

## Biochemical and structural studies of FtsH, a membrane anchored degradation machine

Dias Ribeiro de Carvalho, Vanessa

**DOI**

[10.4233/uuid:ccfb250b-48a4-487a-b6b2-10e7392c1f1a](https://doi.org/10.4233/uuid:ccfb250b-48a4-487a-b6b2-10e7392c1f1a)

**Publication date**

2018

**Document Version**

Final published version

**Citation (APA)**

Dias Ribeiro de Carvalho, V. (2018). *Biochemical and structural studies of FtsH, a membrane anchored degradation machine*. [Dissertation (TU Delft), Delft University of Technology].  
<https://doi.org/10.4233/uuid:ccfb250b-48a4-487a-b6b2-10e7392c1f1a>

**Important note**

To cite this publication, please use the final published version (if applicable).  
Please check the document version above.

**Copyright**

Other than for strictly personal use, it is not permitted to download, forward or distribute the text or part of it, without the consent of the author(s) and/or copyright holder(s), unless the work is under an open content license such as Creative Commons.

**Takedown policy**

Please contact us and provide details if you believe this document breaches copyrights.  
We will remove access to the work immediately and investigate your claim.

**Biochemical and  
structural studies of  
FtsH, a membrane  
anchored degradation  
machine**

Vanessa Isabel Dias Ribeiro de Carvalho



# **Biochemical and structural studies of FtsH, a membrane anchored degradation machine**

Dissertation

for the purpose of obtaining the degree of doctor

at Delft University of Technology

by the authority of the Rector Magnificus Prof. dr. ir. T.H.J.J. van der Hagen

chair of the Board for Doctorates

to be defended publicly on Thursday, 15<sup>th</sup> November 2018 at 10:00 o'clock.

by

Vanessa Isabel DIAS RIBEIRO DE CARVALHO

Master of Science in Applied Biology, Aveiro University, Portugal

born in Viana do Castelo, Portugal

The dissertation has been approved by the promotor.

Composition of the doctoral committee:

Rector Magnificus,	chairperson
Prof. dr. A.H. Engel	Delft University of Technology, promotor
Dr. M.E. Aubin-Tam	Delft University of Technology, copromotor

Independent members:

Prof. dr. C.L. Wyman	Delft University of Technology/Erasmus University
Prof. dr. U. Baumann	U-Köln, Germany
Prof. dr. M. Dogterom	Delft University of Technology
Dr. M. Chami	University of Basel, Switzerland
Dr. A. Jakobi	Delft University of Technology



Bionanoscience Department  
Think big about life at the smallest scale



Keywords: FtsH, Membrane protein, Structural characterization, Proteolysis, AAA proteins

Printed by: Ridderprint

Cover by: Vanessa Isabel Dias Ribeiro de Carvalho

Copyright © 2018 by Vanessa Isabel Dias Ribeiro de Carvalho

Casimir PhD series, Delft-Leiden 2018-40

ISBN 978.90.8593.370.0

An electronic copy of this dissertation is available at:

<http://repository.tudelft.nl/>.

# Contents

<b>CHAPTER 1</b>	<b>INTRODUCTION</b>	<b>1</b>
1.1	PROTEOLYSIS, AN IMPORTANT MECHANISM FOR CELL HOMEOSTASIS MAINTENANCE	2
1.1.1	<i>ATPases associated with diverse cellular activities (AAA+), an elite group of proteases</i>	3
1.1.2	<i>The unique role of FtsH, an AAA+ protease</i>	4
1.1.3	<i>FtsH structural details known</i>	5
1.1.4	<i>FtsH substrates, a variety of possibilities</i>	7
1.1.5	<i>Protease and ATPase activity studies, and what they reveal about FtsH behaviour</i>	9
1.1.6	<i>Membrane proteins, a world of choices</i>	9
1.2	OUTLINE OF THIS THESIS	12
1.3	REFERENCES	13
<b>CHAPTER 2</b>	<b><i>E. COLI</i> FTSH EXPRESSION AND PURIFICATION OPTIMIZATION: A WORLD OF DETERGENTS</b>	<b>19</b>
2.1	INTRODUCTION	20
2.2	MATERIALS AND METHODS	21
2.2.1	<i>Adopted cloning strategies of E. coli FtsH into different expression vectors</i>	21
2.2.2	<i>Optimizing the expression conditions of EcFtsHHis6Myc and EcFtsHX10</i>	22
2.2.3	<i>Solubilization and purification of EcFtsHHis6Myc characterization</i>	23
2.2.4	<i>Solubilization and purification of EcFtsHX10 characterization</i>	24
2.2.5	<i>EcFtsHX6 solubilisation optimization</i>	25
2.2.6	<i>EcFtsHX6 purification using DDM, DM and IGEPAL CA-630 as surfactants</i>	26
2.2.7	<i>EcFtsHX6 purification using LMNG as solubilisation agent</i>	26
2.3	RESULTS	28
2.3.1	<i>Expression and purification of FtsHHis6Myc</i>	28
2.3.2	<i>EcFtsHX6 and EcFtsHX10 cloning</i>	29
2.3.3	<i>Expression and purification of EcFtsHX10</i>	31
2.3.4	<i>EcFtsHX6 solubilization, the proof that the detergent's choice matters</i>	34
2.3.5	<i>Solubilization and purification of EcFtsHX6</i>	36
2.3.6	<i>EcFtsHX6 purification using LMNG as solubilisation agent</i>	39
2.4	DISCUSSION AND CONCLUSIONS	41
2.5	SUPPLEMENTAL DATA	48
2.6	REFERENCES	52
<b>CHAPTER 3</b>	<b><i>AQUIFEX AEOLICUS</i> FTSH EXPRESSION AND PURIFICATION OPTIMIZATION: A DIFFERENT POINT OF VIEW</b>	<b>57</b>
3.1	INTRODUCTION	58

3.2	MATERIAL AND METHODS.....	59
3.2.1	<i>AaFtsH expression and purification characterization</i> .....	59
3.2.1.1	AaFtsH inhibitors.....	59
3.2.1.2	Tests on the effect of ATP concentrations and temperatures .....	60
3.2.2	<i>AaFtsH mutants – site directed mutagenesis</i> .....	61
3.2.2.1	AaFtsH mutants' purification .....	62
3.2.3	<i>Protease activity tests</i> .....	63
3.2.4	<i>Transmission Electron Microscopy analysis</i> .....	63
3.3	RESULTS.....	64
3.3.1	<i>Testing AaFtsH protease activity in different conditions</i> .....	64
3.3.2	<i>AaFtsH purification after inhibition</i> .....	66
3.3.3	<i>Different incubation conditions with ATP lead to different AaFtsH elution profiles</i> 71	
3.3.4	<i>Different mutations of the ATPase and protease domain may affect the elution profile</i> .....	73
3.3.4.1	Mutants protease activity measurements .....	77
3.4	DISCUSSION AND CONCLUSIONS .....	78
3.5	SUPPLEMENTAL DATA .....	83
3.6	REFERENCES .....	85

**CHAPTER 4 LARGE CONFORMATIONAL CHANGES IN FTSH CREATE AN OPENING FOR SUBSTRATE ENTRY .....87**

4.1	INTRODUCTION.....	88
4.2	MATERIALS AND METHODS .....	89
4.2.1	<i>AaFtsH expression and purification</i> .....	89
4.2.2	<i>Transmission Electron Microscopy analysis</i> .....	90
4.2.3	<i>ATPase activity</i> .....	90
4.2.4	<i>Protease activity</i> .....	91
4.2.5	<i>Activity assay in presence of the physiological substrate</i> .....	91
4.2.6	<i>Sequence alignment and structure prediction</i> .....	92
4.2.7	<i>Imaging Processing of negatively stained single particles</i> .....	92
4.3	RESULTS.....	93
4.3.1	<i>Full-length AaFtsH purification</i> .....	93
4.3.2	<i>Electron microscopy of full-length AaFtsH complexes</i> .....	95
4.3.3	<i>2D Class averages and 3D reconstruction of the small AaFtsH complex</i> .....	96
4.3.4	<i>2D Class averages of the large AaFtsH complex highlights large conformational changes</i> .....	97
4.3.5	<i>Dimensions of FtsH subunits and their conformational changes</i> .....	98

4.3.6	<i>Full-length AaFtsH hexamers and dodecamers show similar ATPase and protease activity .....</i>	99
4.3.7	<i>AaFtsH hexamers and dodecamers show similar degradation behaviour in presence of the physiological substrate Sigma 32 .....</i>	101
4.3.8	<i>Bioinformatics tools identify a linker region of ~20aa .....</i>	102
4.4	DISCUSSION AND CONCLUSIONS .....	104
4.5	SUPPLEMENTARY INFORMATION .....	108
4.6	REFERENCES .....	114
<b>CHAPTER 5</b>	<b>CRYO-ELECTRON MICROSCOPY: A LOOK INTO FTSH STRUCTURE .....</b>	<b>119</b>
5.1	INTRODUCTION.....	120
5.2	MATERIALS AND METHODS .....	122
5.2.1	<i>Tilting pairs in negative stain .....</i>	122
5.2.2	<i>Single particle data acquisition and imaging processing in cryo-EM .....</i>	122
5.2.3	<i>AaFtsH reconstitution into proteoliposomes and imaging reconstruction .....</i>	123
5.3	RESULTS.....	123
5.3.1	<i>Random conical tilt of negatively stained pairs .....</i>	123
5.3.2	<i>Single particle image processing of cryo-EM AaFtsH .....</i>	126
5.3.3	<i>Proteoliposomes, a magical recipe for native AaFtsH .....</i>	128
5.4	DISCUSSION AND CONCLUSION .....	132
5.5	SUPPLEMENTARY INFORMATION .....	135
5.6	REFERENCES .....	136
<b>CHAPTER 6</b>	<b>CONCLUSION AND OUTLOOK.....</b>	<b>141</b>
6.1	SUMMARY AND CONTRIBUTIONS TO THE FIELD .....	142
6.2	FUTURE WORK .....	143
6.3	REFERENCES .....	145
	Summary.....	147
	Samenvatting .....	149
	Acknowledgements.....	151
	Curriculum Vitae .....	157
	Publications.....	159



# Chapter 1

## Introduction

“We do not exist in isolation, and science is a human cultural activity, not a purely dispassionate striving after truth, no matter how hard we might try. It is all about where we came from, and where we are going. And it is the most exciting story ever told.”

John Gribbin

Proteins are the main components of all organisms in the Earth surface, playing crucial functions in the control of homeostasis inside the cells. The interest of studying proteins has grown in the scientific community during the last years, especially in what is related with the study of membrane proteins. The possibility of knowing in detail the structural composition and orientations has been a valuable insight to design new and more clever strategies to fight diseases in which different membrane proteins are involved. This introductory chapter describes investigations on a specific protein, FtsH, which will be studied during this thesis, but also describes new techniques and approaches developed to study especially membrane proteins.

## **1.1 Proteolysis, an important mechanism for cell homeostasis maintenance**

Proteins are essential for cells' survival. The set of all proteins, the proteome, proved to be capable of adaptation through the millions of years of evolution. The proteome is what allows cells to maintain and control their mechanisms, as proteins are involved in all cycles that happens inside cells. Even the process that leads to the production of new proteins, translation, is processed by other proteins. Proteins not only control their own production but also their own destruction. The normal cycle of life leads to the use of proteins in some processes and after their use, when no longer needed, these proteins are then in excessive amounts in the cell space, which could become toxic for the cell life. The method that evolution found to avoid protein accumulation inside cells, was through hydrolysis of those proteins down to their basic unit, the amino acids (aa). This process is called proteolysis and it is performed by a specific group of proteins called proteases. Proteases, peptidases or proteinases are enzymes that are found in diverse organisms and they cleave not only surplus proteins but also misfolded or inactive proteins that accumulate in cells. The convergent evolution of proteases resulted in different proteases classes performing a same reaction but employing different catalytic mechanisms. These catalytic proteins produce key signals in different molecular processes inside the cells, acting for example during: embryo development, coagulation, immune response, cell differentiation and death mechanisms. Since their role is of extreme importance, malfunctions associated with these proteins are then related to severe forms of pathological diseases, such as cancer [1].

Proteases are divided in two major groups: the exopeptidases, which cleave peptide bonds of terminal amino acids, and endopeptidases, which catalyse the cleaving of non-terminal amino acids. There are five types of endoproteases, classified by the type of molecular reaction that these proteins control, called: metallo, serine, threonine, cysteine, and aspartate proteases. Metalloproteases are enzymes that possess a catalytic metal ion that serves as base for the hydrolysis of water molecule, an intermediate step in the aa cleavage process. Metalloproteases usually use  $Zn^{2+}$

as a catalytic ion, although some also use  $Mg^{2+}$ ,  $Ni^{2+}$  or  $Cu^{2+}$ , as bases for this catalytical process [2].

One of the most known and complex group of proteases, are the ones within the ATPases associated with diverse cellular activities (AAA+) family. This family of proteins is normally related to several cellular mechanisms such as protein degradation, DNA replication, membrane fusion and signal transduction. They transform the chemical energy contained in the ATP molecule into mechanical energy. In particular, for AAA+ proteases, this mechanical energy is translated into molecular rearrangements that allow the unfolding and cleavage of a target protein, the substrate [3]. The fact that this group of proteases is widely found in eukaryotes, bacteria and archaea proves their evolutive adaptation and, therefore their broad importance [4].

### **1.1.1 ATPases associated with diverse cellular activities (AAA+), an elite group of proteases**

AAA+ proteases are characterized by a barrel shape and an N-terminal conserved adenosine triphosphate (ATP) binding domain (200-250 aa), which is involved in the proteolytical process [5]. They recognize protein substrates for degradation and, in energetically dependent manner fuelled by ATP hydrolysis, they pull the substrates through a central pore. Substrate recognition is mainly performed by the central pore, with the involvement of aromatic aa present in its entrance, which can also be indirectly initiated through proteins called adaptors. The central pore has small dimensions and the mechanical force exerted on the substrates, upon recognition, leads to its unfolding and translocation. The pulling motion is exerted through conformational changes in the ATPase domain, due to ATP hydrolysis [6]. After translocation the substrate enters in a degradation chamber, where the peptide cleaving occurs [7]. Subsequent degradation of the substrate results in a breakdown to smaller-sized peptides, typically around 10-20 amino acids in length [8].

### **1.1.2 The unique role of FtsH, an AAA+ protease**

*Escherichia coli* (*E. coli*) contains five different AAA+ proteases, known as ClpXP, ClpAP, HslUV, Lon and FtsH. From this group, FtsH is the only one that is membrane-anchored, and without it the bacteria do not survive. FtsH plays a crucial role in membrane protein quality control [9]. It is also involved in aminoglycoside antibiotic resistance, possibly by eliminating misfolded proteins disruptive to the membrane [10]. FtsH also regulates the phospholipid to lipopolysaccharide (LPS) ratio in the outer membrane by degrading LpxC, an enzyme involved in LPS biosynthesis [11]. These characteristics make this protein a perfect target for the design of antimicrobial drugs. The abusive use of antibiotics has been reported as a major problem worldwide by the World Health Organization (WHO), since the levels of resistance have been raising dramatically in the last few decades. Large amounts of resources are being invested to overcome this problem, and one of the solutions is to design specific drugs that kill targeted bacteria. FtsH is then an optimal target, since the destruction of this protein would kill all the infectious bacteria. Moreover, malfunctions in the human homologous of *E. coli* FtsH, paraplegin, are associated with disfunction of the muscles and with mistakes in the signal synapse cascade. The mechanism by which this occurs is still unknown, although patients that carry malformations in this protein express a severe form of spastic paraplegia [12]. The description of the FtsH structure and biochemical activity and its response to stimuli presents therefore medical importance.

The gene that codes for FtsH is conserved to at least 40% in distinct organisms as yeast, bacteria, human and plants [13]. Yeast and human have three genes that code for FtsH orthologs, while most of the bacteria have only one and plants have several. In plants, the different FtsH homologous expression is specific for the location, and the protein can be found mainly in the chloroplasts or mitochondria [13].

### **1.1.3 FtsH structural details known**

FtsH name stands for Filamentous temperature sensitive H (FtsH) since the first reports of the expression of this protein were related with a stress response to heat. However, over the years researchers found that HflB, which stands for High frequency lysogenization, refers to exactly the same gene and encodes for FtsH. HflB is related to the elimination of  $\lambda$  phage [14]. For a question of uniformization and since this is the name most often used in the scientific community, the protein will be named FtsH in the context of this thesis.

FtsH is a ~70kDa protein with 650 aa in length, from which ~250 aa are conserved in the AAA+ protease family [15]. It contains both the ATPase and the protease domains in the same polypeptide chain, as opposed to most other AAA+ proteases, which carry these domains in two distinct polypeptide chains [16]. FtsH N-terminal region is composed by two transmembrane helices that are connected to the cytoplasmic (C-terminal) by a small periplasmic region (~75 aa) (Figure 1.1) [17].

Similar to other AAA+ proteases, FtsH assembles in a hexamer complex forming a barrel shape protein with a central pore. The ATPase domain is composed of the Walker A and Walker B motifs which bind and hydrolyse nucleotides, coordinating the ATP,  $Zn^{2+}$  and the water molecules during hydrolysis [15,18]. This domain also contains arginine residues (arginine finger) that compose the second region of homology (SRH), which is believed to be crucial for FtsH oligomerization (Figure 1.1). The FtsH protease domain is composed of an HEXXH motif which is anchored to the ATPase domain through a flexible 12 aa linker, with conserved glycines. This HEXXH motif is transversal to the group of the metalloproteases to which FtsH belongs, and is described as responsible for the coordination of the zinc ion via the two histidines, while the conserved glutamate serves as a catalytic base during the proteolytical process [19].

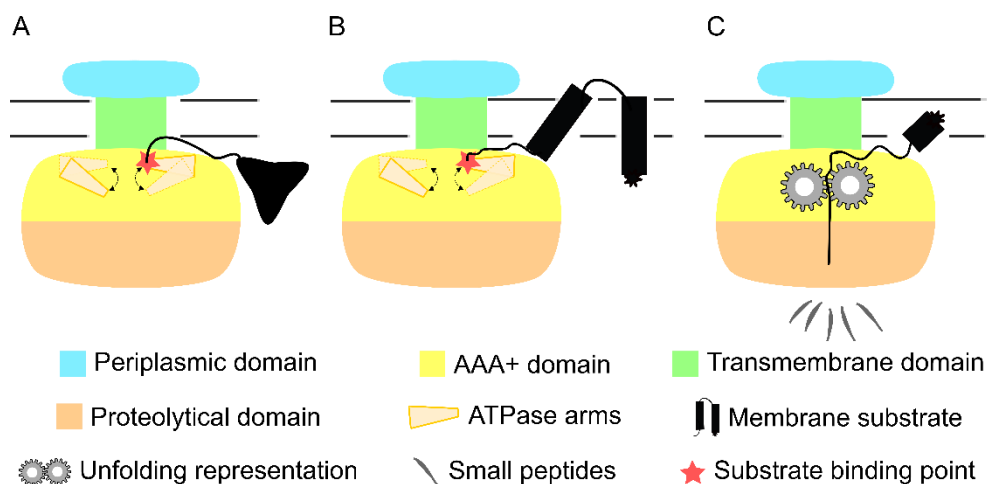


**Figure 1.1 – Illustration of FtsH proteolytical activity and its different domains location in relation to the membrane.** FtsH is capable of degrading soluble and membrane proteins (A and B). The proteolytical process starts with the recognition and binding of the substrate to the ATPase domain (yellow). In this domain, the highly conserved sequence of arginine finger (red) and the Walker A and B domain coordinate the ATP binding and hydrolysis, from which the chemical energy is transformed into mechanical work (movement illustrated by the black arrows). The process progresses, with the pulling and unfolding of the substrate into the protease domain (orange) (C). This results in small peptides (grey strips) that will be recycled to form new and functional proteins. The periplasmic domain of the protein is represented in blue and followed by the transmembrane helices that go through the membrane (green).

Structural studies have used truncated forms of FtsH with only the soluble C-terminal (cytosolic) part [15,17–23] or with only the periplasmic domain [24]. The only full-length structure concerns *m*-AAA, the yeast mitochondrial ortholog of bacterial FtsH, which has been resolved at 12 Å resolution by cryo-electron microscopy (cryoEM) [25]. Therefore, no information on the conformational rearrangement of full-length FtsH in relation to the membrane when bound to nucleotides or to a substrate is available. Crystal structures of the cytosolic domain of FtsH exhibit a six- [18], a two- [15,19] or a three-fold [22] symmetric conformation of the ATPase domain. More recently, the 3.4 Å cryo-electron microscopy map of the inner mitochondrial membrane of the yeast ortholog, YME1, shows a “staircase” symmetry for the ATPase domain [17]. This last model suggests that the “spiral staircase” pore has an opening of 1.4 nm which allows the entrance of small peptides for degradation.

This model also highlights the importance of the tyrosine conserved residues present in loop 1 of FtsH central pore for substrate unfolding and translocation. This model suggests that the ATPase domain can rotate by 35°, which fosters the entrance of peptides to the protease domain. On the other hand, the different conformations, reported in the crystal structures, suggest that the ATPase domain could move polypeptides in steps as long as 45 Å into the central cavity during ATP hydrolysis cycles [18].

In contrast, the C-terminal protease domain always shows a six-fold symmetry for all structures, i.e., the cytosolic domain of *Thermus thermophilus* FtsH [23], of *Thermotoga maritima* FtsH [18,19], of *Aquifex aeolicus* FtsH [15,22], and of YME1 [17]. The proposed mechanism for substrate entry in *m*-AAA is based on substrate recognition by solvent exposed lateral regions of FtsH cytosolic domain. Accordingly, a 13 Å gap between the membrane and the cytosolic domains observed by cryo-electron microscopy would provide access for a substrate, which implies that only (partly) unfolded proteins can reach the translocating loops and be moved through the pore for degradation [25]. Despite the details provided by previous models, there are still open questions related to how FtsH recognizes substrates for degradation and how can insoluble and soluble substrates enter in the central pore of FtsH (Figure 1.1).

#### **1.1.4 FtsH substrates, a variety of possibilities**

Diverse studies on FtsH substrates, show that their recognition by FtsH for degradation does not all occur in the same manner. There is some knowledge on how these substrates are recognized by FtsH inside the cell. If we consider other AAA+proteases, we find that ClpXP is known to recognize five different specific N and C-terminal sequences [7], while the Lon protease recognizes aromatic or hydrophobic rich peptides sequences [26]. FtsH can degrade substrates from either the N or the C-terminal sides. It is capable of degrading both membrane or soluble substrates as long they are unstable, since it possesses only a weak unfoldase capability. A set of FtsH substrates are identified depending on their location and function. Viral soluble substrates include λCII (a gene transcription factor) [27–29], λXis (a subunit of the excision-promoting recombinase) [27], and the CIII gene

product, which allows the virus to initiate latency [30] and influence the lysogenic cycle depending of FtsH overexpression. All these soluble substrates are recognized for degradation by terminal or internal signals. The *E. coli* transcription factors are also regulated by the action of FtsH. The heat shock transcription factor Sigma 32 ( $\sigma_{32}$ ) is one of the most widely studied substrate of FtsH, and it is recognized by an internal sequence [31–33]. Also, the transcription factor SoxS may be degraded by FtsH by its N-terminus [34]. One of the reasons why FtsH is crucial for bacteria survival relates to the substrate LpxC, which plays a key role in controlling the lipopolysaccharide (LPS) to phospholipid ratio inside the cell. FtsH regulates the level of LpxC, whose accumulation would disrupt the lipid cycle inside the cell. LpxC is recognized for degradation by its C-terminus, where the presence of a substrate leads to degradation [35,36]. Furthermore, there are indications that KdtA, involved in the LPS synthesis, is also regulated by FtsH overexpression although this is still unclear [8]. In addition, other unassembled membrane proteins as the subunit SecY of the translocation channel SecYEG is degraded in a  $Zn^{2+}$  and ATP dependent manner by FtsH, when separated from the other units of the SecYEG complex [37,38]. The ATPase subunit a of the  $F_0$  sector is also degraded by FtsH when disassociated from the rotor complex [39]. The membrane protein YccA, which modulates the FtsH protease activity can also be cleaved by FtsH by its 20 aa domain at its N-terminus [40]. There are other membrane substrates identified, such as PspC, DadA, FdoH, YfgM, PpiD, SecD, ExbD and YlaC, for which the mechanism of the recognition is still unclear [41].

The substrates enumerated above belong to a variety of proteins not having a common sequence feature, which complicates the identification of new substrates and the study of the recognition mechanism. There are several biochemical studies concerning FtsH substrate recognition, but we still do not fully understand how substrates are recognized for degradation.

### **1.1.5 Protease and ATPase activity studies, and what they reveal about FtsH behaviour**

To biochemically characterize FtsH behaviour, several studies use  $\sigma 32$  and CII as substrates for *in vitro* reactions [42,43]. Although FtsH is a ATP-dependent protease, it was observed that proteolysis was not inhibited in presence of the ATP analogue cytidine triphosphate (CTP). Proteolytic inhibition is observed when replacing ATP with the following analogous nucleotides: adenosine monophosphate (AMP), guanosine-5'-triphosphate (GTP), uridine-5'-triphosphate (UTP) and adenosine diphosphate (ADP). FtsH protease activity was proven to be reduced by 95% in presence of these nucleotides [43,44]. Moreover, the proteolytical activity is also influenced by the type of ions with which the protein is incubated. The replacement of  $Zn^{2+}$  ions by  $Fe^{2+}$  or the removal of ions in solution completely inhibited  $\sigma 32$  degradation by FtsH [42]. However, the replacement of  $Zn^{2+}$  ions by  $Mn^{2+}$  does not affect the proteolytical process. Several FtsH proteolytical activity inhibitors have also been identified, such as vanadate, o-Phenanthroline and ethylenediamine tetraacetic acid (EDTA); the action of these inhibitors is concentration dependent [42]. From this group only EDTA and vanadate inhibit the ATPase activity, while o-Phenanthroline does not perturb the ATPase activity [45]. It is also known that phenylmethane sulfonyl fluoride (PMSF), azide, potassium nitrate ( $KNO_3$ ) and N-ethylmaleimide (NEM) have no influence on FtsH activity [42]. In absence of substrate, the ATP hydrolysis rate of *E. coli* FtsH is around 459 nmol/min/mg at 37°C [46], with an apparent  $K_m$  around 80  $\mu M$  for ATP [42].

### **1.1.6 Membrane proteins, a world of choices**

Membrane proteins represent around 20 to 30% of all the proteomes in eukaryotes, bacteria and archaea [47]. Around 50% of all human drugs are targeted to membrane proteins, which indicates that several diseases are associated with this group of proteins [48]. Membrane proteins have also several functions associated with the cell maintenance, such as the transport of materials from and into the cell and signal communication with other cells. Despite their evident importance in the cell context, less structural information is available on membrane than on soluble

proteins. In spite of recent advances in structural biology, only 18% of the structure depositions on the Protein Databank (PDB) in 2016 were of membrane proteins [47], which means that although these are important proteins, there are some difficulties in their study. One of the main obstacles for membrane protein characterization is their overexpression at high yields. Usually membrane proteins are expressed in low amounts inside cells and when cells are submitted to overexpression conditions, the expressed membrane proteins are often not functional. Advances in the genetic manipulation of host organisms, especially in *E. coli* strains, has improved the overexpression of these proteins [49]. The other main difficulties in membrane protein studies include the solubilization/extraction of these proteins from the lipid membrane. This process must be performed in such a way that the lipid bilayer is disrupted while keeping the protein assembly stable and functional. To overcome this problem, the constantly evolving surfactants available in the market are of valuable help. The use of novel detergents that are capable of minimal disturbance in the hydrophobic domains of the membrane proteins and in their hydrophilic domains that project out of the membrane, allow to keep them stable in the aqueous medium.

Detergents are constituted by a polar head group and a hydrophobic tail, and they form micelles when present above the critical micellar concentration (CMC) in an aqueous solution (Figure 1.2). Micelle can mimic the natural environment of the membrane protein which destabilizes the lipid bilayer and leads to the extraction of the protein into the detergent micelle [50].

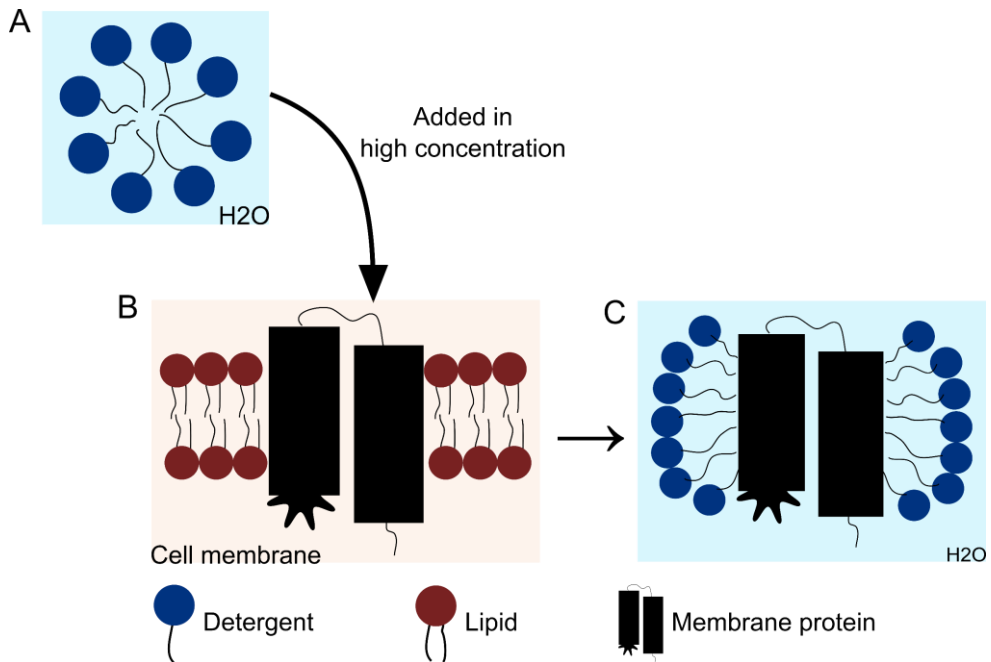


**Figure 1.2 – Illustration of protein isolation by detergents micelles.** Detergents form micelles in aqueous solution (A). When added in excess (20x above the CMC) to cell membranes that overexpress the target membrane protein, they destabilize the lipid bilayer and replace the lipids that surround the protein (B and C). The detergent micelle maintains the membrane protein in aqueous solution to avoid aggregation and enable future studies.

Detergents are classified into four major groups, depending on their structural characteristics: zwitterionic detergents, bile acid salts, ionic and non-ionic detergents. These last two groups are the most successful in membrane protein extraction and are widely used. The right choice of detergent depends mainly on the type of study to which the protein will be submitted, although some characteristics of the detergent may also help in the choice of detergent. The capability of the detergents to form micelles is what prevents the aggregation of membrane proteins when in aqueous solution, which requires the detergent concentration to be above the CMC (Figure 1.2). Diverse types of detergents have been employed during this thesis, which will be further described in the following chapters.

## 1.2 Outline of this thesis

In Chapter 2, the purification of *Escherichia coli* FtsH (EcFtsH) is discussed. Several cloning and overexpression conditions were tested to reach a high yield of protein expression. After establishing the appropriate conditions to overexpress EcFtsH, different solubilization conditions were screened and the conditions that allow to obtain stable EcFtsH were combined with different purification strategies. This study showed that EcFtsH extraction and stabilization in aqueous solution is challenging. However, the screening of the different conditions allowed to conclude that the use of LMNG was the most successful in stabilizing EcFtsH. This effort provided a useful basis for the subsequent studies performed in this thesis, since important knowledge on how to work with FtsH was obtained.

Chapter 3 describes the solubilization and purification of *Aquifex aeolicus* FtsH (AaFtsH). Important advances in the protein stabilization and solubilization in detergent were gained. The finding that temperature influences the purification step allowed to reach more stable proteins. Several protease activity tests were also performed in this chapter, showing that different technical details influenced FtsH stabilization.

In Chapter 4, insights are shared about the capability of the AaFtsH ATPase domain to undergo a large tilting movement. Electron microscopy was used to determine the 3D map of the full-length *Aquifex aeolicus* FtsH hexamer. Moreover, detergent solubilisation induced the formation of fully active FtsH dodecamers, which consist of two FtsH hexamers in a single detergent micelle. FtsH structures reveal that the cytosolic domain can tilt with respect to the membrane. A flexible linker of ~20 residues between the second transmembrane helix and the cytosolic domain permits the observed large tilting movements, thereby facilitating the entry of substrate proteins towards the central pore for translocation.

In Chapter 5, we show the first 2D classes averages of cryo-electron microscopy studies of the full-length FtsH. The determination of the hexameric shape structure is visible in the class assembly as well as in the low-resolution model of the cryo-electron microscopy. FtsH reconstitution into proteoliposomes would allow the

structural characterization of the protein into its native environment. Cryo-electron tomography data show promising results about the insertion of AaFtsH into the membrane and the ability of this technique to reach a structural model of FtsH in its native environment.

Chapter 6 describes the impact that this work will have in the future studies of FtsH. This concerns exploring the importance of the discoveries made during the experimental work, and a vision of the future work that can be performed to make new scientific discoveries about FtsH role in nature.

### 1.3 References

- [1] I. Richard, The genetic and molecular bases of monogenic disorders affecting proteolytic systems., *Journal of Medical Genetics*. 42 (2005) 529–539.
- [2] J.-W. Wu, X.-L. Chen, Extracellular metalloproteases from bacteria, *Applied Microbiology and Biotechnology*. 92 (2011) 253–262.
- [3] R.S. Yedidi, P. Wendler, C. Enenkel, AAA-ATPases in Protein Degradation, *Frontiers in Molecular Biosciences*. 4 (2017) 1–14.
- [4] R.D. Vale, AAA proteins: Lords of the ring, *Journal of Cell Biology*. 150 (2000) F13-9.
- [5] T. Ogura, A.J. Wilkinson, AAA+ superfamily ATPases: common structure-diverse function, *Genes to Cells*. 6 (2001) 575–597.
- [6] G.L. Hersch, R.E. Burton, D.N. Bolon, T.A. Baker, R.T. Sauer, Asymmetric interactions of ATP with the AAA+ ClpX6 unfoldase: allosteric control of a protein machine., *Cell*. 121 (2005) 1017–27.
- [7] R.T. Sauer, T.A. Baker, AAA+ Proteases: ATP-Fueled Machines of Protein Destruction, *Annual Review of Biochemistry*. 80 (2011) 587–612.
- [8] K. Ito, Y. Akiyama, Cellular Functions, Mechanism of Action, and Regulation of FtsH Protease, *Annual Review of Microbiology*. 59 (2005) 211–231.
- [9] S.B. Hari, R.T. Sauer, The AAA+ FtsH Protease Degrades an *ssrA*-Tagged Model Protein in the Inner Membrane of *Escherichia coli*, *Biochemistry*. 55 (2016) 5649–5652.
- [10] A. Hinz, S. Lee, K. Jacoby, C. Manoil, Membrane proteases and aminoglycoside antibiotic resistance, *Journal of Bacteriology*. 193 (2011) 4790–4797.

- [11] M. Schäkermann, S. Langklotz, F. Narberhaus, FtsH-mediated coordination of lipopolysaccharide biosynthesis in *Escherichia coli* correlates with the growth rate and the alarmone (p)ppGpp., *Journal of Bacteriology*. 195 (2013) 1912–9.
- [12] T. Karlberg, S. van den Berg, M. Hammarström, J. Sagemark, I. Johansson, L. Holmberg-Schiavone, H. Schüler, Crystal structure of the ATPase domain of the human AAA+ protein paraplegin/SPG7., *PLoS One*. 4 (2009) e6975.
- [13] H. Janska, J. Piechota, M. Kwasniak, ATP-dependent proteases in biogenesis and maintenance of plant mitochondria, *Biochimica et Biophysica Acta - Bioenergetics*. 1797 (2010) 1071–1075.
- [14] C. Herman, T. Ogura, T. Tomoyasu, S. Hiraga, Y. Akiyama, K. Ito, R. Thomas, R. D'Ari, P. Boulloc, Cell growth and lambda phage development controlled by the same essential *Escherichia coli* gene, *ftsH/hflB*., *Proceedings of the National Academy of Sciences of the United States of America*. 90 (1993) 10861–5.
- [15] M. Vostrukhina, A. A. Popov, B. E. Brunstein, C. M.A. Lanz, D. A. R. Baumgartner, A. C. Bieniossek, E. A. M. Schacherl, C. A. Ulrich, Baumann, C. \*, The structure of *Aquifex aeolicus* FtsH in the ADP-bound state reveals a C2-symmetric hexamer, *Acta Crystallogr D Biol Crystallogr*. D71 (2015) 1307–1318.
- [16] L.-M. Bittner, J. Arends, F. Narberhaus, Mini review: ATP-dependent proteases in bacteria, *Biopolymers*. 105 (2016) 505–517.
- [17] C. Puchades, A.J. Rampello, M. Shin, C.J. Giuliano, R.L. Wiseman, S.E. Glynn, G.C. Lander, Structure of the mitochondrial inner membrane AAA+ protease YME1 gives insight into substrate processing., *Science (New York, N.Y.)*. 358 (2017) eaao0464.
- [18] C. Bieniossek, B. Niederhauser, U.M. Baumann, The crystal structure of apo-FtsH reveals domain movements necessary for substrate unfolding and translocation., *Proceedings of the National Academy of Sciences of the United States of America*. 106 (2009) 21579–21584.
- [19] C. Bieniossek, T. Schalch, M. Bumann, M. Meister, R. Meier, U. Baumann, The molecular architecture of the metalloprotease FtsH., *Proceedings of the National Academy of Sciences of the United States of America*. 103 (2006) 3066–3071.
- [20] S.H. Kim, G.B. Kang, H.E. Song, S.J. Park, M.H. Bea, S.H. Eom, Structural studies on *Helicobacter pylori* ATP-dependent protease, FtsH., *Journal of Synchrotron Radiation*. 15 (2008) 208–10.
- [21] H. Niwa, D. Tsuchiya, H. Makyio, M. Yoshida, K. Morikawa, Hexameric ring structure of the ATPase domain of the membrane-integrated metalloprotease FtsH from *Thermus thermophilus* HB8, *Structure*. 10 (2002) 1415–1423.

- [22] R. Suno, H. Niwa, D. Tsuchiya, X. Zhang, M. Yoshida, K. Morikawa, Structure of the Whole Cytosolic Region of ATP-Dependent Protease FtsH, *Molecular Cell*. 22 (2006) 575–585.
- [23] R. Suno, M. Shimoyama, A. Abe, T. Shimamura, N. Shimodate, Y.-H. Watanabe, Y. Akiyama, M. Yoshida, Conformational transition of the lid helix covering the protease active site is essential for the ATP-dependent protease activity of FtsH, *FEBS Letters*. 586 (2012) 3117–3121.
- [24] F. Scharfenberg, J. Serek-Heuberger, M. Coles, M.D. Hartmann, M. Habeck, J. Martin, A.N. Lupas, V. Alva, Structure and Evolution of N-domains in AAA Metalloproteases., *Journal of Molecular Biology*. 427 (2015) 910–923.
- [25] S. Lee, S. Augustin, T. Tatsuta, F. Gerdes, T. Langer, F.T.F. Tsai, Electron cryomicroscopy structure of a membrane-anchored mitochondrial AAA protease, *Journal of Biological Chemistry*. 286 (2011) 4404–4411.
- [26] E. Gur, R.T. Sauer, Recognition of misfolded proteins by Lon, a AAA(+) protease., *Genes & Development*. 22 (2008) 2267–77.
- [27] O. Kobiler, S. Koby, D. Teff, D. Court, A.B. Oppenheim, The phage lambda CII transcriptional activator carries a C-terminal domain signaling for rapid proteolysis., *Proceedings of the National Academy of Sciences of the United States of America*. 99 (2002) 14964–9.
- [28] A. Kihara, Y. Akiyama, K. Ito, Different pathways for protein degradation by the FtsH/HflKC membrane-embedded protease complex: an implication from the interference by a mutant form of a new substrate protein, YccA, *Journal of Molecular Biology*. 279 (1998) 175–188.
- [29] Y. Shotland, S. Koby, D. Teff, N. Mansur, D.A. Oren, K. Tatematsu, T. Tomoyasu, M. Kessel, B. Bukau, T. Ogura, A.B. Oppenheim, Proteolysis of the phage lambda CII regulatory protein by FtsH (HflB) of *Escherichia coli*, *Molecular Microbiology*. 24 (1997) 1303–1310.
- [30] C. Herman, D. Thévenet, R. D’Ari, P. Bouloc, The HflB protease of *Escherichia coli* degrades its inhibitor lambda cIII., *Journal of Bacteriology*. 179 (1997) 358–63.
- [31] M. Obrist, S. Langklotz, S. Milek, F. Führer, F. Narberhaus, Region C of the *Escherichia coli* heat shock sigma factor RpoH ( $\sigma_{32}$ ) contains a turnover element for proteolysis by the FtsH protease, *FEMS Microbiology Letters*. 290 (2008) 199–208.
- [32] M. Horikoshi, T. Yura, S. Tsuchimoto, Y. Fukumori, M. Kanemori, Conserved region 2.1 of *Escherichia coli* heat shock transcription factor sigma<sub>32</sub> is required for modulating both metabolic stability and transcriptional activity., *Journal of Bacteriology*. 186 (2004) 7474–80.

- [33] C. Herman, D. Thévenet, R. D'Ari, P. Bouloc, Degradation of sigma 32, the heat shock regulator in *Escherichia coli*, is governed by HflB., *Proceedings of the National Academy of Sciences of the United States of America*. 92 (1995) 3516–20.
- [34] K.L. Griffith, I.M. Shah, R. E. Wolf, Proteolytic degradation of *Escherichia coli* transcription activators SoxS and MarA as the mechanism for reversing the induction of the superoxide (SoxRS) and multiple antibiotic resistance (Mar) regulons, *Molecular Microbiology*. 51 (2004) 1801–1816.
- [35] F. Führer, A. Müller, H. Baumann, S. Langklotz, B. Kutscher, F. Narberhaus, Sequence and Length Recognition of the C-terminal Turnover Element of LpxC, a Soluble Substrate of the Membrane-bound FtsH Protease, *Journal of Molecular Biology*. 372 (2007) 485–496.
- [36] T. Ogura, K. Inoue, T. Tatsuta, T. Suzaki, K. Karata, K. Young, L.-H. Su, C.A. Fierke, J.E. Jackman, C.R.H. Raetz, J. Coleman, T. Tomoyasu, H. Matsuzawa, Balanced biosynthesis of major membrane components through regulated degradation of the committed enzyme of lipid A biosynthesis by the AAA protease FtsH (HflB) in *Escherichia coli*, *Molecular Microbiology*. 31 (1999) 833–844.
- [37] Y. Akiyama, A. Kihara, H. Tokuda, K. Ito, FtsH (HflB) is an ATP-dependent protease selectively acting on SecY and some other membrane proteins., *The Journal of Biological Chemistry*. 271 (1996) 31196–201.
- [38] A. Kihara, Y. Akiyama, K. Ito, FtsH is required for proteolytic elimination of uncomplexed forms of SecY, an essential protein translocase subunit., *Proceedings of the National Academy of Sciences of the United States of America*. 92 (1995) 4532–6.
- [39] Y. Akiyama, A. Kihara, K. Ito, Subunit a of proton ATPase F0 sector is a substrate of the FtsH protease in *Escherichia coli*, *FEBS Letters*. 399 (1996) 26–28.
- [40] S. Chiba, Y. Akiyama, K. Ito, Membrane protein degradation by FtsH can be initiated from either end., *Journal of Bacteriology*. 184 (2002) 4775–82.
- [41] L.-M. Bittner, J. Arends, F. Narberhaus, When, how and why? Regulated proteolysis by the essential FtsH protease in *Escherichia coli*, *Biological Chemistry*. 398 (2017) 625–635.
- [42] T. Tomoyasu, J. Gamer, B. Bukau, M. Kanemori, H. Mori, A.J. Rutman, A.B. Oppenheim, T. Yura, K. Yamanaka, H. Niki, *Escherichia coli* FtsH is a membrane-bound, ATP-dependent protease which degrades the heat-shock transcription factor sigma 32., *The EMBO Journal*. 14 (1995) 2551–2560.
- [43] R.L. Bruckner, Robert C.; Gunyuzlu, Paul L. and Stein, Coupled Kinetics of ATP and Peptide Hydrolysis by *Escherichia coli* FtsH Protease, *Biochemistry*. 42 (2003) 10843–10852.

- [44] Y. Asahara, K. Atsuta, K. Motohashi, H. Taguchi, M. Yohda, M. Yoshida, FtsH recognizes proteins with unfolded structure and hydrolyzes the carboxyl side of hydrophobic residues., *Journal of Biochemistry*. 127 (2000) 931–7.
- [45] T. Ogura, T. Okuno, R. Suno, Y. Akiyama, *Handbook of Proteolytic Enzymes*, Elsevier, 2013.
- [46] K. Karata, T. Inagawa, A.J. Wilkinson, T. Tatsuta, T. Ogura, Dissecting the role of a conserved motif (the second region of homology) in the AAA family of ATPases. Site-directed mutagenesis of the ATP-dependent protease FtsH., *The Journal of Biological Chemistry*. 274 (1999) 26225–32.
- [47] R. Fernandez-Leiro, S.H.W. Scheres, Unravelling biological macromolecules with cryo-electron microscopy, *Nature*. 537 (2016) 339–346.
- [48] J.G. Almeida, A.J. Preto, P.I. Koukos, A.M.J.J. Bonvin, I.S. Moreira, Membrane proteins structures: A review on computational modeling tools, *Biochimica et Biophysica Acta (BBA) - Biomembranes*. 1859 (2017) 2021–2039.
- [49] A. Pandey, K. Shin, R.E. Patterson, X.-Q. Liu, J.K. Rainey, Current strategies for protein production and purification enabling membrane protein structural biology, *Biochemistry and Cell Biology*. 94 (2016) 507–527.
- [50] A.M. Seddon, P. Curnow, P.J. Booth, Membrane proteins, lipids and detergents: not just a soap opera, *Biochimica et Biophysica Acta (BBA) - Biomembranes*. 1666 (2004) 105–117.



# Chapter 2

## *E. coli* FtsH expression and purification optimization: a world of detergents

Membrane protein isolation in aqueous solution is possible *in vitro* due to the development of surfactants, which extract protein from the lipid bilayer without disrupting its structure and function. Each membrane protein has its own preferential conditions to be extracted from the membrane partially due to the electrostatic interactions that the protein maintain with the lipid bilayer. In this chapter, we present a diverse set of tests in which detergents and other conditions were explored to extract *E. Coli* FtsH from the membrane.

## 2.1 Introduction

Membrane proteins are important in several biological processes. From the set of membrane proteins identified in cells, 50% are target of drug development [1]. Due to their biological importance, these proteins are studied intensively nowadays, although their *in vitro* study faces several challenges. The major hurdles of biochemical and structural studies of membrane proteins concern the difficulties in the overexpression, membrane extraction, and purification [2,3]. Despite these difficulties, the beginning of this century witnessed an increase in membrane protein structure characterization. These changes were not only accompanied by advances in the improvement of the techniques used in structural characterization (such as cryo-electron microscopy), but also by the development of more efficient detergents [4,5]. In membrane proteins purification, the most crucial step is the choice of the detergent, which destabilizes the lipid bilayer by competing with lipids and breaking the protein-lipid interactions. The choice of the most suitable detergent often involves a long process of trial and error [6].

In this chapter, we describe the optimization of expression and purification protocols of *Escherichia coli* FtsH (EcFtsH). EcFtsH plays a key role in the quality control of proteins inside the cell. It is capable of degrading incompletely assembled or damaged soluble and membrane proteins by ATP-dependent proteolysis. The presence of FtsH is crucial for *E. coli* survival. Due to its importance, FtsH has been the target of several studies over the years [7–19].

The optimization of the expression and purification conditions were performed here taking in account all the previous studies on EcFtsH. Nevertheless, it is important to point out that the major goal of this thesis is to biochemically and structurally characterize FtsH to understand the proteolysis mechanism in a more detailed manner.

## 2.2 Materials and methods

### 2.2.1 Adopted cloning strategies of *E. coli* FtsH into different expression vectors

The synthetic gene of *Escherichia coli* FtsH (EcFtsH) was purchased (Life Technologies) with optimized codon for *E. coli* in a standard vector, containing restriction sites NcoI and SalI/HindIII for 5' and 3' end respectively (Supplementary Figure 2.1). The gene fragment (1959bp) was amplified from the standard vectors by Polymerase Chain Reaction (PCR). Three primers were designed for each PCR reaction. The primer contained the NcoI restriction site (5'-GCATATGAC**CCATGG**CGAAAAACCTAATACTCTGGCTG-3'); the primer for the HindIII restriction site (5'-GGGTAACACCATGTTCAGAGCAGTTAGGCGAC**AAGCTT**GTCGA-3') and the SalI restriction site (5'-CAGAGCAGTTAGGCGACAAGCTT**GTCGACT**GACCGCTG-3'). Using these primers in the PCR reactions, the gene fragments were amplified twice with double restriction sites NcoI/HindIII (Insert 1) and NcoI/SalI (Insert 2). The amplifications were performed using a MyCycler<sup>TM</sup> Thermal Cycler (Bio-Rad) and the DNA Insert 1 and Insert 2 were purified from the PCR mixture by QIAquick<sup>®</sup> PCR Purification Kit (Qiagen) according to the manufacture instructions. The purified DNA inserts were double digested by the corresponding restriction enzymes for 2 hours at 37°C. After double digestion, the restriction enzymes were inactivated at 65°C for 1 hour. Thereafter the double digested inserts were purified by QIAquick<sup>®</sup> PCR Purification Kit (Qiagen) and DNA was quantified by measuring the absorbance at 260 nm ( $A_{260}$ ) (NanoDrop ND-1000 Spectrophotometer Thermo Scientific). Both inserts were cloned into the pET28a expression vector. After cloning insert 1 into pET28a, the FtsH gene will be separated by a sequence of 10 amino acids (aa) (LVDKLAAALE) from a C-terminal His6-tag (EcFtsHX10). After cloning insert 2 into pET28a, the gene is separated by a sequence of 6 aa (LAAALE) from the C-terminal His6-tag (EcFtsHX6). The double digestion of the pET28a was taken in two parallel reactions using the pair NcoI/HindIII and NcoI/SalI restriction enzymes. After digestion, the restriction enzymes were inactivated as described before and the sample was treated with Shrimp Alkaline Phosphatase (SAP) to avoid recircularization of the cloning vectors. Thereafter, the linearized double digested

expression vectors were isolated by agarose gel electrophoresis and purified using the QIAquick® Gel Extraction Kit (QIAGEN). The two, pure double digested inserts were ligated into the pET28a double digested expression vector (Supplementary Figure 2.1). Ligations were performed with 1 U T4 DNA ligase (Fermentas) using a molar ratio of 1:3 (vector to insert) in a total reaction of 10  $\mu$ L, at 22°C for 3 hours, in 1x T4 DNA ligase buffer (50 mM Tris-HCl pH 7.5; 10 mM MgCl<sub>2</sub>, 1mM ATP, 10mM Dithiothreitol, Fermentas). After performing the ligation reaction, 50  $\mu$ L of *E. coli* DH5a competent cells were transformed with 5  $\mu$ L of ligation reaction mixture by heat shock reaction. The positive transformants were grown overnight in Luria-Bertani Broth agar (LB-agar) plate at 37°C. The DNA plasmid was then purified using the PureYield™ Plasmid Miniprep System (Promega). The positive transformants were tested for the insert by performing a colony PCR and the purified DNA sequence was confirmed by sequencing.

### **2.2.2 Optimizing the expression conditions of EcFtsHHis6Myc and EcFtsHX10**

*E. coli* FtsH was cloned into the PSTD113 expression vector, encoding for FtsHHis6Myc. This construct was kindly granted by [20]. Transformed *E. coli* BL21 (DE3) pLysS competent cells were submitted to different expression time points (0, 45, 120, 190, 240, 300 min) after induction with 0.9 mM IPTG at 37°C. Expression was also tested in absence of IPTG for 4hours at 37°C. Induced and non-induced samples were compared by SDS-Page gel. EcFtsHX10 expression was carried using either NiCo (DE3) or Lemo21 (DE3) (New England Biolabs) competent cells at 20°C, 37°C and 25°C and 30°C, respectively. EcFtsHX10 overexpression into NiCo (DE3) cells was firstly carried at 20°C for different expression periods (0, 1, 2, 3, 7 hours) after induction with 0.9 mM IPTG. The resulting cell extract was isolated by centrifugation and solubilised in 10 mM Tris-HCl, 10 mM 2-mercaptoethanol, 1 mM phenylmethane sulfonyl fluoride (PMSF) and 15% glycerol. Cells were lysed by sonication, using a Q125 Sonicator (Qsonica), for 3 min with a 40% duty cycle. Lysates were centrifuged, pellets were isolated and resuspended in 10 mM Tris-HCl, 500 mM NaCl, 10 mM 2-mercaptoethanol, 1 mM PMSF, 10% glycerol, 20 mM

imidazole and 0.5% IGEPAL CA-630. After 30 min on ice, the sample was submitted to a centrifugation for 1 hour at 100 000 *g*. The supernatant and pellet were analysed by SDS-Page gel. Expression of EcFtsHX10 into NiCo (DE3) cells, was also carried at 37 and 25°C for 4 hours after induction with 0.09 and 0.9 mM IPTG. Finally, EcFtsHX10 overexpression was assessed using Lemo21 (DE3). Different L-Rhamnose concentrations were tested (0, 0.1, 0.25, 0.5, 0.75, 1, 2 mM) during induction at 30°C for 4 hours. Unless stated otherwise in this document, all cell extract samples analysed by SDS-Page gel were dissolved in 5x Loading buffer (250 mM Tris-HCl pH6.8, 500 mM dithiothreitol (DTT), 0.25% bromophenol blue and 50% glycerol). The results were analysed by SDS-Page gel.

### **2.2.3 Solubilization and purification of EcFtsHHis6Myc characterization**

*E. coli* BL21 (DE3) pLysS transformed with FtsHHis6Myc, were grown at 37°C until A<sub>600</sub> reached 0.7 - 0.9, FtsHHis6Myc expression was induced by 0.9 mM IPTG for 4 hours. Cells were harvested by centrifugation for 25 min at 3 500 *g* (Beckman JLA-9.1000 rotor, Avanti J-26 XPI). The bacterial pellets were resuspended in 10 mM Tris-HCl pH 8, 500 mM NaCl, 10% glycerol, 10 mM 2-mercaptoethanol, protease inhibitor and 20 mM imidazole (Buffer A). After sonication, the cell extract was centrifuged, and the pellet was solubilised in Buffer A + 0.5% IGEPAL CA-630. The resulting sample was solubilised for 1 hour at 4°C and the supernatant was isolated by centrifugation. The supernatant was loaded on a HisTrap FF 1mL pre-packed column (GE Healthcare) and eluted in an isocratic gradient of Buffer A + 500 mM Imidazole. FtsHHis6Myc sample buffer was exchanged using a Desalting 5mL Prepacked column (GE Healthcare) excluding the salt. The sample was then loaded into a HiTrapQ FF 5mL Prepacked column (GE Healthcare) previously equilibrated with 10 mM Tris-HCl pH 8.1, 10% glycerol, 10 mM 2-mercaptoethanol and protease inhibitor. The protein elution was performed in an isocratic gradient of the same buffer plus 1 M NaCl. FtsHHis6Myc protease activity tests were performed using the same protocol as in 3.2.3. The samples were incubated in presence/absence of 10 mM ATP for 1 hour at 42°C.

### **2.2.4 Solubilization and purification of EcFtsHX10 characterization**

EcFtsHX10 purification and solubilization was first assessed using IGEPAL-CA630 as detergent [21]. EcFtsHX10 overexpression into NiCo or Lemo21 (DE3) was induced at 25 and 30°C for 3 hours, respectively. Cells were lysed using a cell disruptor and further centrifuged, for 10 min at 20 000 *g* and 4°C, the supernatant was collected, and membranes were isolated after ultracentrifugation at 125 000 *g* for 1 hour at 4°C. Membranes were solubilised in 20 mM Tris-HCl pH 8, 200 mM NaCl and 3% IGEPAL CA-630, for 1 hour stirring at 4°C. A two-step purification protocol was used to purify EcFtsHX10 using IGEPAL CA-630. A first step, immobilized metal affinity chromatography was performed incubating the sample with 1 mL of NiNTA beads for 1 hour at 4°C. Elution was made by 20 mM Tris-HCl pH 8, 500 mM NaCl, 1% glycerol, 0.1% IGEPAL CA-630 and 350 mM imidazole. The sample was then analysed by size exclusion chromatography (SEC). An isocratic elution gradient, in gel filtration buffer 20 mM Tris-HCl, 200 mM NaCl, 1% glycerol and 0.1% IGEPAL CA 630, was performed using a Superose 6 10/300 GL column (GE Healthcare). The eluted fractions were analysed by SDS-Page gel. For molecular weight estimations a calibration curve was run in both SEC. The calibration curve was performed using the Gel Filtration High Molecular Weight Calibration Kit (GE Healthcare), following the GE Healthcare instructions.

The cell extract of EcFtsHX10 overexpressed in NiCo (DE3) competent cells at 37°C for 3 hours induced with 0.09 mM IPTG, was also used for further protein purification. The bacterial extract was solubilised into 20 mM monoethanolamine (MEA) pH 9, 100 mM NaCl, 5 mM MgCl<sub>2</sub>, 20% glycerol, 1 mM DTT and 1 mM 4-(2-Aminoethyl) benzenesulfonyl fluoride hydrochloride (AEBSF). Cell extracts and membranes were isolated the same way as explained above. Membrane samples were solubilised in 20 mM MEA pH 9, 10 mM NaCl, 5 mM MgCl<sub>2</sub>, 10% glycerol, 1 mM DTT, 1 mM AEBSF and 2.5% Triton X-100 or 3% DDM, for 1 hour stirring at 4°C. Thereafter, the supernatant containing EcFtsHX10 sample, was isolated by centrifugation for 1 hour at 125 000 *g*. EcFtsHX10 was then purified in presence of

two detergents and using two purification columns: Triton X-100 and loaded into a HiTrapQ 5 mL column, DDM and loaded into a HisTrap 1 mL Prepacked column (GE Healthcare). Both samples were eluted into an isocratic gradient of NaCl (0-1M) and Imidazole (20-500 mM) respectively of 20 mM monoethanolamine pH 9, 5% glycerol, 1 mM DTT, 1 mM AEBSF and 0.2% DDM or Triton X-100 (the buffer used to elute the sample from the HisTrap with DDM contained 500 mM NaCl). Eluted samples were analysed on SDS-Page gel and protease activity of both samples was tested for 1 hour at 42°C in presence/absence of 10 mM ATP (as described in 3.2.3). EcFtsHX10 solubilised with DDM was further purified by a second step of purification, the sample was loaded into a HiTrapQ and eluted in the buffer 20 mM monoethanolamine pH 9, 5% glycerol, 1 mM DTT, 1 mM AEBSF and 0.2% DDM in an isocratic gradient of 0 to 1 M NaCl. EcFtsHX10 purification was also performed on the cell extract that resulted from the overexpression carried at 20°C in NiCo (DE3) competent cells. Except for the solubilization of this membrane pellet which was done with IGEPAL CA-630, all the rest of the purification protocol conditions were the same as described previously.

### **2.2.5 EcFtsHX6 solubilisation optimization**

Solubilisation of EcFtsHX6 was first assessed at analytical scale (a total of 0.8 g of membranes was used for the all experiment) using incomplete factorial (IF) approach [22] combining four detergents (IGEPAL CA-630, DM, DDM or OG), three NaCl concentrations (10, 100 or 300 mM), three incubation periods (2 hours at 4°C; 4 hours at 4°C; or 2 hours at 4°C followed by 1 hour at RT) and two buffers (50 mM Tris-HCl or 20 mM MEA), keeping the samples as much as possible on ice. Using SAMBA software, 16 IF combinations (Supplementary Figure 2.2) can be obtained out of the 72 total combinations (4 detergents x 3 NaCl concentrations x 3 incubations experiments x 2 buffers bases). In all 16 experiments, EcFtsHX6 membrane solubilisation was performed with 50mM Tris-HCl or 20 mM MEA, in presence of 10, 100 or 300 mM NaCl adding 2.5% of IGEPAL CA-630, 2% DM, 2% DDM or 2% OG at 4°C for either 2 hours at 4°C, 4 hours at 4°C, or 2 hours at 4°C followed by 1 hour at room temperature. After solubilisation, membranes were

centrifuged at 110000 *g* for 45 min. The supernatants were analysed on SDS-Page gel.

### **2.2.6 EcFtsHX6 purification using DDM, DM and IGEPAL CA-630 as surfactants**

NiCo (DE3) cells overexpression of EcFtsHX6 was induced with 0.09 mM IPTG at 25°C for 3 hours. Membranes were prepared as described before, with the only change being the buffer to solubilize the cell extract (20 mM MEA pH 9, 100 mM NaCl, 5 mM MgCl<sub>2</sub>, 1 mM DTT, protease inhibitor, 20% glycerol and 0.1 mM ATP). EcFtsHX6 membranes were solubilised for 2 hours at 4°C stirring in presence of 20 mM MEA, 10 mM NaCl, 5mM MgCl<sub>2</sub>, 1mM DTT, protease inhibitor, 10% glycerol and 2% DDM, 2.5% DM or 2.5% IGEPAL CA-630. The buffer in presence of 2% DDM contained 100 mM NaCl and 0.1 mM ATP. After centrifugation, the sample was incubated with 1 mL of NiNTA beads and eluted in 20 mM MEA pH 9, 300 mM NaCl, 5 mM MgCl<sub>2</sub>, 1 mM DTT, protease inhibitor, 250 mM imidazole and 0.2% DDM, 0.5% DM or 0.1% IGEPAL CA-630. Further purification was performed loading the samples into a SEC. The sample purified with DDM was loaded into a Sephacryl S-300 HR (GE Healthcare) and the remaining samples (DM and IGEPAL-CA630 solubilized) were separated by size on a Superose 6 10/300 GL column (GE Healthcare). Samples were analysed by SDS-Page gel and activity tests were performed as in 3.2.3 at 42°C for 1 hour in presence or absence of 10 mM ATP. The different eluted fractions were analysed by negatively stain electron microscopy (as described in 3.2.4).

For molecular weight estimations, a calibration curve was performed using the Gel Filtration High Molecular Weight Calibration Kit (GE Healthcare), following the GE Healthcare instructions.

### **2.2.7 EcFtsHX6 purification using LMNG as solubilisation agent**

Overexpression of EcFtsHX6 was assessed using ArticExpress competent cells (Agilent) as host strain. Cells were incubated for 18 hours after induction with 0.9 mM IPTG at 20°C. Cells were collected by centrifugation and dissolved in 25mM Tris-

HCl (pH 7.5), 20% sucrose, 1mM EDTA and protease inhibitor, and broken as described above. After membrane isolation, EcFtsHX6 was solubilized using Lauryl Maltoside Neopentyl Glycol (LMNG). Membranes were solubilized in 50mM Tris-HCl (pH 8); 1mM DTT; 10% glycerol; 20mM MgCl<sub>2</sub>; protease inhibitor and 2% LMNG, at 4°C for 2 hours stirring. After protein isolation, the supernatant was loaded into a HisTrap 5 mL prepacked column (GE Healthcare) previously equilibrated with 50mM Tris-HCl (pH8), 1mM DTT, 5mM MgCl<sub>2</sub>, 5% glycerol, 500mM NaCl, 0.02% LMNG, 10mM imidazole, protein was eluted in an isocratic gradient up to 500mM imidazole. The eluted fractions containing EcFtsHX6 were directly loaded into a Superose 6 Superose 6 10/300 GL column (GE Healthcare) pre-equilibrated with 50mM Tris-HCl; 1mM DTT; 5mM MgCl<sub>2</sub>; 0,005% LMNG; 5% glycerol. Alternatively, after eluting from the HisTrap column the protein samples were desalted and loaded into an anion exchange chromatography using the same buffer as for the Superose 6 10/300 GL column equilibration and eluting the sample in a isocratic gradient as described before. Thereafter, the sample was loaded into a SEC.

Protease activity was tested on the fractions containing EcFtsHX6 at 42°C for 1 hour in presence of 10 mM ATP or in absence of ATP, as described in 3.2.3. The different eluted fractions were analysed by SDS-Page gel and negative stain electron microscopy (as described in 3.2.4). For molecular weight estimations a calibration curve was run in both SEC, as described in the previous section.

## 2.3 Results

### 2.3.1 Expression and purification of FtsHHis6Myc

FtsHHis6Myc expression was tested using BL21 (DE3) pLysS as host cells. Different induction periods were tested (Figure 2.1 – A). The SDS-Page shows that longer induction periods result in a higher concentration of FtsHHis6-Myc protein (monomer = 74 kDa and hexamer = 444 kDa). To test the IPTG effect in the induction process, a sample was left to grow for four hours with and without IPTG addition (Figure 2.1 – B). IPTG increases FtsHHis6Myc concentration in the sample but also the concentration of other bands around 25 and 35 kDa (Figure 2.1 – B).

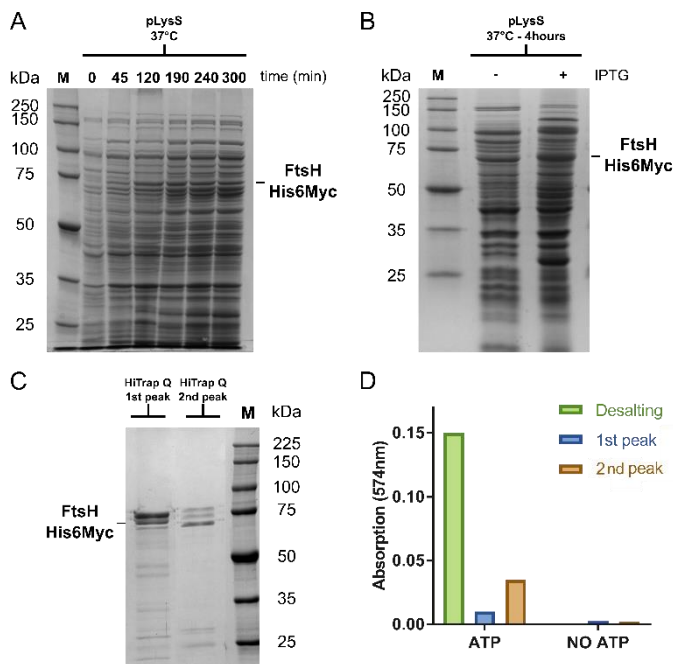


**Figure 2.1 – Expression and purification of FtsHHis6Myc.** Expression tests performed using different inductions periods. The lanes of the SDS-Page gel (A) are labelled with periods of expressions (in min). This gel can be compared with the sample not induced (-) and induced (+) with IPTG for a period of 4 hours (B). EcFtsHHis6Myc concentration increases with longer induction time, but also its expression was observed in the non-induced sample. Anion-exchange purification of the same sample as in the SDS-Page gel in (B) (with IPTG) shows the two first peaks eluted from the HitrapQ (1st and 2nd) (C). Protease activity was tested for both peaks (blue and orange) and for the sample eluted from the desalting column (green) in presence and absence of ATP (D). Protein marker (M).

The purification protocol for FtsHHis6Myc overexpression at 37°C for four hours with IPTG (Figure 2.1 - B) was scaled-up. After membrane solubilization, the solubilized fraction was purified in two chromatography steps: first an ion immobilized affinity chromatography (IMAC), which was followed by an Anion exchange chromatography.

For the first purification step (IMAC), NiNTA beads containing nickel, which is known to bind histidine with high affinity, was used. To separate the EcFtsHHis6Myc from other proteins, a step gradient of imidazole was used. Before loading the protein on the second step of purification, the buffer of the protein was exchanged to exclude salt, using a desalting column. The second step of purification was assessed using an HiTrapQ column and molecules were separated by their charge using an isocratic salt gradient. From the HiTrapQ chromatography profile, two distinct peaks were identified (Figure 2.1 – C). Both samples were analysed by SDS-Page gel, two or three bands with very close molecular size around 75 kDa are identified, demonstrating that EcFtsHHis6Myc indeed enters in a process of self-degradation as described in literature before [14,23–29]. The final purified samples were incubated with resorufin labelled casein, a universal protease substrate, its protease activity was measured at 42°C in presence and absence of ATP. Although the sample that elutes from the desalting column shows high activity, this activity decreases three times after the second purification step. Nevertheless, no activity was detected in absence of ATP.

Despite these positive results, we observe that FtsHHis6Myc protein is not stable and enters in a self-cleaving process which will interfere with further structural characterization studies. For that reason, a synthetic gene coding for *Escherichia coli* FtsH and cloned into expression vectors using different cloning strategies.

### **2.3.2 EcFtsHX6 and EcFtsHX10 cloning**

The synthetic gene coding for the full-length *E. coli* FtsH (EcFtsH) (Uniprot P0AAI3) was purchased from Life technologies with the codon optimized for *E. coli* in the standard vector pMK-RQ (kanR). The gene fragments for EcFtsH were amplified by

PCR including the restriction sites *Nco*I and *Hind*III forming Insert 1, and *Nco*I and *Sal*I forming Insert 2, for the 5' and 3' end respectively. The analysis of the agarose gel (Figure 2.2), shows the amplifications and digestions of gene fragments for Insert 1, Insert 2 and the expression vector pET28a.

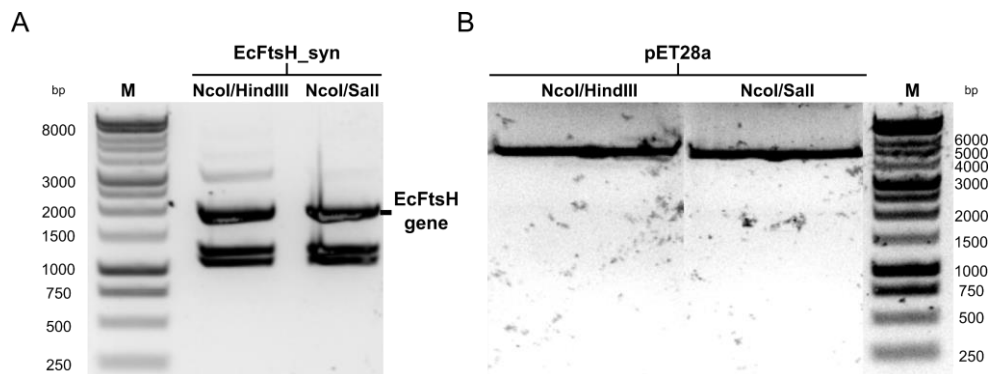


**Figure 2.2 – Agarose gels of the cloning strategy adopted.** Agarose gel of the amplified synthetic gene digestion with the restriction enzymes *Nco*I/*Hind*III and *Nco*I/*Sal*I (A). The insert was purified and then ligated to the pET28a expression vector, previously digested with the corresponding restriction enzymes (B). The molecular sizes of the marker (M) are indicated next to the markers and in base pairs (bp).

The purified PCR products were double digested, within two reactions, with *Nco*I/*Hind*III and *Nco*I/*Sal*I restriction enzymes respectively (Figure 2.2 - A). Thereafter, the expression vector pET28a was prepared for ligation by two double digestion with *Nco*I/*Hind*III and *Nco*I/*Sal*I (Figure 2.2 - B). The double digested expression vectors were isolated and purified from agarose gel. The purified linearized vector was used to ligate Insert 1 and Insert 2. After ligation, the constructs were transformed and the positive transformants were selected by plating onto LB-agar plates supplemented with 50  $\mu$ g/ $\mu$ L Kan and grown overnight at 37°C. The positive transformants, were tested for the insert by performing a colony PCR.

Finally, the tested DNA plasmid samples were sent to Eurofins MWG Operon (Germany) for sequencing. The results were analysed by performing alignments using ClustalW tool (<http://www.ebi.ac.uk/Tools/msa/clustalo/>) [30]. These clones allow the overexpression of EcFtsH with a C-terminal His6-tag. The tag is more

accessible depending on which cloning strategy was used. The linker between the end of the EcFtsH gene sequence and the His6-tag has 10 aa in length (EcFtsHX10), when using Insert 1, and 6 aa in length (EcFtsHX6) when using Insert 2. This cloning strategy was used to allow the overexpression of FtsH with different accessible His6-tag at the C-terminal end.

### 2.3.3 Expression and purification of EcFtsHX10

Transformed NiCo (DE3) competent cells with EcFtsHX10 are induced at different expression temperatures (37, 25 and 20°C) revealing different expression levels. The isolation of the insoluble and soluble fractions of the cell extract, expressed at 20°C, shows that EcFtsHX10 is present at the same concentration on both fractions independently of the induction time (Figure 2.3 - A).

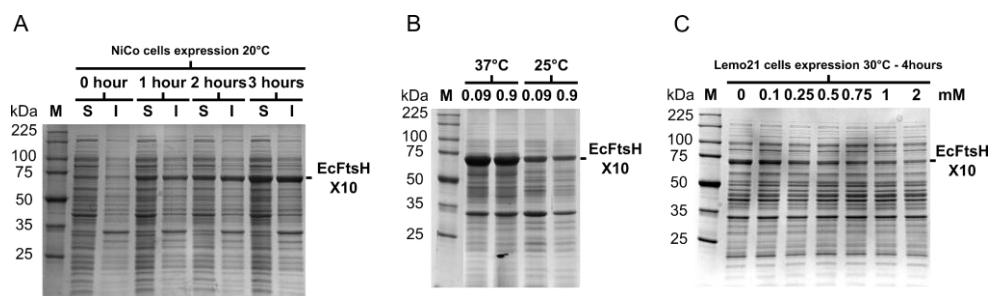


**Figure 2.3 – Expression conditions of EcFtsHX10 protein.** A - The result after membrane solubilisation and isolation of the soluble (S) and insoluble (I) fractions for different induction times (indicated in hours). B – EcFtsHX10 expression on NiCo (DE3) competent cells induced with 0.09 or 0.9 mM IPTG, for 3 hours at 37°C or 25°C. C – EcFtsHX10 expression on Lemo21 (DE3) competent cells induced with 0.9 mM IPTG at 30°C for 4 hours, varying the L-Rhamnose concentration (in mM). Protein marker (M).

On Figure 2.3 B, NiCo (DE3) cells transformed with EcFtsHX10 were induced at 37°C or 25°C for 3 hours and induced with 0.9 or 0.09 mM IPTG. There is no difference in the amount of EcFtsHX10 expressed when induced with these different amounts of IPTG, although there is a higher expression of EcFtsHX10 at 37°C. A lower band around 35 kDa is also overexpressed at both temperatures since when compared with Figure 2.3 A (expression at 20°C) this band does not have the same intensity as in Figure 2.3 B.

Expression tests for EcFtsHX10 were also performed using the expression strain Lemo21 (DE3) competent cells as host. In Lemo21 (DE3) competent cells, concentration of the natural inhibitor of T7-RNA polymerase, lysozyme (*lysY*), is regulated by the addition of different amounts of L-Rhamnose. In absence of L-Rhamnose, the Lemo21 strain works as the BL21 (DE3) pLysS strain. This strain is also described for its capacity of expressing difficult constructs and recognized for achieving more stable and folded proteins [31]. For these reasons, this cell strain was used to express EcFtsHX10. After induction with 0.9 mM IPTG, different L-Rhamnose concentrations were used to tune protein overexpression as suggested by the manufacturer. Figure 2.3 C, shows that smaller amounts of L-Rhamnose (0 and 0.1 mM) lead to a higher yield of EcFtsHX10. Higher concentrations of L-Rhamnose seem to increase the concentration of other proteins and do not improve EcFtsHX10 expression, consequently 0.1mM of L-Rhamnose were used during the following experiments using Lemo21 competent cells.

After performing a global analysis of the expression tests, we further purified the cell extracts that resulted from the overexpression of two different bacterial strains and four different expression conditions: NiCo competent cells induced for 3 hours at 37°C, NiCo competent cells induced for 3 hours at 25°C, NiCo competent cells induced for 18 hours at 20°C and Lemo21 competent cells induced for 4 hours at 30°C.

EcFtsHX10 cell extracts resulting from the expression of NiCo and Lemo21 strains at 25 and 30°C, were also further purified since there is a high yield of expression. IGEPAL CA-630 was used as solubilization surfactant to extract EcFtsHX10 from the membrane. SDS-Page results (Figure 2.4) show that there is a considerable amount of FtsH purified from the first step of affinity chromatography (Figure 2.4 A, B).

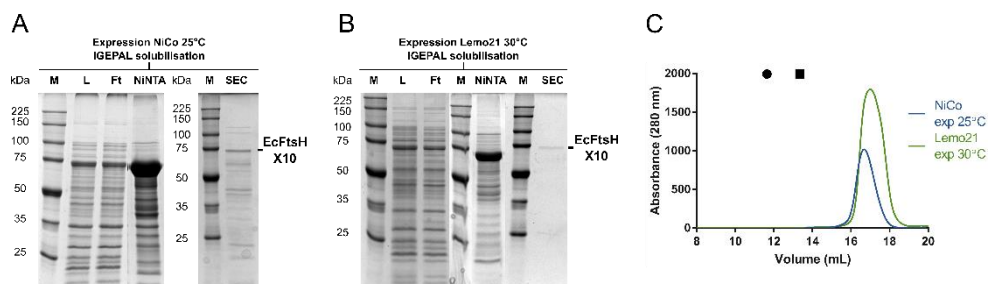


**Figure 2.4 – EcFtsHX10 expression and purification.** SDS-Page gels of EcFtsHX10His purification fractions (A, B), using two cell strains to overexpress EcFtsHX10. NiCo cells were induced at 25°C (A) and Lemo21 cells were induced at 30°C (B) for 3 hours, IGEPAL detergent was used as surfactant in the solubilisation/purification protocol. The SEC profile (C) of both fractions from NiNTA beads (in green, fraction from overexpression of EcFtsHX10 using Lemo21 cells and in blue the fraction of EcFtsHX10 overexpressed by NiCo cells). M – Molecular marker; L – Load fraction into the NiNTA beads; Ft – Flow-through of the NiNTA; SEC – fraction that represents the peak of the SEC profile in C. The elution volumes of some of the standard proteins used to estimate the molecular weight of the eluted fractions are shown on the top of the graph: (●) Tyroglobulin (MW: 669 kDa; Ve: 11.64 ml) and (■) Ferritin (MW: 440 kDa; Ve: 13.35 ml).

The second step of the purification protocol using a SEC, separating molecules by size, show that EcFtsHX10 is lost in this purification step. The molecular weight of both peaks, varies in between 57 kDa (elution volume 16.7 mL) and 49 kDa (elution volume 17 mL), is smaller than the molecular weight expected for the EcFtsHX10 hexamer or monomer (441 kDa or 73.5 kDa).

Since the expression of different strains does not affect the purification of EcFtsHX10, cell extracts resulting from the EcFtsHX10 expression of only NiCo competent cells, at different temperatures (37 and 20°C) were further purified. The membranes were solubilized with Triton X-100, DDM and IGEPAL CA-630. The analysis of the SDS-Page gels (Figure 2.5), shows that Triton X-100 can extract EcFtsHX10 and there is a final band corresponding to EcFtsHX10, although the protein co-elutes with another protein with a very similar molecular weight (Figure 2.5 A), which suggests that the protein may engage in a process of self-cleaving as in 2.3.1. The amount of FtsH purified from Nico cells at 37 and 20°C is very low when using DDM or IGEPAL CA-630 as solubilizing agent, and not pure when using IGEPAL CA-630.

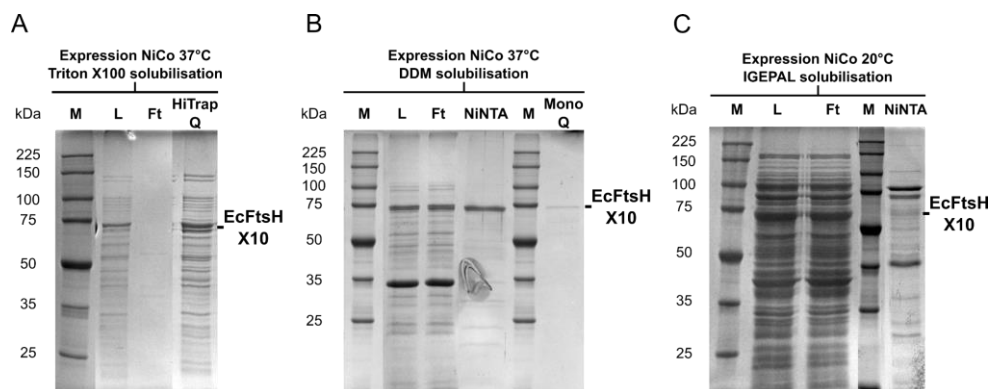


**Figure 2.5 – SDS-Page gels of EcFtsHX10 solubilization using as expression host NiCo competent cells.** A - The final sample coming from the solubilization of the cell extract, expressed at 37°C, using Triton X-100 contains a EcFtsHX10 but also another protein band with a similar molecular weight. B - The same cell extract solubilized with DDM gives a small final amount of EcFtsHX10. The same result is observed when the cell extract originated from the expression using the same cells but changing the expression conditions to 20°C. C. When using IGEPAL CA-630 for solubilisation, small amounts of protein results from the purification steps. L – Sample loaded into the column; Ft – Flow-through of the column loading; M – Molecular marker.

EcFtsHX10 appeared to be difficult upon extraction from the membrane. We hypothesized that the presence of a longer linker between the protein and the exposed HisTag might interfere with EcFtsH assembly into a hexamer (details of this hypothesis will be discussed in 2.4). Therefore, the expression and purification of this construct was not further explored. The expression and purification of EcFtsHX6 is described below.

### 2.3.4 EcFtsHX6 solubilization, the proof that the detergent's choice matters

Expression of EcFtsHX6 was performed using the same conditions as in 2.3.3 using the same expressions conditions and strains (data not shown). The best conditions to express EcFtsHX6 were established to be using NiCo cells at 25°C for 3 hours induced with 0.09 mM IPTG. Membranes were purified using a series of centrifugation steps as described in 2.2.4. EcFtsHX6 solubilization was assessed at analytical scale (0.8 g of membranes were used for the total experiment) using an incomplete factorial (IF) approach combining four detergents (IGEPAL CA-630, DM,

DDM and OG), three NaCl concentrations (10, 100 and 300 mM), three incubation periods (2 hours at 4°C; 4 hours at 4°C; or 2 hours at 4°C followed by 1 hour at RT) and two buffers bases (50 mM Tris-HCl and 20 mM MEA). The solubilization patterns of 16 experiments (72 IF combinations, see section 2.2.5) were analysed by SDS-Page gels (Figure 2.6 A-D).

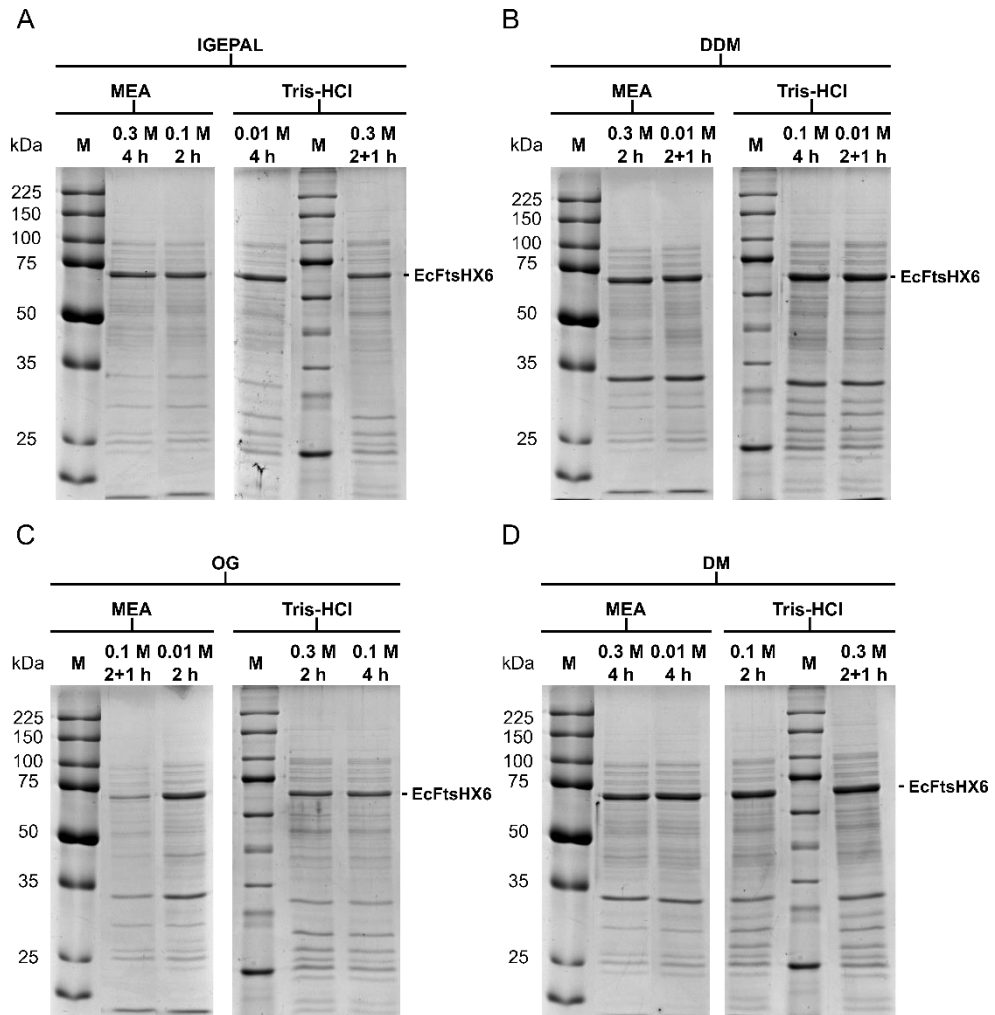


**Figure 2.6 – SDS Page gels resulting from the incomplete factorial approach.** They show the influence of different detergents (A – IGEPAL; B – DDM; C – OG and D – DM), buffers (MEA and Tris-HCl), salt concentrations (0.01, 0.1 and 0.3 M) and time incubation (2, 4 and 2+1 hours), during membrane solubilisation of EcFtsHX6. All the conditions are indicated on top of the gels.

The results show that EcFtsHX6 final concentration in the supernatant of different conditions is almost the same in all conditions. The only exception are the membranes that were solubilized with OG in presence of 100 mM NaCl and 20 mM MEA, where the yield of EcFtsHX6 is slightly lower than in the rest of the conditions tested (Figure 2.6 C). Even though there is no difference in terms of EcFtsHX6 amounts using the different detergents, there is a difference in the other bands that are co-solubilized with it. IGEPAL CA-630 is the detergent that provides a higher EcFtsHX6 purity after solubilization (Figure 2.6 A). The presence of different bands is mainly observed in Figure 2.6 B and D, in which DDM and DM are used as solubilization agents. Furthermore, the results show no difference in concentration of FtsHX6 extracted using different buffer, salt concentrations and incubation periods used (excluding the case of OG already mentioned before).

### **2.3.5 Solubilization and purification of EcFtsHX6**

After the results shown in section 2.3.4, solubilization of EcFtsHX6 was performed in presence of 2% DDM, 2.5% DM or 2.5% IGEPAL CA-630. Further purification steps were performed to reach a pure and active EcFtsHX6 protein. The first solubilization and purification step was performed using 2% DDM as solubilization buffer and a two-step purification protocol (Figure 2.7). The first purification step was an affinity chromatography resulting in a high concentration of EcFtsHX6 (as shown on the SDS-Page gel, Figure 2.7 A), which is further purified by the second purification step using a SEC (Figure 2.7 B).

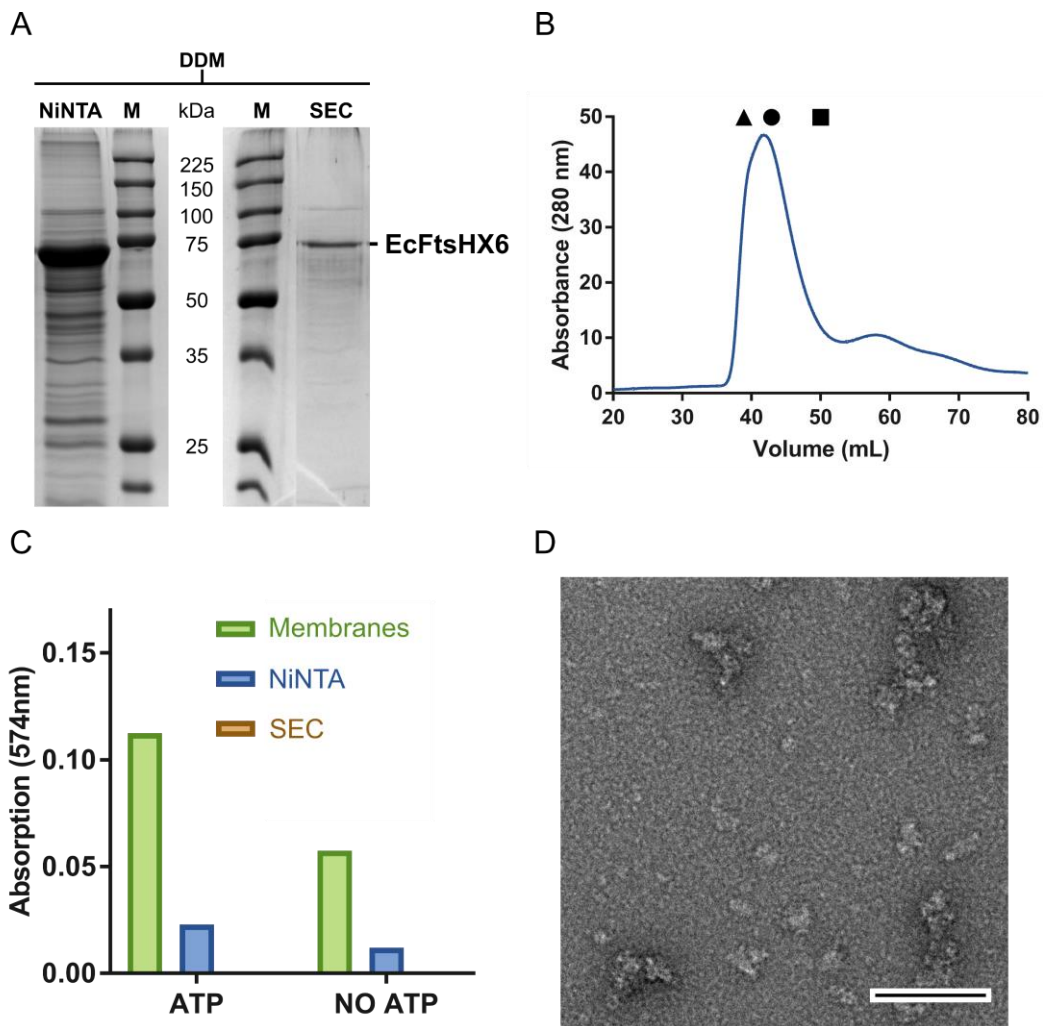


**Figure 2.7 – EcFtsHX6His purification using DDM as surfactant.** The purification was performed using a two-step protocol, with a first step using NiNTA beads followed by a second step of SEC (A). The SEC profile (B) shows the elution of one peak and the protease activity assay was performed in all the purification steps (C), testing the membranes, NiNTA and SEC fractions. The resulting peak of B was further analysed by negative stain TEM (D).

The Sephacryl S-300 elution profile, shows that EcFtsHX6 elutes mainly in one broad peak around 41.9 mL which corresponds to a molecular weight of 747 kDa. The second peak elutes at a volume of 58.5 mL, which corresponds to a molecular weight of 154 kDa. Membrane, NiNTA and SEC fractions were tested for proteolytical activity in presence and absence of ATP (Figure 2.7 C). The results show that the further

the purification protocol progresses, the lower is the activity detected in presence of ATP. SEC fractions do not show any activity in both conditions tested. This is also corroborated by the negatively stained EM analysis in which big aggregates are observed. No particle with dimensions expected for EcFtsHX6 are observed.

EcFtsHX6 was also purified with either IGEPAL CA-630 or DM. The resulting SDS-Page gels show that EcFtsHX6 is extracted and purified after the SEC profile (Figure 2.8 A). The sample eluted from the NiNTA beads using IGEPAL CA-630 is less pure than the one coming from the same elution step using DM. However, when comparing the SDS-Page gel bands resulting from the SEC elution, only a minor difference is observed. When comparing the chromatography profile between samples (Figure 2.8 B), there is a broad peak around 11.9 mL, which corresponds to a molecular weight of 968 kDa, in the sample solubilized with DM. Not only is the peak broad, but that peak also contains a shoulder around 12.9 mL (MW: 364 kDa) which means that complexes of close sizes eluted together and were not separated in the elution. The differences between the sample solubilized with DM to the one solubilized with IGEPAL CA-630 are evident in the SEC profile. The latter elutes in two distinct peaks: a first peak around 11.1 mL which corresponds to a molecular weight of 878 kDa, and a second peak around 17.6 mL, which corresponds to a molecular weight of 36 kDa. The eluted fractions from the SEC, were tested for proteolytical activity (Figure 2.8 C), showing that only the fraction solubilized with IGEPAL CA-630 is active after the SEC elution. This fraction was also analysed by negative stain, some characteristic particles features are observed, although aggregation is evident all around the grid and a contamination with the GroEL protein is seen.

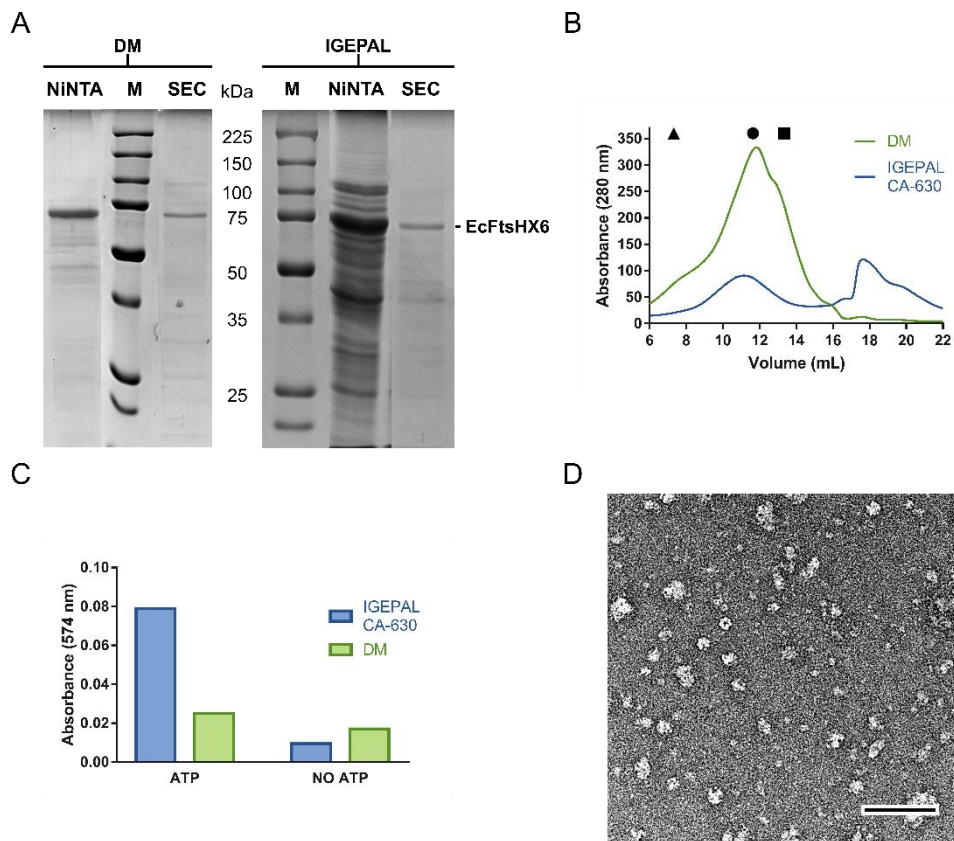


**Figure 2.8 – EcFtsHX6His was purified in a two-step purification protocol.** Affinity chromatography was followed by size exclusion chromatography, using DM or IGEPAL as surfactants in the buffers, samples resulting from both steps were analysed by SDS-Page gel (A). Blue Dextran (▲) used to calculate the void volume of the column (7.32 mL). The elution volumes of some of the standard proteins used to estimate the molecular weight of the eluted fractions are shown on the top of the graph: (●) Tyroglobulin (MW: 669 kDa;  $V_e$ : 11.54ml) and (■) Ferritin (MW: 440 kDa;  $V_e$ : 13.35 ml). The SEC profiles of both DM (green) and IGEPAL (blue) purifications show a different distribution. SEC eluted fraction were assessed for proteolytical activity in presence/absence of ATP (C). The SEC fraction resulting from the IGEPAL purification was analysed by negative stain (D). Scalebar = 100 Å.

### 2.3.6 EcFtsHX6 purification using LMNG as solubilisation agent

EcFtsHX6 expression was assessed using Artic competent cells (Agilent) has host organism. Cells were expressed at 20°C for 18 hours after induction with 0.9 mM IPTG, and after membrane isolation, EcFtsHX6 was solubilized with LMNG. The

protein was purified in a two-step purification protocol as explained before. The results show that there is no difference between directly loading the eluted fraction from the NiNTA column into a SEC column compared to performing an extra anion exchange chromatography purification step (Supplementary Figure 2.4). The Superose 6 10/30 GL profile shows that the protein elutes in two distinct peaks, the first peak elutes around 11.2 mL which corresponds to 837 kDa, and the second peak elutes approximately at 15.1 mL which corresponds to 124 kDa (Figure 2.9 A).

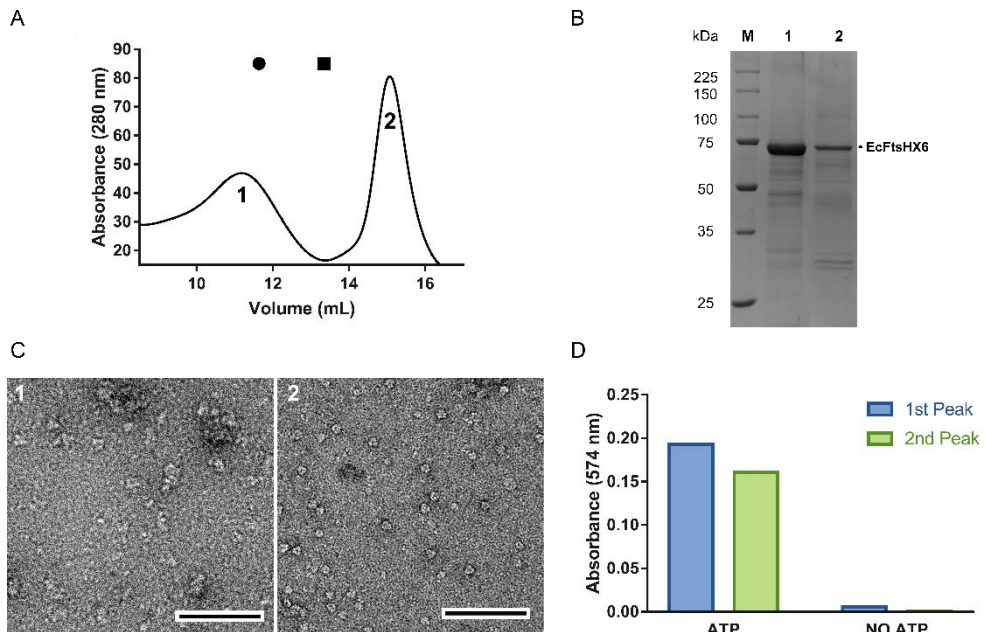


**Figure 2.9 – EcFtsHX6His purification solubilised with LMNG.** SEC profile (A) shows the elution of two different peaks a first peak corresponding to a molecular size of 837 kDa (1) and a second of 124 kDa (2). The elution volumes of some of the standard proteins used to estimate the molecular weight of the eluted fractions are shown on the top of the graph: (●) Tyroglobulin (MW: 669 kDa;  $V_e$ : 11.54ml) and (■) Ferritin (MW: 440 kDa;  $V_e$ : 13.35ml). The resulting fractions were analysed by SDS-Page gel (B) and by negative stain (C), particles differ in size and shape in both fractions. Both SEC peaks were tested for proteolytical activity (D) demonstrating that both samples are active in ATP presence. Scalebar = 100 Å.

Both peaks were analysed by SDS-Page gel (Figure 2.9 B), showing that both lanes have the same protein composition. Negatively stained microscopy analysis (Figure 2.9 C) illustrates that the particles size is different from the first to the second peak

sample. In the first peak diverse aggregates and bigger particles are present, while the second peak sample exhibits a homogeneous distribution of particles over the grid with a size of 10.7 nm (N=12, SD=0.9), compatible to what is expected for the EcFtsHX6 complex. Moreover, the protease activity was assessed, and both fractions from the two eluted peaks from the SEC were active in presence of ATP and did not show any activity in absence of ATP.

## **2.4 Discussion and conclusions**

EcFtsH expression and purification was first assessed using the construct kindly provided by the Akiyama group. The induction of PlysS competent cells for different periods of time and in presence or absence of IPTG at 37°C (Figure 2.1), revealed that EcFtsHHis6Myc is co-expressed together with other proteins. After a two-step purification protocol, we show that it is possible to isolate EcFtsHHis6Myc and to observe degradation activity from EcFtsHHis6Myc. As previously reported in literature [14,17,29,32], we suspected that EcFtsH can recognize the His6Myc tag and cleave it from the construct. Moreover, the first peak of the HiTrapQ elution, which has a more preeminent band for EcFtsHHis6Myc, shows almost no proteolytic activity, while the second step shows higher activity and smaller amounts of EcFtsHHis6Myc. The activity of the Desalting column fraction was assessed when compared with other studies, which used resorufin labelled casein as substrate to test the proteolytic activity, the absolute numbers of absorption at 574 nm are the same around 0.18 [14]. Nevertheless, the fact that the activity values decrease in between purification steps is a clear sign of protein degradation, possibly due to FtsH self-degradation, which introduces complications towards achieving a stable and pure sample for structural and biochemical studies. Even though this process could be decreased if the His6Myc tag was cleaved, we opted not to continue with the purification of EcFtsH using this construct.

Instead, two different constructs were used. A first construct with EcFtsH with a 10 aa linker plus a 6 x Histidines tag at its C-terminus, and a second construct with EcFtsH with a 6 aa linker plus a 6 x Histidines tag. This strategy was adopted with the intent of expressing a more stable protein. The longer linker could help the

affinity chromatography purification protocol due to a better exposure of the his-tag to the chromatography medium, while the smaller linker could stop or decrease the process of self-cleaving due to its reduced availability for EcFtsH degradation. We first assessed the expression and purification of EcFtsHX10 using two different competent cell strains (Lemo21 and NiCo), different inducer concentrations and temperatures. The first assessment of the EcFtsHX10 purification was performed using the cell extracts resulting from the expression of NiCo cells (induced at 25°C) and Lemo21 (induced at 30°C). A small amount of EcFtsHX10 is isolated, with a molecular weight around 50-60 kDa, which is lower than the one expected for EcFtsHX10 molecular weight of 73.5 kDa. This experiment also showed that there is no difference between the cell strain (Lemo21 or NiCo cells) used to express EcFtsHX10 and the resulting amount of protein purified (Figure 2.4). For this reason, we chose to use NiCo competent cell strain as host organism for further expression of EcFtsHX10 in the following experiments. As the results confirm that EcFtsHX10 is a difficult protein to purify in its hexameric state as demonstrated in literature before [13], we decided to test a range of detergents to solubilize EcFtsHX10 from the membrane. Membrane protein solubilization is one of the most sensible steps in the purification protocol. If the protein is not well extracted, this will lead to aggregation. Moreover, it has been reported in literature that different detergents have different effects when solubilizing the same membrane protein [33]. A good range of detergents should be tested adapting the purification protocol to the different ionic forces present in solution. We began by testing two different detergents Triton X-100 and DDM. These detergents have different critical micelle concentration (CMC): Triton X-100 has a CMC of 0.3 mM, while the CMC of DDM is half of this. The CMC of a detergent is the detergent concentration at which detergent micelles start to form. This parameter and others (ionic strength and pH of the used buffers (salt concentration), the detergent cloud point and aggregation number) all have an influence in the detergent solubility and in the correct formation of the micelles. Micelles disrupt the membrane, surround the protein to extract it from the membrane and keep it soluble in the aqueous medium. Since this solubilization step is critical for membrane protein isolation, many detergents are tested for the solubilization of

EcFtsH, to increase the chances to find the optimum conditions to produce pure and stable protein. DDM turned out to be unsuitable for EcFtsHX10 extraction since the protein is not stable during the purification process (Figure 2.5 B). The concentration of EcFtsHX10 after the final purification step was very low, which is a sign of degradation (or aggregation) of the protein. Triton X-100 seems to work better since it is possible to observe a band corresponding to EcFtsHX10 in the final purified sample (Figure 2.5 A), together with another band of very similar size. Although it is not impossible that FtsH elutes together with a protein of very similar molecular weight, it is likely to be the same self-processing mechanism observed for the EcFtsHHis6Myc purification. Although the use of more harsh detergents such as Triton X-100 helped in the extraction of EcFtsHX10, it seems that the protein is not stable either. With the intention of increasing the proper folding of EcFtsHX10 the expression temperature was decreased to 20°C. Lower expression temperatures result in slower protein production inside the cell, which might increase the proper folding of the protein expressed. Also a lower protein concentration inside the cell reduces the chance for aggregation [31]. The expression of EcFtsHX10 using NiCo competent cells as host showed that the lower temperature and higher period of expression leads to a higher expression of other proteins (Figure 2.5 C). Not only the expression temperature was changed at this step, but also the surfactant was changed to IGEPAL CA-630, which has a CMC of 0.08 mM. This detergent is the replacement of Nonidet P-40, reported as one of the most used detergents to extract EcFtsH [14,17,21,29,32,34–36]. The purification was performed using only an affinity purification (Figure 2.5 B and C lane Ft). There is a significant difference in between the results depending on the type of detergent used. The use of mild detergents (Triton X-100 and DDM) seems to lead to the extraction of EcFtsHX10, but the size of the linker seems to induce the process of self-cleaving observed before. Since our goal is to characterize EcFtsH biochemically and structurally, it is necessary to have a stable and pure protein. We believe that it is hard to isolate EcFtsH even if a larger scan of detergents and purification protocols were executed. Some other results were obtained during the development of this expression and purification approach, but only the preeminent results are discussed here. Since the

experiments with this construct did not show any advantage for the work planned for this thesis, we decided to abandon EcFtsHX10 and optimize the purification of the other construct left, EcFtsHX6. This construct has a less accessible tag and we assumed that the smaller linker would abolish or decrease the process of self-cleaving.

Different expression conditions and cell lines were explored for optimizing EcFtsHX6 expression, although they are not shown in this thesis since the results are very similar to ones obtained for the expression conditions of EcFtsHX10. As the results with EcFtsHX10 revealed that the choice of detergent is crucial for the correct extraction of EcFtsH from the membrane, a first analytical test of different conditions to use in the extraction of EcFtsHX6 was accomplished. To scan different conditions and factors at the same time, an incomplete factorial (IF) approach was used. This reduced the time of the experiments and enhanced the number of variables that influence the extraction of EcFtsHX6 from the membrane. This experiment was divided into the analysis of two SDS-Page gels: the first loaded with the fractions resulting from the membrane solubilization (Supplementary Figure 2.3) and the second loaded with the supernatant of the same fractions after a centrifugation step (Figure 2.6). Analysis of these two gels allows to decide whether the detergent used to solubilize the membranes was efficient. If the detergent used was not able to solubilize EcFtsHX6, all the protein sample will be in the pellet after the centrifugation step. The comparison of both gel results (Figure 2.6 and Supplementary Figure 2.3), shows that EcFtsHX6 was entirely solubilized in almost all cases except the one mentioned below. Although four different detergents were used: IGEPAL CA-630, DDM, OG and DM; there is only one condition in which it was possible to observe a difference. Extraction of EcFtsH in presence of 20mM MEA pH9, 100mM NaCl and 2%OG for 2 hours at 4°C plus 1 hour at RT, results in a low amount of EcFtsHX6. This phenomenon might be related to the fact that the protein was exposed to RT for 1 hour. In this condition, the protein might have aggregated during the solubilization process, being lost in the centrifugation process. This step was eliminated for further scanning since it appeared not to be a good condition to extract EcFtsHX6 from the membrane. The use of IGEPAL CA-630 showed to extract

slightly purer amounts of EcFtsHX6, in agreement with the literature [10,14,17,21,29,32,34–37]. The use of detergents as DDM and DM results in the co-purification of other proteins, showing that the isolation of pure EcFtsHX6 is indeed detergent dependent. No difference in the extracted amount of EcFtsHX6 is observed when changing the other parameters tested, showing that those are not influencing the extraction of the protein from the membrane as much as the type of detergent used, at least not in the combinations explored. The IF approach was used before to test crystallization conditions, but here it proved to be also a valuable tool to test other experiments not having to scale-up all of experiments [22,38]. This approach allows several numbers of conditions to be tested in fewer experiments and helping in decision making concerning which route to take when scaling-up an experiment.

The purification of EcFtsHX6 was scaled-up using a two-step protocols and the three different detergents that gave better results in the IF approach. The composition of the buffers was influenced by the literature available for EcFtsH [7,8,29,32,36,39–45,10,13,15,17,20,21,24,28] and it was adapted as the experiments were being performed and better results achieved.

The first purification scaled-up was performed using 2% DDM as surfactant. Despite the pure fraction obtained from the SEC (Figure 2.7 A), almost no protease activity was measured for this sample. Moreover, there is a decrease of the activity measured when advancing in the purification protocol, which is an indicator that the protein is degrading in between these steps. Additionally, a close analysis of the negatively stained sample shows that the sample aggregates and no single particle can be observed on the grid. We conclude that the sample extracted with DDM did not provide stable EcFtsHX6, which is in accordance with the results observed previously for EcFtsHX10. DDM was found to be incapable of extracting and stabilizing EcFtsH in either forms. For this reason, the purification of EcFtsHX6 was further assessed using DM and IGEPAL CA-630 and a comparison of both was made (Figure 2.8). In this comparison both elution profiles show the elution of molecules with around 900 kDa, the profile with DM shows a broader peak which suggests that the elution fraction is a mix of particles with different molecular weights. The

shoulder of the DM elution profile may belong to EcFtsHX6 although the separation of this shoulder was not possible by further purification steps. Although the size of the particles is in a different range than what would be expected for EcFtsHX6 (900 kDa compared with 441 kDa plus detergent), the peak of the IGEPAL elution profile is sharper which means that the particles eluted in this peak have a close molecular weight. There is also the elution of a later peak in the IGEPAL CA-630 purification step close to 40 kDa, which is not comparable to the monomer of EcFtsHX6. This protein may be one of the contaminants that are seen in the fraction that eluted from the NiNTA column (Figure 2.8). Although the amount of this contaminants was much higher in this fraction it is important to mention that a 100 kDa AMICON Filter was used to concentrate the protein after the NiNTA and before the SEC. This step eliminated all the smaller proteins that did not stick to bigger particles and for this reason they are not seen in the SDS-Page gel or SEC profile (Figure 2.8 A and B). The activity tests made with the IGEPAL CA-630 and DM purifications show that there is a difference in activity when ATP is present, although the absolute numbers provided are low compared to the ones previously reported. Moreover, some activity is also observed in absence of ATP, which may be an indicator of other non-ATP-dependent proteases present in the solution. FtsH was reported to degrade the substrates only in presence of ATP. The electron microscopy analysis of negatively stained samples eluted from the IGEPAL CA-630 purification shows the presence of only few particles with the expected size of EcFtsHX6. Aggregation is also observed. Moreover, the contamination of the sample with GroEL, which is a chaperone responsible for the correct folding of proteins inside the cell, suggests that the expression conditions used to express EcFtsHX6 might be stressing the cells. The stress could originate from the overexpression of EcFtsH, the temperature change or the chemicals used, which might also cause a non-correct folding of EcFtsHX6.

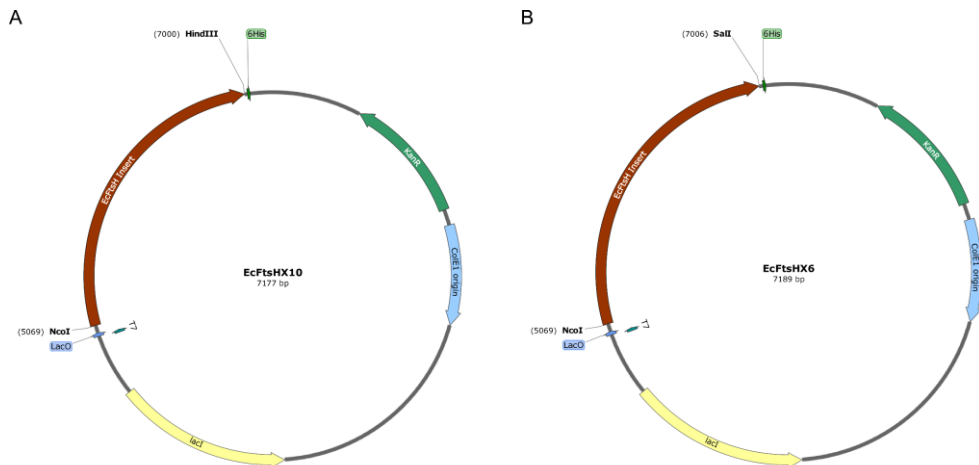
All these experiments show that the detergent seems to influence EcFtsHX6 extraction, but none of the detergents tested yielded satisfactory results in the stabilization of the protein in its solubilized state. As, the extraction of EcFtsH has proven to be difficult independently of the tag used in the protein purification, we conclude that the most important parameter is the detergent used.

A final test was performed to extract EcFtsHX6 with LMNG (CMC = 0.01mM) a detergent with a lower CMC than IGEPAL CA-630 (CMC = 0.08mM). LMNG allowed the high resolution structural characterization of several membrane proteins [4] proving efficient in the extraction of several types of membrane proteins. The very low CMC allows this detergent to tightly bind to the membrane protein and stabilize it in solution [46]. Not only the detergent, but also the cell strain used for expressing the protein might be influencing the oligomerization state of EcFtsHX6. Therefore, we tested another type of cells described in literature, the Arctic competent cells. These cells are described by the manufacturer as engineered to produce improved amounts of correctly folded protein at lower expression temperatures. Instead of using the common chaperonins, as GroEL, they co-express the cold-adapted chaperonins Cpn10 and Cpn60 from *Oleispira antarctica*, an extremophilic organism that grows and reproduces at -20 to 10°C. This mechanism is used since at low temperatures GroEL and GroES do not have full activity. For this reason, Arctic competent cells seemed a valid solution to decrease the amount of GroEL co-expressed with EcFtsHX6 and improve the correct folding of EcFtsH. When EcFtsHX6 was extracted from Arctic cells using LMNG, the resulting purification using SEC shows the elution of two peaks (Figure 2.9 A). The first peak has a molecular weight of 837 kDa and the second peak one of 124 kDa. The analysis of the SDS-Page gels does not show a significant difference in composition between these two fractions, but the analysis of the negatively stain sample shows a distinct presence of particles on the grid (Figure 2.9 B and C). The first eluted peak shows the presence of big agglomerates corresponding to aggregates and smaller particles, while the second peak fraction shows a homogeneous particle distribution on the grid. The particles have a diameter of 107 Å, which is close to the size expected for the top views of EcFtsH. However, the height of EcFtsH is expected to be 5-6 Å larger. This difference led us to think that there might be some hexamers in this sample, but that the majority of the sample is a different oligomeric state of EcFtsH. A hypothesis is that this sample is composed by a mixture of dimers (2 x monomers) plus detergent and some monomers that co-eluted. The assembly of EcFtsH in a dimeric state was

previously reported by [47], which describes a similar SEC profile for the protein elution and also that protease activity is detected for these smaller particles.

In summary, EcFtsH was found to be a difficult protein to express and extract from the membrane. Different purification protocols did not influence the outcome apart from the change of detergent and cell strain used to express the protein. Nevertheless, this chapter gave valuable insights for the continuation of the thesis.

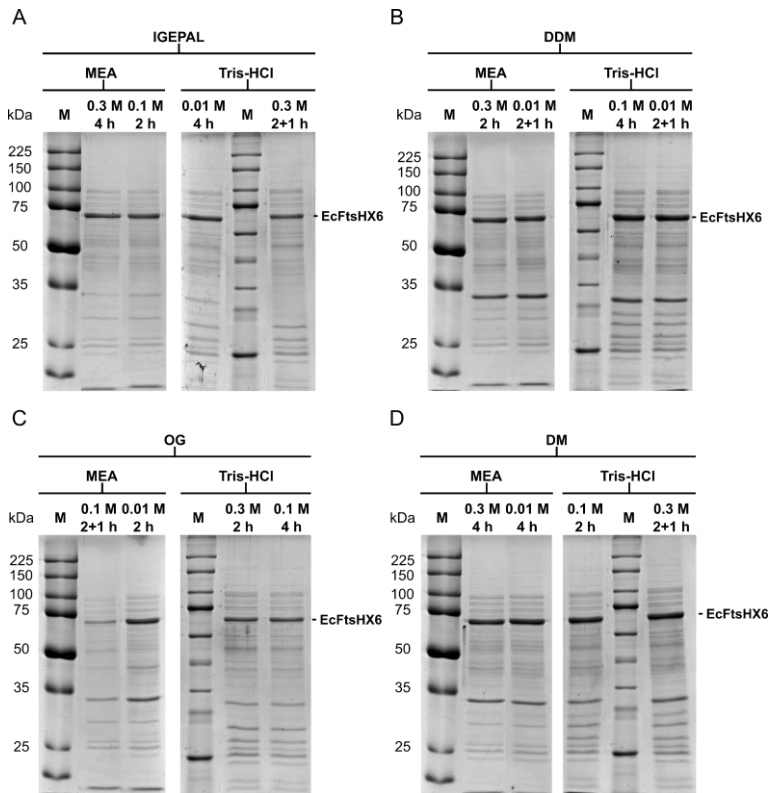
## 2.5 Supplemental data



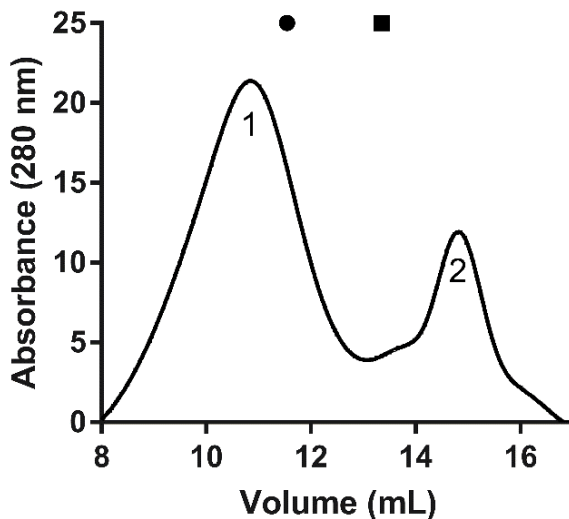
**Supplementary Figure 2.1 – EcFtsH vectors constructions.** The EcFtsH insert (brown) was cloned into a pET28a expression vector optimized for *E. coli* expression. (A) Represents the EcFtsHX10 construction in which the EcFtsH gene is separated from the His-tag by a 10 aa sequence. While (B) represents the construction of the EcFtsH gene separated from the His-tag by a 6 aa sequence. In green the Kanamycin resistance sequence; in yellow the LacI gene repressor of the tac promoter; LacOperator (LacO) in blue arrow; T7 promoter (T7). The position of the six histidine's tag is indicated by 6His and the restriction enzymes sites are indicated for NcoI, HindIII and SalI.

Experiment	Detergent	NaCl concentration (mM)	Incubation time(hours)	Buffer composition
1	IGEPAL	10	4	TrisHCl 50mM pH 7
2	DDM	10	2+1	
3	DDM	100	4	
4	DM	100	2	
5	OG	100	4	
6	OG	300	2	
7	IGEPAL	300	2+1	
8	DM	300	2+1	
9	IGEPAL	300	4	Monoethanolamine pH9
10	DM	300	4	
11	DDM	300	2	
12	IGEPAL	100	2	
13	OG	100	2+1	
14	DDM	10	2+1	
15	DM	10	4	
16	OG	10	2	

**Supplementary Figure 2.2 – Incomplete factorial experimental details.** All the conditions were tested in the same amount of EcFtsHX6 membranes, after solubilization the samples were treated with a centrifugation step and both supernatant and pellets were analysed.



**Supplementary Figure 2.3 – SDS-Page gels of the Incomplete Factorial approach.** All samples were collected after solubilization and before centrifugation. These results can be compared with the amount of EcFtsHX6 present in the gels presented in Figure 2.6. M – Molecular marker.



**Supplementary Figure 2.4 – Size exclusion chromatography profile of the purification of EcFtsHX6, after affinity chromatography and ion exchange chromatography.** The elution profile shows the elution of two different peaks a first peak corresponding to a molecular size of 837 kDa (1) and a second of 124 kDa (2). An extra step of purification does not improve the separation between the two peaks, as can be concluded from the comparison with the SEC profile of Figure 2.9 A. The elution volumes of some of the standard proteins used to estimate the molecular weight of the eluted fractions are shown on the top of the graph: (●) Tyroglobulin (MW: 669 kDa;  $V_e$ : 11.54ml) and (■) Ferritin (MW: 440 kDa;  $V_e$ : 13.35ml).

## 2.6 References

- [1] J.P. Overington, B. Al-Lazikani, A.L. Hopkins, How many drug targets are there?, *Nature Reviews Drug Discovery*. 5 (2006) 993–996.
- [2] S. Eshaghi, M. Hedrén, M.I.A. Nasser, T. Hammarberg, A. Thornell, P. Nordlund, An efficient strategy for high-throughput expression screening of recombinant integral membrane proteins., *Protein Science: A Publication of the Protein Society*. 14 (2005) 676–83.
- [3] F. Mancia, J. Love, High-throughput expression and purification of membrane proteins., *Journal of Structural Biology*. 172 (2010) 85–93.
- [4] K.H. Cho, M. Husri, A. Amin, K. Gotfryd, H.J. Lee, J. Go, J.W. Kim, C.J. Loland, L. Guan, B. Byrne, P.S. Chae, Maltose neopentyl glycol-3 (MNG-3) analogues for membrane protein study, *The Analyst*. 140 (2015) 3157–3163.
- [5] T.E. Kraft, R.C. Hresko, P.W. Hruz, Expression, purification, and functional characterization of the insulin-responsive facilitative glucose transporter GLUT4., *Protein Science: A Publication of the Protein Society*. (2015).
- [6] A.M. Seddon, P. Curnow, P.J. Booth, Membrane proteins, lipids and detergents: not just a soap opera, *Biochimica et Biophysica Acta (BBA) - Biomembranes*. 1666 (2004) 105–117.
- [7] M.M.K. Jayasekera, S.K. Foltin, E.R. Olson, T.P. Holler, *Escherichia coli* requires the protease activity of FtsH for growth., *Archives of Biochemistry and Biophysics*. 380 (2000) 103–7.
- [8] R. Srinivasan, H. Rajeswari, P. Ajitkumar, Analysis of degradation of bacterial cell division protein FtsZ by the ATP-dependent zinc-metalloprotease FtsH in vitro, *Microbiological Research*. 163 (2008) 21–30.
- [9] S.H. Kim, G.B. Kang, H.E. Song, S.J. Park, M.H. Bea, S.H. Eom, Structural studies on *Helicobacter pylori* ATP-dependent protease, FtsH., *Journal of Synchrotron Radiation*. 15 (2008) 208–10.
- [10] R. Suno, M. Shimoyama, A. Abe, T. Shimamura, N. Shimodate, Y.-H. Watanabe, Y. Akiyama, M. Yoshida, Conformational transition of the lid helix covering the protease active site is essential for the ATP-dependent protease activity of FtsH, *FEBS Letters*. 586 (2012) 3117–3121.
- [11] Z. Adam, A. Rudella, K.J. van Wijk, Recent advances in the study of Clp, FtsH and other proteases located in chloroplasts, *Current Opinion in Plant Biology*. 9 (2006) 234–240.
- [12] M. Schäkermann, S. Langklotz, F. Narberhaus, FtsH-mediated coordination of lipopolysaccharide biosynthesis in *Escherichia coli* correlates with the growth rate and the alarmone (p)ppGpp., *Journal of Bacteriology*. 195 (2013) 1912–9.

- [13] R.L. Bruckner, Robert C.; Gunyuzlu, Paul L. and Stein, Coupled Kinetics of ATP and Peptide Hydrolysis by *Escherichia coli* FtsH Protease, *Biochemistry*. 42 (2003) 10843–10852.
- [14] N. Saikawa, K. Ito, Y. Akiyama, Identification of Glutamic Acid 479 as the Gluzincin Coordinator of Zinc in FtsH (HflB), *Biochemistry*. 41 (2002) 1861–1868.
- [15] C. Herman, S. Prakash, C.Z. Lu, A. Matouschek, C.A. Gross, Lack of a Robust Unfoldase Activity Confers a Unique Level of Substrate Specificity to the Universal AAA Protease FtsH, *Molecular Cell*. 11 (2003) 659–669.
- [16] T. Yamada-Inagawa, T. Okuno, K. Karata, K. Yamanaka, T. Ogura, Conserved Pore Residues in the AAA Protease FtsH Are Important for Proteolysis and its Coupling to ATP Hydrolysis, *Journal of Biological Chemistry*. 278 (2003) 50182–50187.
- [17] Y. Akiyama, K. Ito, Reconstitution of membrane proteolysis by FtsH, *Journal of Biological Chemistry*. 278 (2003) 18146–18153.
- [18] S. Makino, T. Makino, K. Abe, J. Hashimoto, T. Tatsuta, M. Kitagawa, H. Mori, T. Ogura, T. Fujii, S. Fushinobu, T. Wakagi, H. Matsuzawa, Second transmembrane segment of FtsH plays a role in its proteolytic activity and homo-oligomerization, *FEBS Letters*. 460 (1999) 554–558.
- [19] F. Scharfenberg, J. Serek-Heuberger, M. Coles, M.D. Hartmann, M. Habeck, J. Martin, A.N. Lupas, V. Alva, Structure and Evolution of N-domains in AAA Metalloproteases., *Journal of Molecular Biology*. 427 (2015) 910–923.
- [20] Y. Akiyama, T. Yoshihisa, K. Ito, FtsH, a membrane-bound ATPase, forms a complex in the cytoplasmic membrane of *Escherichia coli*, *Journal of Biological Chemistry*. 270 (1995) 23485–23490.
- [21] Y. Akiyama, A. Kihara, H. Tokuda, K. Ito, FtsH (HflB) is an ATP-dependent protease selectively acting on SecY and some other membrane proteins., *The Journal of Biological Chemistry*. 271 (1996) 31196–201.
- [22] I. Benoit, B. Coutard, R. Oubelaid, M. Asther, C. Bignon, Expression in *Escherichia coli*, refolding and crystallization of *Aspergillus niger* feruloyl esterase A using a serial factorial approach., *Protein Expression and Purification*. 55 (2007) 166–74.
- [23] S. Langklotz, U. Baumann, F. Narberhaus, Structure and function of the bacterial AAA protease FtsH., *Biochimica et Biophysica Acta*. 1823 (2012) 40–8.
- [24] Y. Akiyama, K. Ito, Roles of multimerization and membrane association in the proteolytic functions of FtsH (HflB)., *The EMBO Journal*. 19 (2000) 3888–95.

- [25] Y. Shotland, D. Teff, S. Koby, O. Kobiler, A.B. Oppenheim, Characterization of a conserved  $\alpha$ -helical, coiled-coil motif at the C-terminal domain of the ATP-dependent FtsH (HflB) protease of *Escherichia coli*, *Journal of Molecular Biology*. 299 (2000) 953–964.
- [26] K. Ito, Y. Akiyama, Cellular Functions, Mechanism of Action, and Regulation of FtsH Protease, *Annual Review of Microbiology*. 59 (2005) 211–231.
- [27] T. Langer, AAA proteases: Cellular machines for degrading membrane proteins, *Trends in Biochemical Sciences*. 25 (2000) 247–251.
- [28] Y. Asahara, K. Atsuta, K. Motohashi, H. Taguchi, M. Yohda, M. Yoshida, FtsH recognizes proteins with unfolded structure and hydrolyzes the carboxyl side of hydrophobic residues., *Journal of Biochemistry*. 127 (2000) 931–7.
- [29] Y. Akiyama, Self-processing of FtsH and its implication for the cleavage specificity of this protease, *Biochemistry*. 38 (1999) 11693–11699.
- [30] J.D. Thompson, D.G. Higgins, T.J. Gibson, CLUSTAL W: improving the sensitivity of progressive multiple sequence alignment through sequence weighting, position-specific gap penalties and weight matrix choice., *Nucleic Acids Research*. 22 (1994) 4673–80.
- [31] G.L. Rosano, E.A. Ceccarelli, Recombinant protein expression in *Escherichia coli*: advances and challenges., *Frontiers in Microbiology*. 5 (2014) 172.
- [32] Y. Akiyama, Proton-motive force stimulates the proteolytic activity of FtsH, a membrane-bound ATP-dependent protease in *Escherichia coli*., *Proceedings of the National Academy of Sciences of the United States of America*. 99 (2002) 8066–8071.
- [33] H. Ilgü, J.-M. Jeckelmann, M.S. Gachet, R. Boggavarapu, Z. Ucurum, J. Gertsch, D. Fotiadis, Variation of the detergent-binding capacity and phospholipid content of membrane proteins when purified in different detergents., *Biophysical Journal*. 106 (2014) 1660–1670.
- [34] K. Westphal, S. Langklotz, N. Thomanek, F. Narberhaus, A trapping approach reveals novel substrates and physiological functions of the essential protease FtsH in *Escherichia coli*, *Journal of Biological Chemistry*. 287 (2012) 42962–42971.
- [35] A. Kihara, Y. Akiyama, K. Ito, Different pathways for protein degradation by the FtsH/HflKC membrane-embedded protease complex: an implication from the interference by a mutant form of a new substrate protein, YccA, *Journal of Molecular Biology*. 279 (1998) 175–188.
- [36] K. Karata, T. Inagawa, A.J. Wilkinson, T. Tatsuta, T. Ogura, Dissecting the role of a conserved motif (the second region of homology) in the AAA family of ATPases. Site-directed mutagenesis of the ATP-dependent protease FtsH., *The Journal of Biological Chemistry*. 274 (1999) 26225–32.

- [37] C. Katz, E.Z. Ron, Dual role of FtsH in regulating lipopolysaccharide biosynthesis in *Escherichia coli*, *Journal of Bacteriology*. 190 (2008) 7117–22.
- [38] Q. Kuang, P. Purhonen, H. Hebert, Two-Dimensional Crystallization Procedure, from Protein Expression to Sample Preparation., *BioMed Research International*. 2015 (2015) 693869.
- [39] A. Kihara, Y. Akiyama, K. Ito, FtsH is required for proteolytic elimination of uncomplexed forms of SecY, an essential protein translocase subunit., *Proceedings of the National Academy of Sciences of the United States of America*. 92 (1995) 4532–6.
- [40] T. Okuno, K. Yamanaka, T. Ogura, Characterization of mutants of the *Escherichia coli* AAA protease, FtsH, carrying a mutation in the central pore region., *Journal of Structural Biology*. 156 (2006) 109–14.
- [41] M. Graef, G. Seewald, T. Langer, Substrate recognition by AAA+ ATPases: distinct substrate binding modes in ATP-dependent protease Yme1 of the mitochondrial intermembrane space., *Molecular and Cellular Biology*. 27 (2007) 2476–2485.
- [42] T. Tomoyasu, J. Gamer, B. Bukau, M. Kanemori, H. Mori, A.J. Rutman, A.B. Oppenheim, T. Yura, K. Yamanaka, H. Niki, *Escherichia coli* FtsH is a membrane-bound, ATP-dependent protease which degrades the heat-shock transcription factor sigma 32., *The EMBO Journal*. 14 (1995) 2551–2560.
- [43] T. Okuno, K. Yamanaka, T. Ogura, An AAA protease FtsH can initiate proteolysis from internal sites of a model substrate, apo-flavodoxin., *Genes to Cells*. 11 (2006) 261–8.
- [44] Y. Shotland, S. Koby, D. Teff, N. Mansur, D.A. Oren, K. Tatematsu, T. Tomoyasu, M. Kessel, B. Bukau, T. Ogura, A.B. Oppenheim, Proteolysis of the phage lambda CII regulatory protein by FtsH (HflB) of *Escherichia coli*, *Molecular Microbiology*. 24 (1997) 1303–1310.
- [45] R. Srinivasan, G. Anilkumar, H. Rajeswari, P. Ajitkumar, Functional characterization of AAA family FtsH protease of *Mycobacterium tuberculosis*, *FEMS Microbiology Letters*. 259 (2006) 97–105.
- [46] S.K. Singh, F.J. Sigworth, Cryo-EM: Spinning the Micelles Away, *Structure*. 23 (2015) 1561.
- [47] C. Bieniossek, T. Schalch, M. Bumann, M. Meister, R. Meier, U. Baumann, The molecular architecture of the metalloprotease FtsH., *Proceedings of the National Academy of Sciences of the United States of America*. 103 (2006) 3066–3071.



# Chapter 3

## *Aquifex aeolicus* FtsH expression and purification optimization: a different point of view

FtsH purification proved to be a challenging task in the last chapter. Membrane protein studies have adopted different strategies to study membrane proteins and one of them is the use of homologous thermophile versions of the proteins. Those reveal to be more stable, decreasing the difficulties of protein extraction and stabilization in an aqueous medium, since these organisms are more resistant than non-thermophilic bacteria. In this chapter, all the procedures performed during this dissertation to purify and obtain a solubilized form of the thermophilic *Aquifex aeolicus* FtsH are described, as well as all the assays performed to confirm that the protein was kept stable and active during the period of the duration of the experiments.

### 3.1 Introduction

The choice of thermophiles as an alternative source to unstable natural *E. coli* proteins is widely used by the scientific community. Homologous thermophilic proteins are usually expressed at a higher yield and have a more stable conformation than proteins from bacteria growing at lower temperatures (e.g., *E. Coli*). This is directly linked to the resistance of these proteins to temperature changes [1]. *Aquifex aeolicus* (*A. aeolicus*) is a rod-shaped bacterium that grows optimally at 95°C in water. Its genome is only one third of size of the total *E. coli* genome [2]. The sequence coding for the full-length FtsH from *A. aeolicus* (AaFtsH) has been cloned into an expression vector to express and purify AaFtsH [3]. Previous work has described a purification protocol for the full-length *A. aeolicus* FtsH, but no structural information is provided yet about this protein. The proteolytical and ATPase activity has been partly characterized and compared with several mutants of FtsH carrying only the cytoplasmic domain, revealing that the full-length protein has higher proteolytical activity than its cytoplasmic part. Previous work has also shown that mutating the glycine linker between the protease and ATPase domain (G399L) leads to loss of FtsH activity [3]. Cytoplasmic domains of other thermophilic FtsH homologs were crystallized, those of *Thermus thermophiles* FtsH [4] and of *Thermotoga maritima* FtsH [5,6]. Although several crystal structures of the cytoplasmic domain of thermophilic FtsH have been solved, the structure of the full-length FtsH from either thermophile or non-thermophile bacteria has not been described.

In this chapter, we present the optimization of the purification protocols of AaFtsH. Taking in account the knowledge obtained in the last chapter, where a range of detergents were explored, we combined that knowledge and applied it to the purification protocols tested for this new construct.

Having the same goal as in the previous chapter, the purification of AaFtsH was optimized to obtain a protein as stable as possible in solution, such that it could be submitted to different biochemical and structural studies.

## **3.2 Material and methods**

### **3.2.1 AaFtsH expression and purification characterization**

Full-length *Aquifex aeolicus* FtsH (AaFtsH) cloned into pET22a vector was kindly granted by Ulrich Baumann and the same expression conditions were employed [3]. Cells were harvested at 3500 *g* for 25 min at 4 °C and disrupted in a cell disruptor. The resulting cell debris was purified at 20000 *g* for 15 min and membranes were isolated at 125000 *g* for 3 hours. Membranes were solubilised in 20 mM Tris-HCl pH 8.0; 150 mM NaCl; 1%(w/v) Lauryl Maltose Neopentyl Glycol (LMNG) (Anatrace) for 3 hours at 4 °C and cleared at 125000 *g* for 1 hour at 4 °C. The sample was first purified by affinity chromatography, using a HisTrap-5 mL column (GE Healthcare). FtsH fractions were eluted in 20 mM Tris-HCl pH 8.0; 500 mM NaCl; 0.01%(w/v) LMNG and 200 mM imidazole. The eluted fractions were pooled together and directly loaded into the Superose 6 Increase 10/300 GL previously equilibrated with 10 mM Tris-HCl pH8.0; 150 mM NaCl; 0.01%(w/v) LMNG; 5% Glycerol. A separate purification protocol of AaFtsH was also performed using DDM instead of LMNG in all buffers used to reproduce the purification in [3].

Moreover, different optimizations were performed in the AaFtsH purification protocol. After the samples elution from the HisTrap column, the fractions were subjected to different conditions in an attempt to enhance the hexameric oligomeric state. All the conditions tested are described below and were performed before the second step of purification, which consisted of size exclusion chromatography (SEC).

#### **3.2.1.1 AaFtsH inhibitors**

Inhibition of the ATPase domain was attempted by incubating the resulting HisTrap fractions with 5 mM 1,10-Phenanthroline (Sigma-Aldrich) for 30 min at room-temperature, at 50°C for 3 hours and at 50°C for 2 hours adding 5 mM ATP, 10 mM MgCl<sub>2</sub>, 25 μM ZnAc. The inhibition of the ATPase domain was also attempted in an earlier stage of the purification protocol during membrane solubilization. 1,10-Phenanthroline was added to the slurry to a final concentration of 20 nM, and the solubilization was performed for 3 hours at 4°C. After membrane solubilization the

purification was performed as described above for the sample that did not undergo any incubation after the first step of purification (in 3.2.1).

Adenylyl-imidodiphosphate (AMP-PNP) was also used to inhibit AaFtsH activity after the HisTrap purification step. The fractions were concentrated and incubated with 10 mM AMP-PNP for 20 min at 80°C and with 5 mM AMP-PNP for 1 hour at 60°C with and without 2 µM of GST-CII; to all these conditions was added, to a final concentration, 10mM MgCl<sub>2</sub> and 25 µM ZnAc. GST-CII was purified in house (GST-CII purification protocol in 4.2.5). After the incubation, the fractions were filtrated and loaded into the Superose 6 Increase 10/300 GL pre-equilibrated with 10 mM Tris-HCl pH8.0; 150 mM NaCl; 0.01%(w/v) LMNG; 5% glycerol.

The inhibition of AaFtsH activity was also tested by the incubation of the HisTrap fractions with Adenosine 5'-diphosphate (ADP) in two different conditions: 10 mM ADP for 1 hour at 50°C and 5 mM ADP, 5 mM ATP for 2 hours at 50°C. The incubation buffer also contained 10 mM MgCl<sub>2</sub> and 25 µM ZnAc. After incubation, both samples were concentrated and loaded into the SEC as previously described.

### **3.2.1.2 Tests on the effect of ATP concentrations and temperatures**

The effect of adding ATP to the fractions eluting from the HisTrap column was also tested. The fractions containing AaFtsH, after HisTrap purification, were pooled together and incubated with 5 mM ATP in the following conditions: for 2 hours at 50°C; over-night at 25°C or 60°C in presence or in absence of 2 µM GST-CII. All the incubations with ATP were performed in presence of 10 mM MgCl<sub>2</sub> and 25 µM ZnAc.

After the HisTrap column chromatography AaFtsH fractions incubation in presence of 10 mM ATP was also tested under the following incubation conditions: for 4 and 7 hours at 50°C; overnight at 60°C; or overnight at 80°C. The final ATP concentration was also increased to 20 and 40 mM and the incubation was performed at 60°C overnight. The incubated sample was concentrated to 500 µL and loaded into a SEC Superose 6 Increase 10/300 GL column (GE Healthcare) pre-equilibrated with 10

mM Tris-HCl pH8.0; 150 mM NaCl; 0.01%(w/v) LMNG; 5% Glycerol. The AaFtsH monomer concentration was measured with a Nanodrop.

The best purification protocol revealed to be the one where the sample from HisTrap is incubated with 20 mM ATP, 10 mM MgCl<sub>2</sub> and 25 μM ZnAc overnight at 60°C. The profile of the chromatogram was reproducible after repeating the purification protocol several times. For this reason, the graph presented in this thesis was determined by the fitting of Gaussian functions to 10 SEC profiles, to determine the centre position of the two largest peaks. A calibration curve of the Superose 6 Increase 10/300 GL was performed using the Gel Filtration High Molecular Weight Calibration Kit (GE Healthcare), following the GE Healthcare instructions. All fractions were analysed by SDS-PAGE gels, to confirm the molecular weight of the different protein samples eluted.

### **3.2.2 AaFtsH mutants – site directed mutagenesis**

Three different AaFtsH mutants were produced in this chapter by site directed mutagenesis (SDM). This method allows site-specific mutation in any double-stranded plasmid. The pET22a vector cloned with the full-length AaFtsH gene and kindly granted by Ulrich Baumann was used as template in the mutagenesis reaction to produce the mutants R316L and H418Y. Another mutant of the AaFtsH full-length gene cloned into the pET22b expression vector was commercially produced by GeneScript, the mutation introduced was K201A. This commercially produced vector was the template for the third mutant produced carrying the H418Y mutation (K201A\_H418Y). For the three SDM reactions (R316L, H418Y and H418Y+K201A), three pairs of primers were designed using the software provided by Stragene Genomics® (<https://www.genomics.agilent.com/primerDesignProgram.jsp>). These primers are two complementary DNA oligonucleotides that contain the desired mutation, flanked by unmodified nucleotide sequence. With R316L mutagenic primers (5' – TTTGGGTATAAATATCTGCCTGTCAAAAAGTCCGGGCCTTAAAAGA GCCGGGTCTAAGATGTC - 3' and 5' – TTAGACCCGGCTCTTTTAAGGCCCGGA CTTTTTGACAGGCAGATATTTATACCCAAACCTGACG -3') the amino acid arginine (R) in position 316 was mutated to a leucine (L) to create the AaFtsH mutant R316L.

Furthermore, with H418Y mutagenic primers (5' - GAGTCCCATGAGGGCGTGTCCGGCTTC**ATA**TATAGCTATCTTCTCCTTTTCTTTTGGCGA TATGGT- 3' and 5' - AAAGAAAAGGAGAAGATAGCTATA**TAT**GAAGCCGGACACGCC TCATGGGACTCGTCTCCGAT - 3') the amino acid histidine (H) at position 418 was mutated for a tyrosine (Y) to create the mutant H418Y. These two primers were also used to mutate the synthetic gene at position 418, produced by GenScript, that already had the amino acid lysine (K) mutated to an alanine (A) at position 201 forming the mutant K201A. This mutant has two mutations and was designated H418Y\_K210A.

The SDM was performed using Phusion HF polymerase (New England Biolabs) for high fidelity and robust amplification DNA. Using a cycling PCR reaction, the product was then cleaned and treated with 10 units of DpnI endonuclease for 1 hour at 37°C. The product was cleaned and transformed into *E. coli* DH5α competent cells. The positive transformants were selected by plating onto LB-agar plates supplemented with 100 µg/ml Ampicillin and growing overnight. DNA plasmid isolation and purification were performed in the positive transformants and the pure DNA plasmid samples were sent for sequencing.

### **3.2.2.1 AaFtsH mutants' purification**

The same expression and purification steps accomplished in 3.2.1 were executed to express the different mutants described in 3.2.2. Similar experiments were performed to determine the best conditions, to produce AaFtsH mutants in the hexameric form.

HisTrap fractions of AaFtsH R316L were submitted to an incubation with either 10mM or 20 mM ATP overnight at 60°C in presence of 10 mM MgCl<sub>2</sub> and 25µM ZnAc. HisTrap fractions of AaFtsH K201A were either submitted to an incubation with 20 mM ATP overnight at 60°C in presence of 10 mM MgCl<sub>2</sub> and 25µM ZnAc, or were concentrated and directly loaded into the SEC. Furthermore, the H418Y fractions were submitted to different incubation conditions with: 10 mM ATP overnight at 4°C or 60°C; 20 mM ATP overnight at 60°C; 5 mM AMP-PNP for 3 hours at 60°C; or

directly loaded into the SEC after the elution from the HisTrap column. All the incubation buffers had 10 mM MgCl<sub>2</sub> and 25 μM ZnAc.

### **3.2.3 Protease activity tests**

Protease activity tests were performed with samples from the early steps of purification: isolated membranes, fraction that was loaded into the HisTrap column, and HisTrap fractions. The protease activity was tested in presence and absence of 10 mM ATP. The protease activity of these fractions was tested by incubating 25 μL of sample with 25 μL of resorufin-labelled casein substrate (Roche), 30 μL of [50 mM Tris-HCl pH 8.0; 80 mM NaCl; 12.5 μM ZnCl<sub>2</sub>; 5 mM MgCl<sub>2</sub>; 1 mM dithiothreitol; 0.01% LMNG; protease inhibitor], and 20 μL of MiliQ water; overnight at 50°C. 240 μL of 5% trichloroacetic acid was added and incubated at 37 °C for 30 min. Proteins were precipitated at 16100 g for 30 min and 300 μL from the supernatant was mixed with 700 μL of 500 mM Tris-HCl pH 8.8 and added to a 1 mL cuvette. The OD574nm was immediately measured using a Nanodrop 2000 (Thermo Fisher). The sample that was loaded into the HisTrap column was also tested in the same conditions to measure protease activity, although this sample was incubated with the substrate for 2 hours instead of overnight. To test the effect of imidazole, the fractions that were loaded onto the HisTrap column, were incubated with and without 500 mM imidazole for 0/30/60/120 min in presence and absence of 10 mM ATP. The protease activity of the HisTrap fractions was measured before and after an overnight incubation at 60°C as previously described.

The protease activity of the sample eluted from the SEC was also assessed using the same protocol as described in Chapter 4. The protease activity was tested for all fractions collected from the purification of AaFtsH WT, R316L, K201A, H418Y and K201A\_H418Y.

### **3.2.4 Transmission Electron Microscopy analysis**

3 μL of AaFtsH dodecamer or hexamer fractions was loaded on a carbon-coated 400 square mesh copper grid (Aurion) previously glow-discharged for 1 min. The liquid drop was absorbed with filter paper after 1 min and quickly washed with a drop of

water that was again blotted with filter paper. This procedure was repeated 3 times to rinse all the detergent present in the samples. Finally, a 3  $\mu$ L drop of 3 % uranyl-acetate was added to the grid, incubated for 1 min and absorbed with a filter paper. Transmission electron microscopy was performed using a Philips CM-200T, JEOL JEM-1400 or a JEOL 3200 FSC.

### **3.3 Results**

#### **3.3.1 Testing AaFtsH protease activity in different conditions**

The expression and the first attempt of purification of AaFtsH was performed as described in [3]. The size exclusion profile of the purification performed, using DDM in the buffers, shows that the protein elutes in a broad peak around 11.6 mL, which corresponds to approximately 1020 kDa (see Figure 3.1 A). Since the elution of AaFtsH did not correspond to the expected molecular weight, another purification step was performed using LMNG as detergent in the buffers. The choice of this detergent was influenced by the results obtained in Chapter 2, which showed that EcFtsHX6 was more stable when solubilized in LMNG. The purification using LMNG in the buffer for loading the HisTrap fraction into the SEC, also showed the elution of a broad peak at 12.2 mL (around 924 kDa) which is not compatible with the expected 432 kDa plus detergent of the hexameric AaFtsH (see Figure 3.1 A). In order to study the behaviour of this protein at various temperature, the protease activity of the samples eluted from the HisTrap was tested at different temperatures. For the membrane and the samples loaded into the HisTrap protease activity were tested at 50°C overnight (Figure 3.1 B). The protease activity of the HisTrap samples was tested at 50, 37 and 25°C in presence and absence of ATP. Figure 3.1 B shows that in absence of ATP, almost no activity is seen, whereas all fractions show activity in presence of ATP. The protease activity results demonstrate that the temperature at which the assay is executed influences the level of protease activity. Higher temperatures resulted in higher activity levels (in presence of ATP, Figure 3.1 B). A distinct activity increment is observed in absence of ATP when the temperature increases.

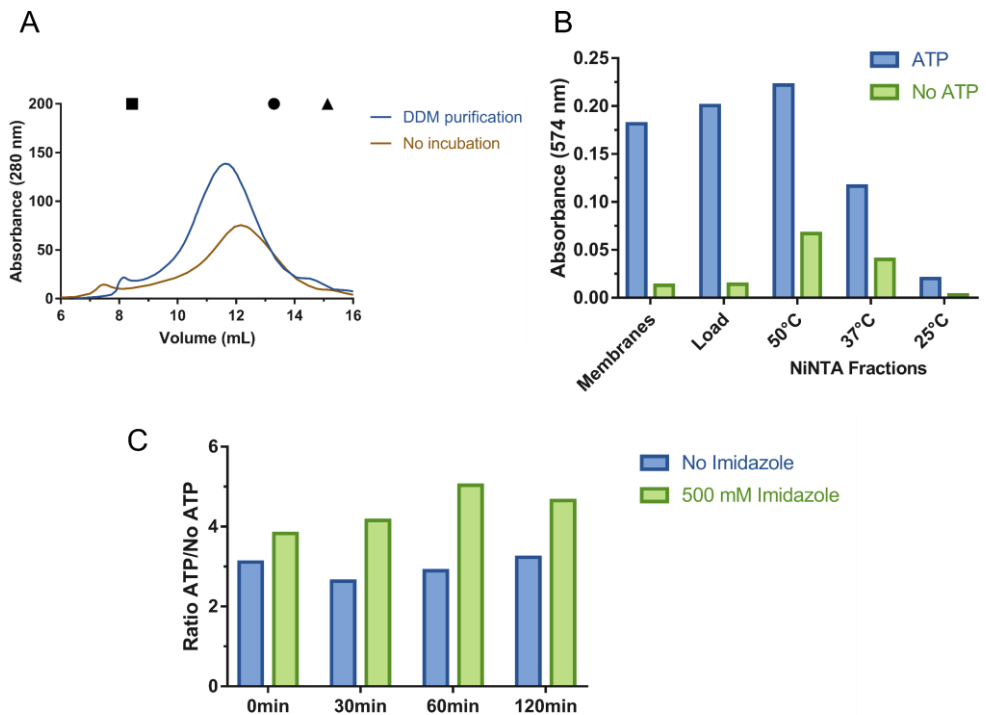


**Figure 3.1 – Size exclusion chromatography profile of samples purified with either DDM or LMNG directly loaded from the HisTrap elution into the Superose 6 10/300 GL column (no incubation).** (A). Blue Dextran (■) is used to calculate the void volume of the column (8.47mL). The elution volumes of standard proteins used to estimate the molecular weight of the eluted fractions are shown on the top of the graph: (●) Tyroglobulin (MW: 669 kDa; Ve: 13.27 ml), (▲) Ferritin (MW: 440 kDa; Ve: 15.13 ml), (◆) Aldolase (MW: 158 kDa; Ve: 16.62 ml) and (★) Ovalbumin (MW: 44kDa; Ve: 17.76 ml). In B, the protease activity assay shows that all fractions (membranes, fractions loaded on the HisTrap column, and fractions eluting from the affinity chromatography) are active. The protease activity of the HisTrap was tested at different temperatures (50, 37 and 25°C) to assess the effect of temperature on the protease activity. C reveals the ratios of activity in presence and absence of 10 mM ATP. To study the influence of 500mM imidazole, an incubation for 0/30/60/120 min was performed at 4°C (C). D shows that the HisTrap fractions have the same level of activity after an incubation at 60°C overnight.

Since the goal of these experiments was to identify conditions favourable for AaFtsH stability, the influence of imidazole was also tested by measuring the protease activity at different temperatures. Imidazole can help in aggregation inhibition, although depending on the hydrophobic interactions of this amino acid with the

protein its presence can also be responsible for protein aggregation when using affinity chromatography [7]. The fraction that was loaded in the HisTrap column was incubated for 0/30/60/120 min with and without 500 mM imidazole; and after the incubation, protease activity was tested at 50°C for 2 hours. The experiment was performed for 2 hours to uniformize the incubation time with the substrate. Figure 3.1 C shows the ratios of activity between the samples incubated in presence and in absence of ATP. In all the conditions tested, the presence of imidazole does not significantly affect the protease activity. With this experiment, it is also possible to observe that although the samples were kept at 4°C for at least 120 min, the samples were still fully active. Finally, the influence of temperature on the AaFtsH protease activity was tested by measuring the protease activity before and after an incubation at 60°C overnight. No significant difference was observed during 120 min (Figure 3.1 D)

Since the protease activity is not influenced by the different temperatures tested during overnight incubation, several incubation conditions were assessed till the first step of purification, although none of them seemed to influence the resulting SEC profile. Moreover, because only the affinity chromatography highly increased FtsH purity, only the results of changes made after protein elution from the HisTrap column are discussed. Different incubation periods, temperatures and buffers were tested, and the most meaningful results will be summarized in the following sections.

### **3.3.2 AaFtsH purification after inhibition**

Several FtsH inhibitors have been reported in literature, some reducing the ATPase activity such as ADP and AMP-PNP [8,9], and others reducing the proteolytical activity such as EDTA and phenanthroline [10]. The results shown in 3.3.1 demonstrated that AaFtsH is not stable enough and aggregates when it is directly loaded into the SEC after the HisTrap purification. For that reason, inhibition of both protease and ATPase activity was attempted in the hope to prevent aggregation. The use of 20 nM of 1,10-phenanthroline incubated with the membranes during solubilization has no significant effect on the elution profile as shown in Figure 3.2 A (blue trace). The protein elutes as a broad peak with its maximum at 11.9 mL

(around 972 kDa). The same profile is observed when incubating the HisTrap eluted fractions with 5mM of 1,10-phenanthroline at room temperature for 30 min (elution volume at 11.7 mL, with an estimated molecular weight of 1004 kDa) (Figure 3.2 A green trace). As we have seen that temperature influences the protein activity, we increased the incubation temperature to 50°C and the incubation period to 3 hours. However, no change in the elution profile was observed, the peak was even broader, and it remained at the same elution volume as the last one (Figure 3.2 A red trace). Only when repeating the experiment in the presence of 5 mM ATP, 10 mM MgCl<sub>2</sub> and 25 μM ZnAc, the elution profile exhibited two distinct narrow peaks instead of one broad peak. A first peak elutes at 11.6 mL (estimated molecular weight 1020 kDa) and a second peak elutes at 13.2 mL (with a molecular weight of around 779 kDa) (Figure 3.2 A orange trace). Despite not being shown in Figure 3.2 A, a third peak is also detected at around 20 mL, which does not contain AaFtsH as verified by SDS-Page gel.

As the hydrolysis of ATP plays an important role in the mechanics of FtsH process, the HisTrap fractions were incubated with adenosine nucleotides to test whether it could have an effect on AaFtsH stability. The inhibition of the HisTrap fraction using nucleotides was first attempted by incubating it with 10 mM of ADP at 50°C for either 1 hour or 2 hours in presence of 10 mM ATP (Figure 3.2 B green and orange trace respectively). The SEC profiles in Figure 3.2 B show that no effect is detected as compared with the SEC elution profiles where HisTrap fractions were directly loaded into the Superose 6 10/300 GL column.

Furthermore, FtsH fractions were also incubated with AMP-PNP, which is an adenine nucleotide that FtsH cannot degrade [10]. The results of the profiles in Figure 3.2 A of the different incubations indicate that a second peak is formed when incubating with AMP-PNP.

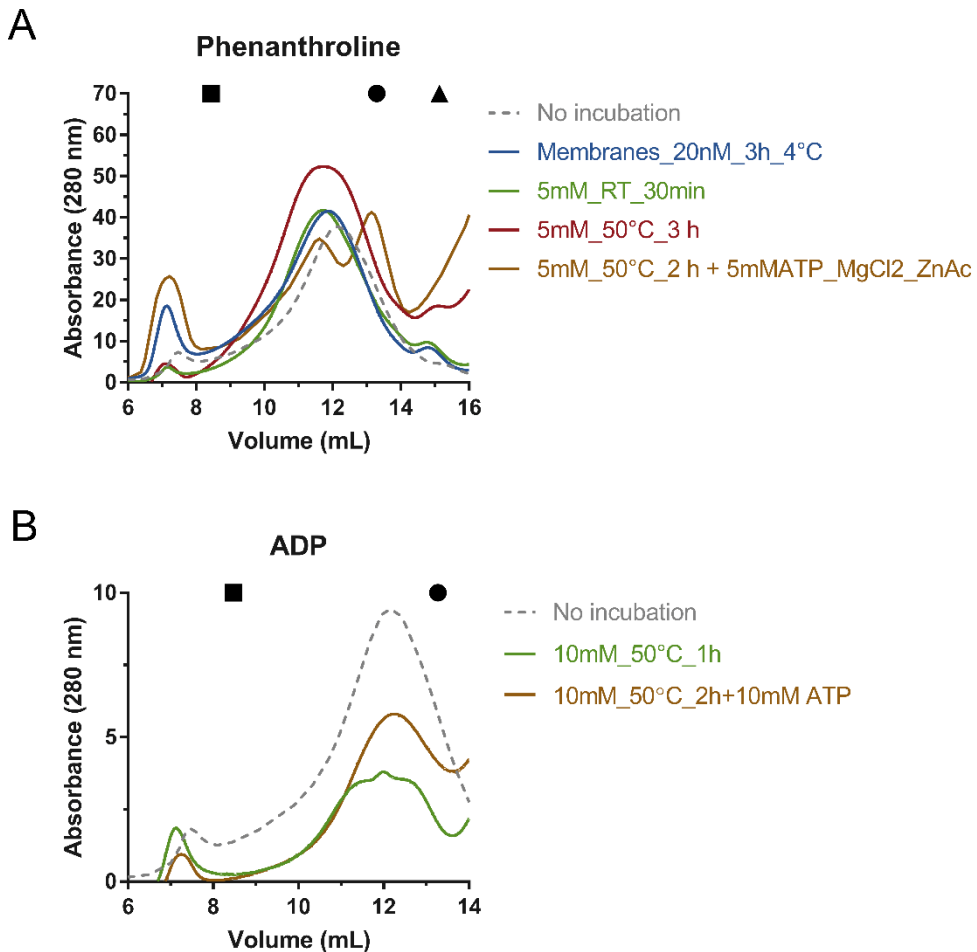


**Figure 3.2 – AaFtsH size exclusion profiles after incubation with 1, 10 – phenanthroline and ADP (A and B).** Only the elution profile that resulted from the HisTrap fractions incubation at 50 °C with 1, 10 – phenanthroline and ATP shows a profile different from the elution profile with no incubation (grey trace) (A). B shows the SEC elution profiles after incubating the HisTrap fractions with ADP. No significant difference is detected between conditions. The grey traces on the graphs indicate the SEC elution profile of the HisTrap fractions which were directly loaded into the Superose 6 10/300 GL column. Blue Dextran (■) is used to calculate the void volume of the column (8.47mL). The elution volumes of standard proteins used to estimate the molecular weight of the eluted fractions are shown on the top of the graph: (●) Tyroglobulin (MW: 669 kDa;  $V_e$ : 13.27 ml), (▲) Ferritin (MW: 440 kDa;  $V_e$ : 15.13 ml), (◆) Aldolase (MW: 158 kDa;  $V_e$ : 16.62 ml) and (★) Ovalbumin (MW: 44kDa;  $V_e$ : 17.76 ml).

A short incubation of 20 min at 80°C with AMP-PNP shows a profile with two peaks, the first at an elution volume of 12.1 mL (around 940 kDa) and a second peak with an elution volume of 13.5 mL (estimated molecular weight 715 kDa) (Figure 3.3 A brown trace). When decreasing the incubation time to 1 hour and decreasing the incubation temperature to 60°C the elution profiles shifts to even later elution volumes: first peak at 12.5 mL (estimated molecular weight 876 kDa) and second peak at 14 mL (around 634 kDa) (Figure 3.3 A blue trace). The same experiment was repeated in presence of 2  $\mu$ M GST-CII, a known FtsH substrate [11], but no difference in the elution profile was detected (Figure 3.3 B green trace). The execution of the experiment with AMP-PNP revealed to be difficult as the incubation of AaFtsH with AMP-PNP necessitated to first concentrate the sample before performing the experiment. AMP-PNP is also expensive when used in such high concentrations. With a volume of 500  $\mu$ L (maximum volume that can be loaded into the Superose 6 10/300 GL), the overnight incubation with AMP-PNP led to the total aggregation of the protein (data not shown). The samples incubated with 5 mM AMP-PNP at 60°C for 1 hour were further analysed by negative stain electron microscopy (Figure 3.3 B and C). The micrographs show the presence of small particles with an average length of  $152 \text{ \AA} \pm 15 \text{ \AA}$  (SD, N=50) which eluted in the second peak, and bigger particles with a length of  $229 \text{ \AA} \pm 25 \text{ \AA}$  (SD, N=50). Side views are preferentially observed in the micrographs.

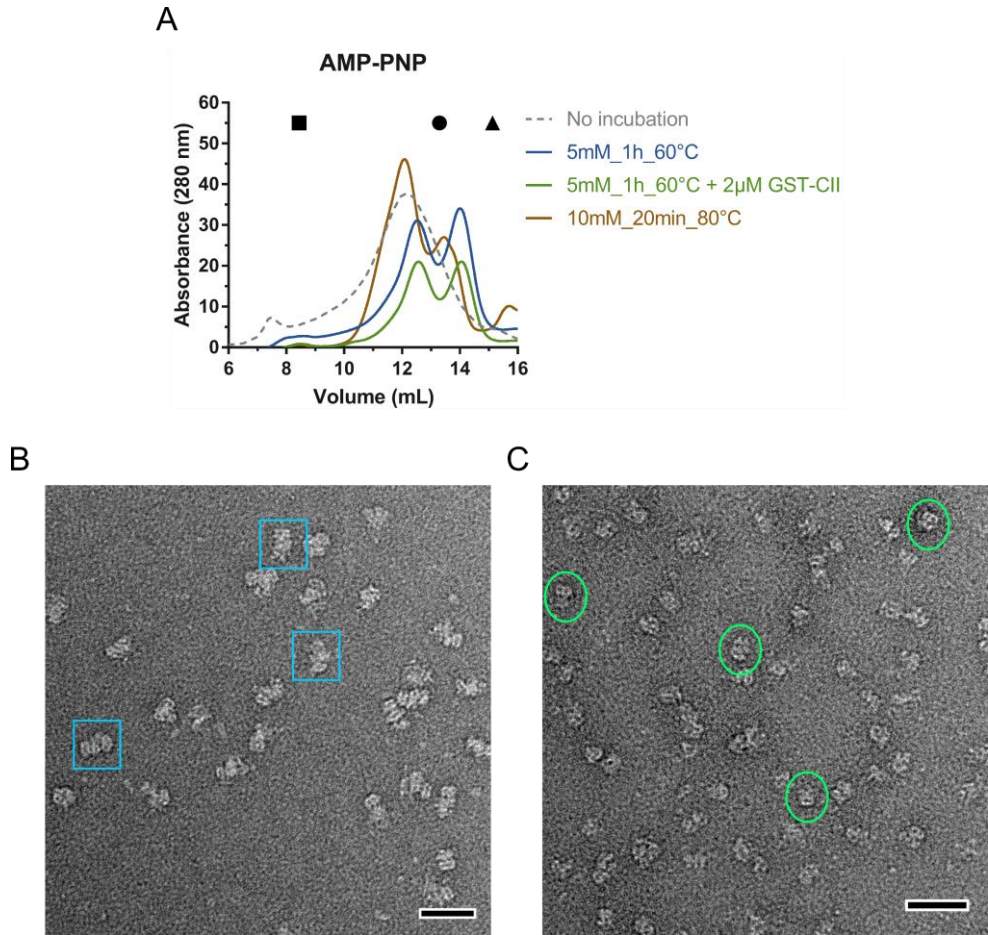


**Figure 3.3 - The size exclusion profile and negatively stained images of the fractions incubated with AMP-PNP.** The profile shows a two-peak chromatogram independent of the condition tested (A). The graph has a grey trace that indicates the SEC elution profile of the HisTrap fractions which were directly loaded into the Superose 6 10/300 GL column. Blue Dextran (■) is used to calculate the void volume of the column (8.47mL). The elution volumes of standard proteins used to estimate the molecular weight of the eluted fractions are shown on the top of the graph: (●) Tyroglobulin (MW: 669 kDa; Ve: 13.27 ml), (▲) Ferritin (MW: 440 kDa; Ve: 15.13 ml), (◆) Aldolase (MW: 158 kDa; Ve: 16.62 ml) and (★) Ovalbumin (MW: 44kDa; Ve: 17.76 ml). B and C show electron micrographs of the negatively stained samples from the first and second peaks, respectively. Side views are preferentially obtained. Blue squares correspond to dodecamers particles and green circles to hexamers. Scale bar is 500 Å.

### **3.3.3 Different incubation conditions with ATP lead to different AaFtsH elution profiles**

In the same fashion, the HisTrap fractions were incubated with two different concentrations of ATP (10 mM and 20 mM) at different temperatures (50, 60 and 80°C) and for three different periods (4, 7 hours and overnight). The incubation with ATP was always performed in presence of 10 mM MgCl<sub>2</sub> and 25 μM ZnAc, since these are essential for FtsH activity [10]. The incubation of the AaFtsH HisTrap fractions with 10 mM ATP at 50°C for 4 and 7 hours revealed a very similar profile (Figure 3.4 A green and blue traces respectively), in which the two peaks overlapped and are detected between the 11 - 12 mL of elution volume. The two elution profiles show that smaller molecular weight proteins are also eluted with the two peaks. SDS-PAGE analysis confirmed that AaFtsH was present in those fractions (Supplementary Figure 3.1). The elution profile of samples previously incubated overnight at 60°C with 10 mM ATP show a profile similar to the one detected for the incubation in 3.3.2 with AMP-PNP (Figure 3.3 A blue trace). The first peak elutes at a volume of 12.2 mL and the second peak at 13.6 mL (Figure 3.4 A orange trace). The profile of the sample incubated at 80°C shows a higher and sharper second peak at the elution volume of 13.8 mL (estimated molecular weight 666 kDa), although the first peak is still present as a shoulder and an earlier third peak is observed at the elution of 11.3 mL (around 1069 kDa) (Figure 3.4 A red trace). Despite this profile being satisfying, many attempts to reproduce this profile failed, which can be due to the elevated temperature at which the assay was performed. Both peaks were loaded into a SDS-Page gel to further comparison in Supplementary Figure 3.1, although the concentration of protein loaded on the gel was not the same it is possible to observe that only the fractions which eluted from the SEC after an incubation at 80°C are not contaminated with other impurities.

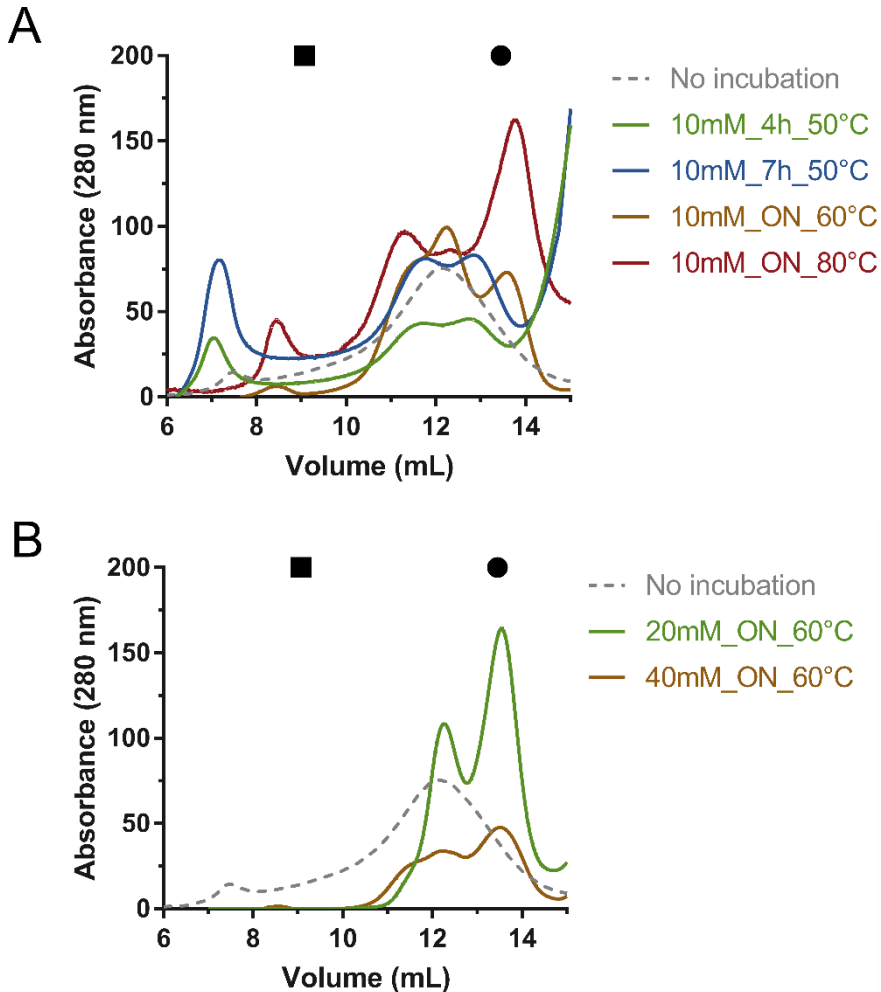


**Figure 3.4 – Size exclusion chromatography profiles with different ATP concentrations.** The elution profiles of the SEC after incubation with 10 mM ATP (A) and 20 and 40 mM ATP (B). The profiles show that at higher temperatures, a second sharper peak is obtained in the elution profile (A) and the same is true for the increase of the ATP amount (B). The graphs have a grey trace that indicates the SEC elution profile of the HisTrap fractions which were directly loaded into the Superose 6 10/300 GL column. Blue Dextran (■) is used to calculate the void volume of the column (8.47mL). The elution volumes of standard proteins used to estimate the molecular weight of the eluted fractions are shown on the top of the graph: (●) Tyroglobulin (MW: 669 kDa; Ve: 13.27 ml), (▲) Ferritin (MW: 440 kDa; Ve: 15.13 ml), (◆) Aldolase (MW: 158 kDa; Ve: 16.62 ml) and (★) Ovalbumin (MW: 44kDa; Ve: 17.76 ml).

Furthermore, the influence of higher ATP concentrations during this incubation period was tested with 20 mM and 40 mM (Figure 3.4 B orange and green trace). Both conditions show an increase of the second peak at the same elution volume, although the elution profile of the sample incubated with 40 mM ATP shows a less sharp peak around 13.5 mL as for the elution profile of the samples incubated with 20 mM ATP (Figure 3.4 B green trace). The profile represented by the green trace in Figure 3.4 B was determined by a Gaussian fit of 10 elution profiles. This profile is highly reproducible, and the protein is fully active as described in detail in Chapter 4.

### **3.3.4 Different mutations of the ATPase and protease domain may affect the elution profile**

Three AaFtsH mutants were produced by SDM. The R316L mutant, which has a mutation at position 316, changing an arginine (R) for a leucine (L), is described in literature as having no *in vivo* protease activity and no *in vitro* ATPase activity, although there are suspicions that ATP still binds to the ATPase domain [12]. Since no ATPase activity is detected *in vitro* for the R316L mutant, the effect of an incubation in presence of ATP was tested for the AaFtsH R316L mutant. The expression and purification protocol of the R316L mutant is the same as the one optimized for AaFtsH wild type (WT). The fractions resulting of the HisTrap chromatography were subjected to an incubation with 10 and 20 mM ATP at 60°C overnight (Figure 3.5 A orange and blue traces respectively). Both conditions show a three-peak profile: the first peak elutes at 12.1 mL with an estimated molecular weight of 940 kDa, while the second peak has a molecular weight of around 763 kDa eluting at 13.2 mL, and the third peak elutes at 15.2 mL with an estimated molecular weight of 441 kDa (Figure 3.5 A).

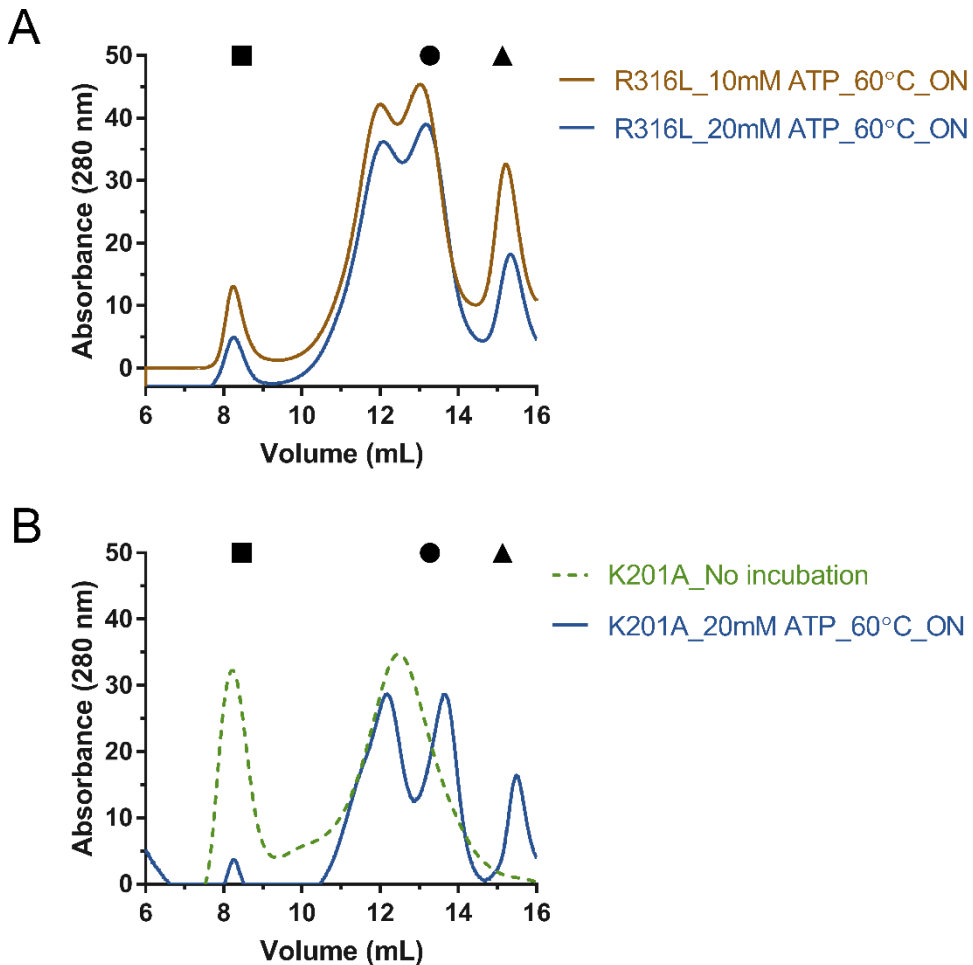


**Figure 3.5 - Size exclusion elution profiles of the R316L (A) and the K201A (B) mutants.** Both HisTrap fractions were incubated with 20 mM ATP at 60°C overnight. The R316L was also incubated with 10 mM ATP. The K201A was also directly loaded into the SEC (traced green line). Blue Dextran (■) is used to calculate the void volume of the column (8.47mL). The elution volumes of standard proteins used to estimate the molecular weight of the eluted fractions are shown on the top of the graph: (●) Tyroglobulin (MW: 669 kDa;  $V_e$ : 13.27 ml), (▲) Ferritin (MW: 440 kDa;  $V_e$ : 15.13 ml), (◆) Aldolase (MW: 158 kDa;  $V_e$ : 16.62 ml) and (★) Ovalbumin (MW: 44kDa;  $V_e$ : 17.76 ml).

The K201A was commercially produced having as template the pET22b of AaFtsH, with the mutation at position 201 corresponding to the change of a lysine (K) for an alanine (A). This mutant is described in literature as not having ATPase activity and

not binding ATP [13]. The fractions from the first step of purification were directly loaded into the SEC and the elution profile shows a first peak of aggregates and a second wide peak with its maximum around 12.5 mL (estimated molecular weight of 876 kDa) (Figure 3.5 B dashed green trace). The K201A fractions that were incubated with 20 mM ATP at 60°C overnight show sharper peaks at 12.2, 13.7 and 15.5 mL of elution volume (Figure 3.5 B blue trace).

The two other AaFtsH mutants produced by SDM are: H418Y which has a mutation at position 418 (a histidine (H) is replaced by a tyrosine (Y)), and K201A\_H418Y which is a mutant that has both the H418Y mutation and the K201A mutation). The mutation at position 418 leads to complete loss of FtsH protease activity [14]. The fractions obtained from the HisTrap purification step were first directly loaded into the size exclusion chromatography. The profile in Figure 3.6 A (dashed blue line) shows the elution of a single broad peak at 12.4 mL and a first peak of aggregates. The fraction that was incubated with AMP-PNP at 60°C for 3 hours also shows aggregates and higher peak at 12.5 mL and a smaller peak at 13.9 mL (Figure 3.6 A green trace). The big differences, compared with this last profile, are seen when comparing the elution profiles of the samples incubated at 4 and 60°C (Figure 3.6 orange and red traces). Both elution profiles show a sharper second peak that elutes at 13.8 mL while the first peak is a small shoulder which elutes at 12.5 mL. Finally, a significant difference is seen when observing the elution profile of the fractions which were incubated at 60°C overnight with 20 mM ATP (Figure 3.6 A purple trace). The profile shows a sharp peak which elutes at 14.1 mL (estimated molecular weight 618 kDa) with a smaller shoulder. All the elution profiles of the H418Y samples that were incubated with nucleotides show a peak at 15.7 mL which the SDS-PAGE gel analysis proves not to belong to FtsH (Supplementary Figure 3.2). In Supplementary Figure 3.2 a representative SDS-Page gel example is provided for the H418Y since the separation of the fractions on the gel does not change depending on the conditions in which the samples were incubated. The protein eluted from the second peak (14.1 mL).

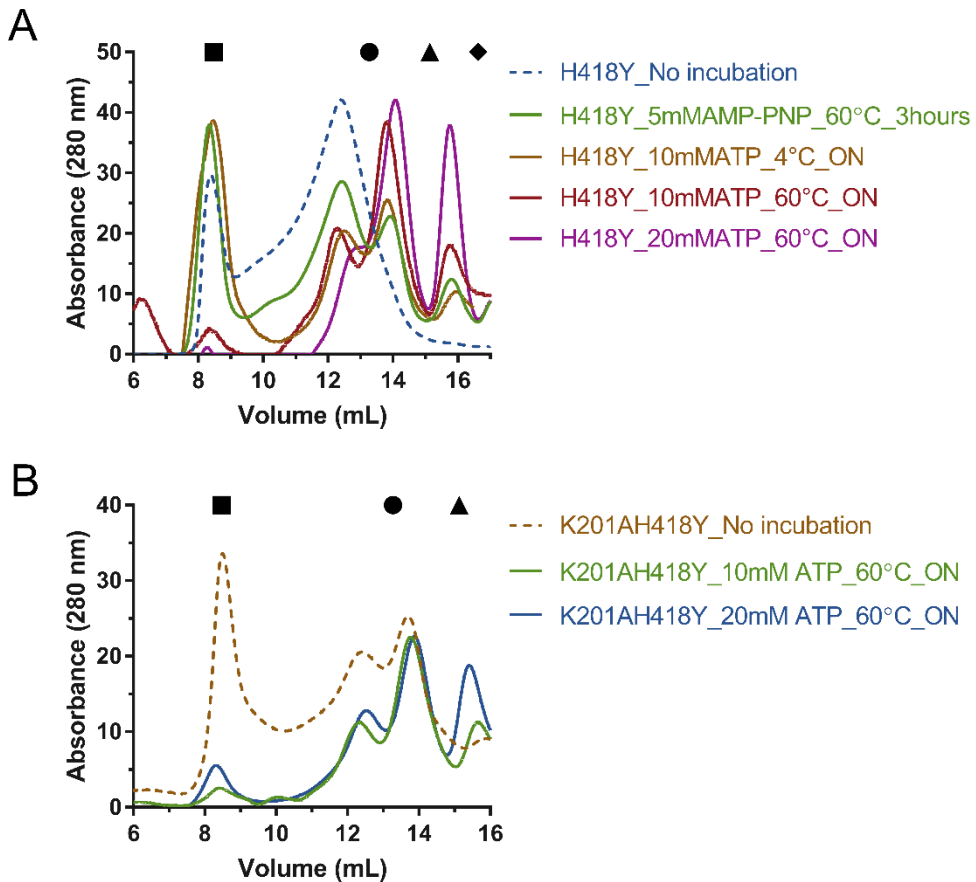


**Figure 3.6 – The elution profile of the size exclusion chromatography of the H418Y and K201A\_H418Y mutants (A and B).** Both fractions were either directly loaded into the Superose 6 10/300 GL (profiles represented by the dashed lines in both chromatograms) or incubated with nucleotides at different temperatures (nucleotide concentration, incubation temperature and incubation time are shown in the legend). Blue Dextran (■) is used to calculate the void volume of the column (8.47mL). The elution volumes of standard proteins used to estimate the molecular weight of the eluted fractions are shown on the top of the graph: (●) Tyroglobulin (MW: 669 kDa; V<sub>e</sub>: 13.27 ml), (▲) Ferritin (MW: 440 kDa; V<sub>e</sub>: 15.13 ml) and (◆) Aldolase.

The purification of the K201A\_H418Y mutant was performed in a two-step purification. In a first assay, the samples eluted from the first purification step (the affinity chromatography) were directly loaded into the SEC (Figure 3.6 B orange dashed trace). This mutant is the only one presented in this thesis in which the SEC profile of the sample directly loaded into the SEC gives two peaks. An aggregation

peak is first observed, followed by a peak that elutes at 12.4 mL and a second one at 13.8 mL, both are broad peaks. The incubation of the HisTrap fractions with 10 and 20 mM ATP at 60°C overnight leads to a similar SEC profile (Figure 3.6 B green and blue traces). A first peak at 12.5 mL is followed by a second one at 13.9 mL, sharper and higher than the first one. The third peak is also observed, and this was also analysed by SDS-Page gel showing that no band corresponding to AaFtsH molecular weight was present (an example of the profile of the SDS-Page gel for this case is given in Supplementary Figure 3.2). The negatively stained samples resulting of the H418Y and K201A\_H418Y purification after incubated at 60°C with 20 mM ATP overnight, show an increase of the amount of the hexameric particles on the grid (Figure 3.7 A and B)

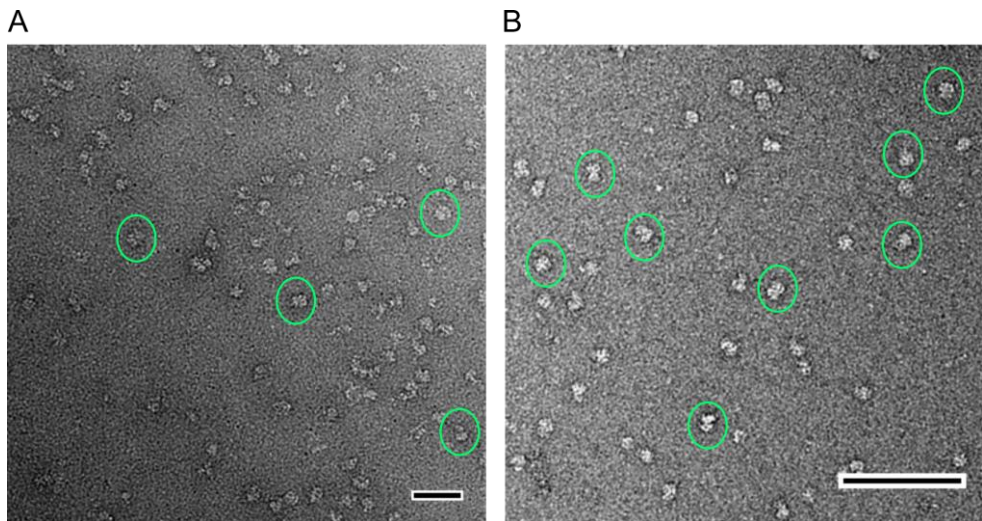


**Figure 3.7 – Negatively stained samples of the purified mutants H418Y (A) and K201A\_H418Y (B) after incubation at 60°C overnight with 20 mM ATP.** Scale bars are 500 Å.

### 3.3.4.1 Mutants protease activity measurements

Protease activity tests were performed for the four mutants produced in this chapter. The protocol used for the protease activity tests is explained in Chapter 4. To assess the protease activity of the different mutants, 2  $\mu$ M of AaFtsH purified by SEC after incubation with 20 mM ATP at 60°C overnight was used. The samples corresponding to the dodecamers (first peak) and the hexamers (second peak) were tested

separately at 0/30/60 min time points (Figure 3.8). The protease activity measurements corresponding to the wild type AaFtsH and a control with no protein are also plotted for further comparison. As can be observed, the only mutant that shows some remaining activity is K201A. Compared with the WT AaFtsH, this mutant shows a decrease of 60% in its proteolytic activity, which means that even though it cannot bind ATP, this mutant is still capable of degrading a substrate in its proteolytic chamber.

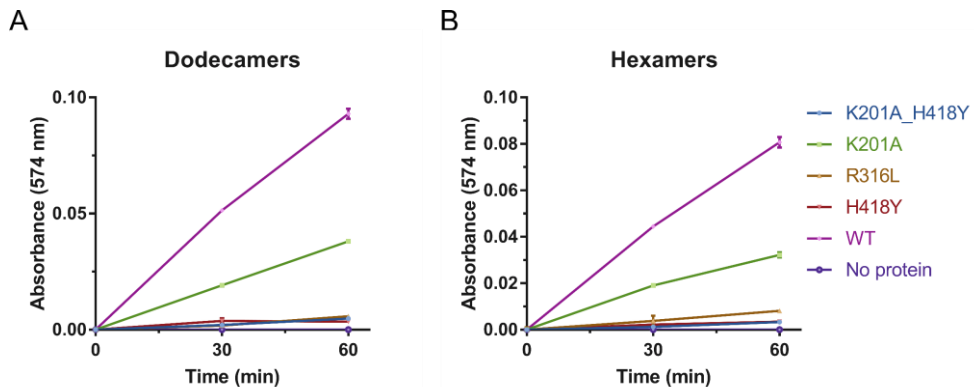


**Figure 3.8 – The proteolytic activity of the four mutants, the WT AaFtsH and the negative control with no protein is plotted for the dodecamer and hexamer fractions (A and B).** The fractions studied here come from the SEC purification performed after the incubation of the different samples with 20 mM ATP at 60°C overnight. Protease activity was measured for 0/30/60 min with 10 mM ATP as described in 4.2.4. All experiments were replicated three times and the standard deviations are plotted, although for some of the measurements they are not visible, since they are smaller than the thickness of the line.

### 3.4 Discussion and conclusions

As demonstrated in Chapter 2 the expression and purification of FtsH reveals to be challenging, especially with the goal of obtaining samples with a high purity and stability in solution to be used for structural studies. For that reason, this chapter describes different purification protocols to help understanding the behaviour of the protein when solubilized with detergent. The choice of the *Aquifex aeolicus* construct was made with the intention to work with a more stable protein, since this microorganism is a thermophile which lives under extreme temperature conditions

[1]. The AaFtsH sample indeed revealed to be more resistant to several conditions and extreme temperatures. This is first shown by the observation of the high protease activity when FtsH was incubated with the substrate at 50°C and in presence of imidazole (Figure 3.1 B, C and D). After following the same purification protocol as in Vostrukhina et al. [3] the elution profile shows no sharp peak of pure AaFtsH. However, this elution profile is not new to the scientific community since other FtsH homologous, from which mainly only FtsH cytoplasmic domain was purified [5,6,15,16] or the full-length FtsH [17], also do not elute purely in the hexameric form.

The elution profiles reported in this chapter show that the protein tends to elute not only as a hexamer but also as dodecamers (earlier peak in the SEC profile), this phenomenon is explained later in Chapter 4. Both SEC fractions of the WT AaFtsH showed ATPase and protease activity, which means that the dodecamer conformation is stable. For this reason, we believe that the previous mechanistic models described for FtsH function is different than what was previously reported. We explore this hypothesis further in the following chapter. Although this is an important finding for the scientific community, a FtsH full-length structure is still needed. To reach a high amount of pure AaFtsH hexamers, we tried to “freeze” the ATPase and protease domains of this highly dynamic protein by introducing mutations that interfere with FtsH activity, and by using chemically inhibitors/enhancers of FtsH activity.

To decrease the motion of the ATPase arms or completely “freeze” them, we tested a series of inhibition and stimulation of the ATPase domain. For this we used three types of ATPase and protease activity inhibitors: 1,10 – phenanthroline, ADP and AMP-PNP; which were incubated with purified samples. Despite ADP being reported to be an inhibitor for the ATPase activity, no effect was seen in the chromatography profile after incubating AaFtsH with this nucleotide [18] (Figure 3.2 B). This could mean that ADP is not capable of occupying the ATPase site and maintaining the protein in a stable state, leading to a disruption of the hexamers, which would be consistent with the SEC showing a broad peak. For this reason, we tried to replace

the ATP molecules, inside the ATPase domain, by other molecules that are not hydrolysable by AaFtsH and which decrease FtsH proteolytical activity, such as *o*-phenanthroline and AMP-PNP [10,17,18]. The incubation with these two inhibitors shows that indeed the samples which were incubated with AMP-PNP, a nucleotide that cannot replace ATP in the hydrolysis process, is the most effective at obtaining an elution profile in which one of the peaks contains AaFtsH hexamers plus the LMNG micelle molecular weight (this concept is further explored in Chapter 4). Moreover, the SEC profile resulting from the incubation with AMP-PNP shows a first eluted peak with an estimated molecular weight of 876 kDa compatible with the molecular weight of two hexamers in the same micelle complex, as the negatively stained electron microscopy analysis show on the grid bigger particles with the expected shape (Figure 3.3 B and C). The fact that the formation of the dodecamers is not blocked by the addition of both ATPase and protease inhibitor led us to think that some stronger stabilization of both ATPase and protease domains was mandatory to obtain a pure sample of AaFtsH hexamers. The fact that a protease inhibitor can promote the hexameric form of the protein, indicates that the proteolytical domain also plays a crucial role in the stabilization of AaFtsH in solution.

But since the use of inhibitors did not prevent the formation of particles larger than AaFtsH hexamers efficiently, we tried to stabilize the protein by incubating the protein at various temperatures and ATP concentrations before loading onto the SEC column. It was found that changes in temperature and ATP concentrations in the medium are key to separate the dodecamers from the hexamers. Moreover, protease activity tests were performed to all fractions eluted from the SEC profile, showing that the eluted protein maintains its proteolytic activity. An incubation step with 20mM ATP at a temperature of 60°C was found to be optimum and to lead to a SEC profile that was highly reproducible as discussed further in Chapter 4.

Although a satisfactory condition to purify AaFtsH (incubation with 20 mM ATP at 60°C overnight) was found, we considered mutating one of the AaFtsH domains to further stabilize the protein and favour the hexameric conformation. Four mutants were produced, one in which the protein can bind but cannot hydrolyse ATP thereby

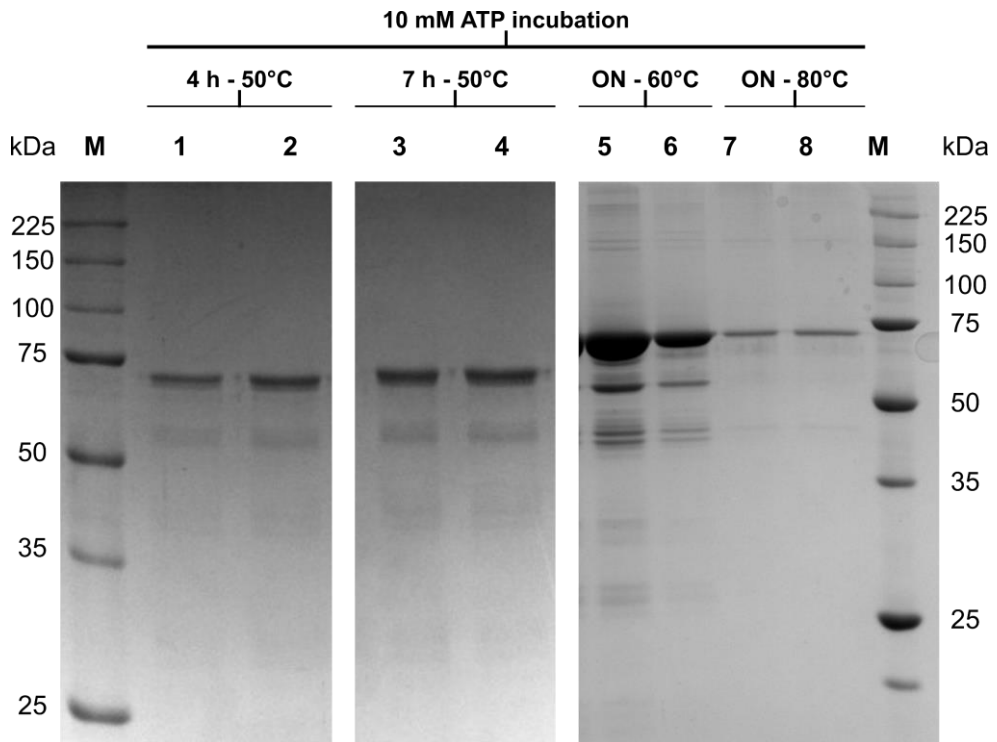
losing its protease activity (R316L), another which cannot bind ATP at all but keeps some protease activity (K201A), a third one which does not have proteolytic activity (H418Y), and finally a fourth one which does not have ATPase nor proteolytic activity (K201A\_H418Y) [5,12,14,19]. The characteristics of these mutants are linked with the role of the mutated amino acid in the protein structure: R316 is one of the arginine fingers which is linked to FtsH oligomerization state; K201 is part of the Walker A motif and coordinates the ATP binding and hydrolysis; and H418 is part of the HEXXH motif responsible for the coordination of the zinc ion via the two histidine during the proteolytic process [3,6]. The protease assays performed in this chapter compare the protease activity of each of the mutants with the activity of the WT AaFtsH. The results agree with what is described in literature. The K201A maintains 60% of the protease activity when compared with the WT AaFtsH, which means that although this mutant does not bind any ATP there is still some remaining activity that leads to the proteolytic process.

The purification of AaFtsH mutants showed to be more challenging than expected. When directly loading the HisTrap fractions into the SEC, K201A and H418Y mutants' elution profile still showed a broad peak where no clear hexameric peak is identified (Figure 3.5 B and Figure 3.6 A), while the K201A\_H418Y showed a different result, which might be related to the fact that indeed the protein is in a more frozen conformational when not having either protease or ATPase activity. In the SEC profile, a second peak is present which indicates that this mutant is more prone to form the hexameric form (Figure 3.6 B dashed trace). For that reason, and gathering all the information previously collected, two incubation conditions were tested at 60°C overnight with 10 and 20 mM ATP which show a clear increase of the amount of AaFtsH hexamers. Testing a new condition of higher temperature was not explored for this mutant since, as previously shown at 80°C in 3.3.3, this leads to aggregation/degradation of AaFtsH. A significant effect on the oligomeric state is noticed when purifying H418Y (in presence of 20 mM overnight at 60°C, Figure 3.6 A purple trace). These are encouraging results that show that point mutations, of the protease domain isolated (H418Y) and in combination with the K201A mutation of the ATPase domain (preventing binding to ATP) (K201A\_H418Y), lead to a more

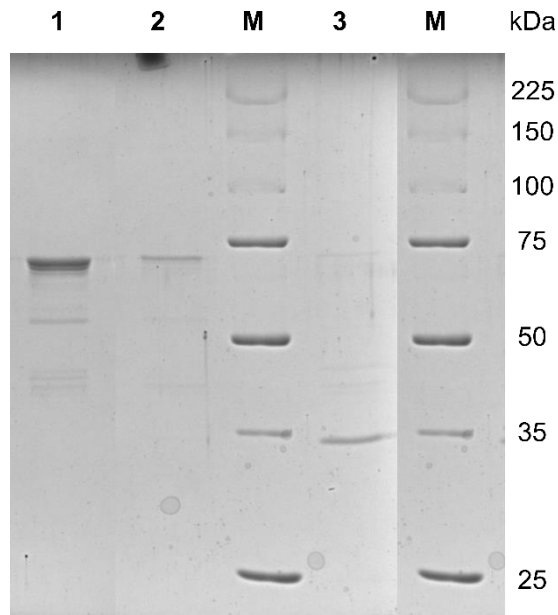
satisfactory profile where most of the sample is purified in its hexameric shape. The negatively stained microscopy analysis also shows that the type of particles obtained from the purification of these two mutants is mainly hexameric (Figure 3.7). An alternative approach to increase even more the amount and purity of AaFtsH hexamers is to produce mutants in which the amino acids have a higher crucial role in the oligomeric state of the protein, which from our observations should relate to the loss of proteolytical and ATPase activity. A suggestion is to test the expression and purification of the same construct that Vostrukhina et al. suggest, the mutation of the glycine (G399L) amino acid positioned in the linker between the AAA and proteolytical domain, since it is described that this mutant retains only 5% of the proteolytical activity and 40% of the ATPase activity.

We conclude that the work presented in this chapter is of major importance, showing the capability of alternatives to the standard purification protocols in which normally only purification methods are employed without in-between incubation steps. In this chapter, we report the use of chemicals and temperature to favour the more stable hexameric conformation. Also, important knowledge was acquired regarding AaFtsH stability at high temperatures and in presence of diverse nucleotides. This knowledge can be further explored to achieve even more stable and pure AaFtsH in solution.

### 3.5 Supplemental data



**Supplementary Figure 3.1 – The peaks resulting from the size exclusion profile, after an incubation of the NiNTA fractions with 10 mM ATP were loaded into a SDS-Page gel.** In 1 and 2 the first and second peak of the incubation for 4 hours at 50°C are shown, while in 3 and 4 the first and second peak of the incubation for 7 hours at 50°C, in 5 and 6 the first and second peaks after an incubation at 60°C over-night and 7 and 8 correspond to the first and second peaks after an incubation at 80°C over-night. The molecular markers (M).



**Supplementary Figure 3.2 – SDS-Page gel loaded with the fractions from H418Y mutant elution from the SEC.** The first and second peak (1 and 2) contain the corresponding band to the protein size around 72 kDa, while the third peak (3) eluted contains a protein of around 35 kDa that does not correspond to AaFtsH size. The molecular markers (M).

### 3.6 References

- [1] A. Razvi, J.M. Scholtz, Lessons in stability from thermophilic proteins., *Protein Science: A Publication of the Protein Society*. 15 (2006) 1569–78.
- [2] G. Deckert, P. V. Warren, T. Gaasterland, W.G. Young, A.L. Lenox, D.E. Graham, R. Overbeek, M.A. Snead, M. Keller, M. Aujay, R. Huber, R.A. Feldman, J.M. Short, G.J. Olsen, R. V. Swanson, The complete genome of the hyperthermophilic bacterium *Aquifex aeolicus*, *Nature*. 392 (1998) 353–358.
- [3] M. Vostrukhina, A. A. Popov, B. E. Brunstein, C, M.A. Lanz, D. A, R. Baumgartner, A, C. Bieniossek, E. A, M. Schacherl, C, A. Ulrich, Baumann, C, \*, The structure of *Aquifex aeolicus* FtsH in the ADP-bound state reveals a C2-symmetric hexamer, *Acta Crystallogr D Biol Crystallogr*. D71 (2015) 1307–1318.
- [4] R. Suno, M. Shimoyama, A. Abe, T. Shimamura, N. Shimodate, Y.-H. Watanabe, Y. Akiyama, M. Yoshida, Conformational transition of the lid helix covering the protease active site is essential for the ATP-dependent protease activity of FtsH, *FEBS Letters*. 586 (2012) 3117–3121.
- [5] C. Bieniossek, B. Niederhauser, U.M. Baumann, The crystal structure of apo-FtsH reveals domain movements necessary for substrate unfolding and translocation., *Proceedings of the National Academy of Sciences of the United States of America*. 106 (2009) 21579–21584.
- [6] C. Bieniossek, T. Schalch, M. Bumann, M. Meister, R. Meier, U. Baumann, The molecular architecture of the metalloprotease FtsH., *Proceedings of the National Academy of Sciences of the United States of America*. 103 (2006) 3066–3071.
- [7] W. Wang, S. Nema, D. Teagarden, Protein aggregation—Pathways and influencing factors, *International Journal of Pharmaceutics*. 390 (2010) 89–99.
- [8] Y. Shotland, S. Koby, D. Teff, N. Mansur, D.A. Oren, K. Tatematsu, T. Tomoyasu, M. Kessel, B. Bukau, T. Ogura, A.B. Oppenheim, Proteolysis of the phage lambda CII regulatory protein by FtsH (HflB) of *Escherichia coli*, *Molecular Microbiology*. 24 (1997) 1303–1310.
- [9] T. Okuno, K. Yamanaka, T. Ogura, An AAA protease FtsH can initiate proteolysis from internal sites of a model substrate, apo-flavodoxin., *Genes to Cells*. 11 (2006) 261–8.
- [10] T. Tomoyasu, J. Gamer, B. Bukau, M. Kanemori, H. Mori, A.J. Rutman, A.B. Oppenheim, T. Yura, K. Yamanaka, H. Niki, *Escherichia coli* FtsH is a membrane-bound, ATP-dependent protease which degrades the heat-shock transcription factor sigma 32., *The EMBO Journal*. 14 (1995) 2551–2560.

- [11] T. Okuno, T. Yamada-Inagawa, K. Karata, K. Yamanaka, T. Ogura, Spectrometric analysis of degradation of a physiological substrate sigma32 by *Escherichia coli* AAA protease FtsH., *Journal of Structural Biology*. 146 (2004) 148–54.
- [12] K. Karata, T. Inagawa, A.J. Wilkinson, T. Tatsuta, T. Ogura, Dissecting the role of a conserved motif (the second region of homology) in the AAA family of ATPases. Site-directed mutagenesis of the ATP-dependent protease FtsH., *The Journal of Biological Chemistry*. 274 (1999) 26225–32.
- [13] M.M.K. Jayasekera, S.K. Foltin, E.R. Olson, T.P. Holler, *Escherichia coli* requires the protease activity of FtsH for growth., *Archives of Biochemistry and Biophysics*. 380 (2000) 103–7.
- [14] N. Saikawa, K. Ito, Y. Akiyama, Identification of Glutamic Acid 479 as the Gluzincin Coordinator of Zinc in FtsH (HflB), *Biochemistry*. 41 (2002) 1861–1868.
- [15] Y. Akiyama, Proton-motive force stimulates the proteolytic activity of FtsH, a membrane-bound ATP-dependent protease in *Escherichia coli*., *Proceedings of the National Academy of Sciences of the United States of America*. 99 (2002) 8066–8071.
- [16] R. Suno, H. Niwa, D. Tsuchiya, X. Zhang, M. Yoshida, K. Morikawa, Structure of the Whole Cytosolic Region of ATP-Dependent Protease FtsH, *Molecular Cell*. 22 (2006) 575–585.
- [17] R.L. Bruckner, Robert C.; Gunyuzlu, Paul L. and Stein, Coupled Kinetics of ATP and Peptide Hydrolysis by *Escherichia coli* FtsH Protease, *Biochemistry*. 42 (2003) 10843–10852.
- [18] Y. Asahara, K. Atsuta, K. Motohashi, H. Taguchi, M. Yohda, M. Yoshida, FtsH recognizes proteins with unfolded structure and hydrolyzes the carboxyl side of hydrophobic residues., *Journal of Biochemistry*. 127 (2000) 931–7.
- [19] P.I. Hanson, S.W. Whiteheart, AAA+ proteins: Have engine, will work, *Nature Reviews Molecular Cell Biology*. 6 (2005) 519–529.

# Chapter 4

## Large conformational changes in FtsH create an opening for substrate entry

Protein structural rearrangements during mechanical processes leading to proteolysis are of interest by the scientific community. In the case of FtsH, few details of these rearrangements in relation to the membrane are known. In this chapter we show that the AAA domain can tilt much more than previously reported. Creating a large gap between the membrane and the AAA domain. Structural rearrangements are explained and shown by the protein activity assays and electron microscopy studies.

\*Parts of this chapter is included in: *V. Carvalho, R. Kieffer, N. de Lange, A. Engel, M.E. Aubin-Tam, submitted (2018)*

## 4.1 Introduction

Reported FtsH structural studies have used truncated FtsH forms with only the soluble C-terminal (cytosolic) part [1–7] or with only the periplasmic domain [8]. The single full-length structure concerns m-AAA, the yeast mitochondrial ortholog of bacterial FtsH, which has been resolved at 12 Å resolution by cryo-electron microscopy [9]. Therefore, no information on the conformational rearrangement of full-length FtsH in relation to the membrane when bound to nucleotides or to a substrate is available. Crystal structures of the cytosolic domain of FtsH exhibit a six- [1], a two- [2–5] or a three-fold [4] symmetric conformation of the ATPase domain. These different conformations suggest that the ATPase domain could move polypeptides in steps as long as 45 Å into the central cavity during ATP hydrolysis cycles [1]. In contrast, the C-terminal protease domain always shows a six-fold symmetry for all crystal structures, i.e., the cytosolic domain of *Thermus thermophilus* FtsH (15), of *Thermotoga maritima* FtsH [1,5] and of *Aquifex aeolicus* FtsH [2,4]. The proposed mechanism for substrate entry in m-AAA is based on substrate recognition by solvent exposed lateral regions of FtsH cytosolic domain. Accordingly, a 13 Å gap between the membrane and the cytosolic domain observed by cryo-electron microscopy would provide access to substrate, which implies that only (partly) unfolded proteins can reach the translocating loops and be moved through the pore for degradation [9].

Here we report the first full-length structure of *Aquifex aeolicus* FtsH (AaFtsH), which we determined by negative stain electron microscopy to a resolution of 20 Å. Unexpectedly, upon detergent solubilisation not only hexamers of AaFtsH formed, but also fully stable and active dodecamers of AaFtsH. The dodecamer structure is solved to a resolution of 25 Å, showing two AaFtsH hexamers sharing a single Lauryl Maltoside Neopentyl Glycol (LMNG) micelle, with the periplasmic domain of one hexamer touching the cytosolic domain of the other hexamer. This arrangement induces a tilt of the periplasmic domain with respect to the cytoplasmic domain. While AaFtsH hexamers and dodecamers have similar ATPase and proteolytic activity, the latter exhibit a substantial larger gap between the cytosolic domain and

the transmembrane domain. Therefore, we propose that the cytosolic domain can tilt with respect to the membrane plane for substrates to reach the translocating pore loops, as required for substrate unfolding and degradation.

## 4.2 Materials and methods

### 4.2.1 AaFtsH expression and purification

Full-length *Aquifex aeolicus* FtsH (AaFtsH) cloned into pET22a vector was kindly granted by Ulrich Baumann and the same expression conditions were employed [2]. Cells were harvested at 3500 g for 25 min at 4 °C and disrupted in a cell disruptor. The resulting cell debris was purified at 20000 g for 15 min and membranes were isolated at 125000 g for 3 hours. Membranes were solubilised in 20 mM Tris-HCl pH 8.0; 150 mM NaCl; 1%(w/v) Lauryl Maltose Neopentyl Glycol (LMNG) (Anatrace) for 3 hours at 4 °C and cleared at 125000 g for 1 hour at 4 °C. The sample was first purified by affinity chromatography, using a HisTrap-5 mL column (GE Healthcare). FtsH fractions were eluted in 20 mM Tris-HCl pH 8.0; 500 mM NaCl; 0.01%(w/v) LMNG and 200 mM imidazole. AaFtsH fractions were then incubated at 60 °C overnight with 20 mM ATP; 10 mM MgCl<sub>2</sub>; and 25 μM ZnCl<sub>2</sub> or directly loaded into the SEC. The incubated sample or the sample directly eluted from the HisTrap column, were concentrated to 500 μL and loaded into a SEC Superose 6 Increase 10/300 GL column (GE Healthcare) pre-equilibrated with 10 mM Tris-HCl pH8.0; 150 mM NaCl; 0.01%(w/v) LMNG; 5% Glycerol. After analysis of the SEC profile was possible two peaks were detected, and the second peak was reloaded onto the SEC to assess the composition of the second peak alone. AaFtsH monomer concentration was measured with a Nanodrop. A representative SEC run is plotted in Figure 4.1 A. The elution volume value was determined by the centre position of the two largest peaks by fitting Gaussian functions to 10 SEC profiles which are plotted in Supplementary Figure 4.1. A calibration curve of the Superose 6 Increase 10/300 GL was performed using the Gel Filtration High Molecular Weight Calibration Kit (GE Healthcare), following the GE Healthcare instructions. AaFtsH fractions were

analysed by Native PAGE gels using the MiniPROTEN®TGX™ Precast Protein Gels (Biorad).

### **4.2.2 Transmission Electron Microscopy analysis**

3  $\mu$ L of AaFtsH dodecamer or hexamer fractions was loaded on a carbon-coated 400 square mesh copper grid (Aurion) previously glow-discharged for 1 min. The liquid drop was absorbed with filter paper after 1 min and quickly washed with a drop of water that was again blotted with filter paper. This procedure was repeated 3 times to rinse all the detergent present in the samples. Finally, a 3  $\mu$ L drop of 3 % uranyl-acetate was added to the grid, incubated for 1 min and absorbed with a filter paper. Transmission electron microscopy was performed using a Philips CM-200T and a JEOL 3200 FSC both equipped with a TemCam-F416 (TVIPS) and recorded at 50000x magnification using the EM-MENU software with a sampling rate of 2.23  $\text{\AA}$ /pixel.

### **4.2.3 ATPase activity**

The ATPase activity was measured using the High Throughput Colorimetric ATPase Assays kit (Innova Biosciences). Free phosphate from the AaFtsH dodecamers and hexamers was eliminated by an incubation with 100  $\mu$ L of PiBind™ resin (Innova Bioscience) for 30 min. Also mix A [50 mM Tris-HCl pH 8.0; 150 mM NaCl; 10 mM MgCl<sub>2</sub>], was previously incubated with PiBind™ resin (Innova Bioscience). Initial ATPase activity assays were performed in presence of 2 or 5 mM ATP, started by mixing AaFtsH (2  $\mu$ g) in mix A. Reaction rates were measured in one time point of 60 min. 25 $\mu$ L of PiColorLock™ mix was added to stop the reaction, and after 5 min, 10  $\mu$ L of stabiliser reagent was added. OD650 was measured after 30 min using a CLARIOstar (BMG-Labtech) microplate reader. With the goal of studying the influence in the medium of other components the ATPase activity was measured in presence of 2 mM ATP and 2  $\mu$ g of AaFtsH, adding 50  $\mu$ M ZnAc, 100  $\mu$ M ZnAc or 4  $\mu$ M Sigma 32 (purified in house as described in 4.2.5).

For detailed description of the AaFtsH ATPase activity, reactions were started by mixing AaFtsH (0.25  $\mu$ M final concentration) in mix A with either 50, 100, 250, 500, 1000, or 1800  $\mu$ M ATP (final concentrations). Reaction rates were measured every

2 min for a total of 10 min, in triplicates. ATP concentrations were chosen such that the maximum concentrations were more than 10x the previously reported  $K_M$  values [10,11]. 25  $\mu$ L of PiColorLock<sup>TM</sup> mix was added to stop the reaction, and after 5 min, 10  $\mu$ L of stabiliser reagent was added. OD650 was measured after 30 min using a CLARIOstar (BMG-Labtech) microplate reader, every replica was measured 3 times and an average of these readings was calculated for each replica (Supplementary Figure 4.2). Released Pi concentrations were calculated from a calibration curve of standard Pi concentrations measured.  $K_M$  and  $K_{cat}$  were calculated for both hexamers and dodecamers. Michaelis-Menten constants were obtained, assuming the steady-state of the reaction, with GraphPad Prism software with a 95% Confidence Interval (CI).

#### **4.2.4 Protease activity**

AaFtsH protease activity was assessed using the Resorufin labelled casein kit (Roche). 0.25, 0.5, 1.0 or 2.0  $\mu$ M (final concentrations) of AaFtsH dodecamers or hexamers were incubated with 50  $\mu$ M of resorufin labelled casein in [50 mM Tris-HCl pH 8.0; 80 mM NaCl; 12.5  $\mu$ M ZnCl<sub>2</sub>; 5 mM MgCl<sub>2</sub>; 1 mM dithiothreitol; 0.01% LMNG and 10 mM ATP] at 60 °C. Triplicates of these measurements were taken. Reaction rates were measured every 10 min for 30 min (Supplementary Figure 4.3). 160  $\mu$ L of 5% trichloroacetic acid was added and incubated at 37 °C for 30 min. Proteins were precipitated at 16100 g for 30 min and 120  $\mu$ L from the supernatant was mixed with 80  $\mu$ L of 500 mM Tris-HCl pH 8.8 and added to a 96 well transparent plate. The OD574nm was immediately measured using an Infinite® 200PRO (TECAN) plate reader.

#### **4.2.5 Activity assay in presence of the physiological substrate**

GST-Sigma 32 factor was kind gift of Okuno, et al [12] and the same purification protocol was performed to obtain pure Sigma 32 factor. The activity assay was performed mixing 2  $\mu$ M of AaFtsH with 1  $\mu$ M Sigma 32 in presence of 50 mM Tris-HCl pH 8.0; 80 mM NaCl; 12.5  $\mu$ M ZnCl<sub>2</sub>; 5 mM MgCl<sub>2</sub>; 1 mM dithiothreitol; 0.01% LMNG and 10 mM ATP or 10 mM ADP. The Sigma 32 degradation by AaFtsH was

detected by SDS-Page gel analysis. Both AaFtsH fractions eluting from the SEC were tested for its capability to degrade Sigma 32, but also the AaFtsH fraction eluting directly from the HisTrap was used to perform this assay.

#### **4.2.6 Sequence alignment and structure prediction**

The AaFtsH and *E. coli* FtsH sequences were aligned with ESPript 3 [13]. Part of the AaFtsH sequence (1-144 aa) sequence was submitted to different transmembrane helices structure predictors: RHYTHM [14], CCTOP [15], TMHHM [16], HMMTOP [17], TOPCONS [18] and TMpred (Expasy) [19]. Prediction of the transmembrane helices was performed to identify the beginning of the linker between membrane and AAA domains. To explore whether this 20 aa linker has a known structure, part of the sequence (110-148) was submitted to the structure predictors SCRATCH [20], PRE-FOLD 3 [21] and PREDICTPROTEIN [22]. Sequence similarity search was performed with BLAST (blast.ncbi.nlm.nih.gov) [23]. Residue conservation was assessed with the ConSurf server [24].

#### **4.2.7 Imaging Processing of negatively stained single particles**

Single particle imaging processing was performed using Xmipp and Eman, using Scipion 1.1 interface [25] and Eman2.12 software packages [26]. A set of 15000 particles was manually picked using a semi-automated mode, the particles were 2D averaged into 100 classes. To measure the dimensions of the negatively stain particles two approaches were taken. First, the height of dodecamers and hexamers was measured directly from 280 particles in the micrographs. Measurements referring to the different domains were done on 10 class averages chosen. The resolution of the maps was calculated from the Fourier Shell Correlation (FSC) values as implemented in Eman2.12. Using Chimera4.0.4 [27] different crystal structures of the cytoplasmic domain *Aquifex aeolicus* (PDB 4WW0), the CryoEM of the full-length m-AAA (EMDB 1712) and the crystal structure of the *E. coli* periplasmic domain (PDB 4V0B) were automatically fitted into our 3D map.

## 4.3 Results

### 4.3.1 Full-length AaFtsH purification

AaFtsH with a C-terminal His-tag was overexpressed in *E. Coli* cells and extracted from purified membranes with the use of a mild detergent, LMNG [28]. Ni-NTA chromatography followed by size-exclusion chromatography (SEC) using Superose 6 10/300 GL yielded pure AaFtsH complexes (Figure 4.1). Best results were obtained by incubating the AaFtsH containing fractions, collected from Ni-NTA chromatography, overnight at 60°C in presence of 20 mM ATP, 10 mM MgCl<sub>2</sub> and 25 μM ZnCl<sub>2</sub> just before the SEC purification. The SEC profile shows a first peak that is centred at 12.1 mL ± 0.2 mL (SD, N=10) and a second peak at 13.4 mL ± 0.2 mL (SD, N=10) (Figure 4.1 A green trace). Peak positions are determined by simultaneously fitting two Gaussian functions. Native gel electrophoresis suggests that the second peak likely contains hexameric AaFtsH as it runs at ~700 kDa, while the first peak indicates a higher oligomeric state (Figure 4.1 B). The molecular weight of the eluted complexes was estimated using the partition coefficient ( $K_{av}$ ) values extracted from a calibration curve of the Superose 6 column, and the positions of fitted Gauss functions. The second peak is centred at a molecular weight of 730 kDa, which is larger than the size expected for AaFtsH hexamers (~432 kDa). Extrapolating the calibration curve to smaller elution volumes, the first peak corresponds to a molecular weight of 940 kDa. The non-incubated sample was directly loaded into a SEC after eluting from the Ni-NTA (Figure 4.1 A dashed trace).

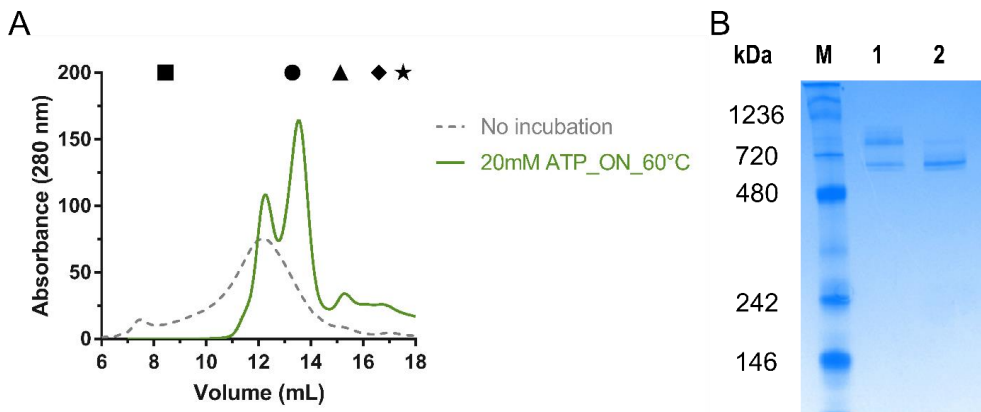


**Figure 4.1 – Size exclusion profile and native gel of *Aquifex aeolicus* FtsH.**

FtsH oligomers elute in two peaks from sizing chromatography. A - Representative size exclusion chromatography run of the elution profile after incubation at 60°C ON (green trace) and from the elution profile with no incubation after elution from the NiNTA (dashed trace). Blue Dextran (■) used to calculate the void volume of the column (8.47mL). The elution volumes of standard proteins used to estimate the molecular weight of the eluted fractions are shown on the top of the graph: (●) Tyroglobulin (MW: 669 kDa; Ve: 13.27 ml), (▲) Ferritin (MW: 440 kDa; Ve: 15.13 ml), (◆) Aldolase (MW: 158 kDa; Ve: 16.62 ml) and (★) Ovalbumin (MW: 44kDa; Ve: 17.76 ml). B - Native PAGE gel of peak 1 and 2 (lanes 1 and 2) and molecular marker (M).

With intention of verify if there is an transformation of the amount of hexamers into dodecamers to reach an equilibrium. The second peak of the SEC, the hexamers, was isolated and reloaded into the SEC using the same conditions. The profile shows that there are still present some dodecamers in the hexamers peak, despite that peak which is sharper is the second peak that corresponds to the hexamers fraction.

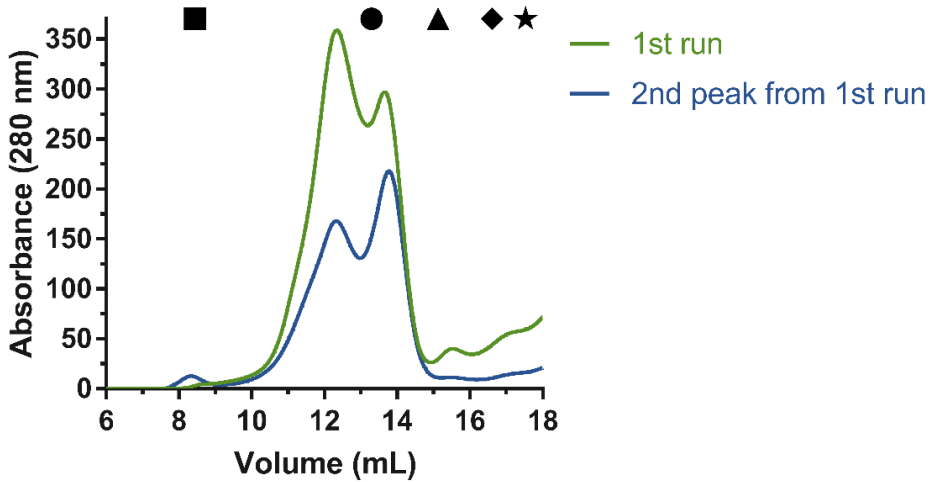


**Figure 4.2 - FtsH hexamers elute in two peaks from sizing chromatography after being reloaded.** The green peak shows the first profile after incubation at 60°C ON. The peak eluting at 13.4 mL was isolated and reloaded into a SEC resulting in the profile in blue trace. Blue Dextran (■) used to calculate the void volume of the column (8.47mL). The elution volumes of standard proteins used to estimate the molecular weight of the eluted fractions are shown on the top of the graph: (●) Tyroglobulin (MW: 669 kDa; Ve: 13.27 ml), (▲) Ferritin (MW: 440 kDa; Ve: 15.13 ml), (◆) Aldolase (MW: 158 kDa; Ve: 16.62 ml) and (★) Ovalbumin (MW: 44kDa; Ve: 17.76 ml).

#### 4.3.2 Electron microscopy of full-length AaFtsH complexes

Transmission electron microscopy (EM) visualized the difference of negatively stained samples from each peak. Preparations from the first peak revealed elongated particles with an average length of  $231 \text{ \AA} \pm 15 \text{ \AA}$  (SD, N=280; Figure 4.3 A). Most particles from the second peak are smaller and exhibit an average length of  $154 \text{ \AA} \pm 13 \text{ \AA}$  (SD, N=280) (Figure 4.3 B). Particles from the first peak appear to house two AaFtsH oligomers from the second peak, although their average length is less than twice the average length of the smaller particles.

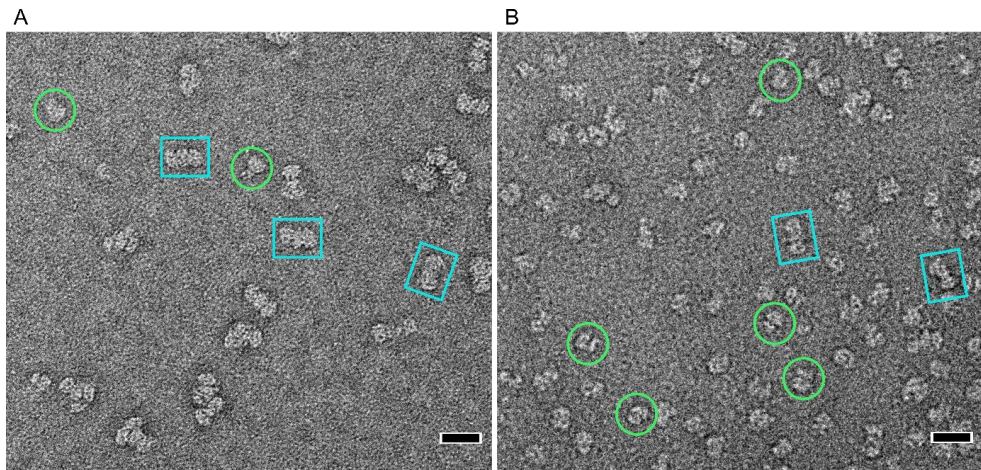


**Figure 4.3 - Micrographs of the first (A) and second (B) SEC eluted fractions prepared by negative staining.** Side views are preferentially obtained. Blue squares correspond to dodecamers particles and green circles to hexamers. Scale bar is 200 Å.

### 4.3.3 2D Class averages and 3D reconstruction of the small AaFtsH complex

15000 projections of the smaller AaFtsH complex prepared by negative staining were selected and classified using the image processing software packages Xmipp [25] and Eman2.12 [26]. The class average corresponding to the infrequent, approximately axial projections is compatible with the hexameric nature of the small AaFtsH complex (Figure 4.4 A), while Figure 4.4 B-D display representative side or tilted views of AaFtsH hexamers. From such class averages EMAN2.12 calculated starting models and refined one of them against all particle projections, imposing 6-fold symmetry. Figure 4.4 F displays the 20 Å resolution 3D map of the AaFtsH hexamer, which accommodates the crystal structure of the AaFtsH cytosolic domain (PDB 4WW0) and the *E. coli* periplasmic domain (PDB 4V0B; Figure 4.4 G).

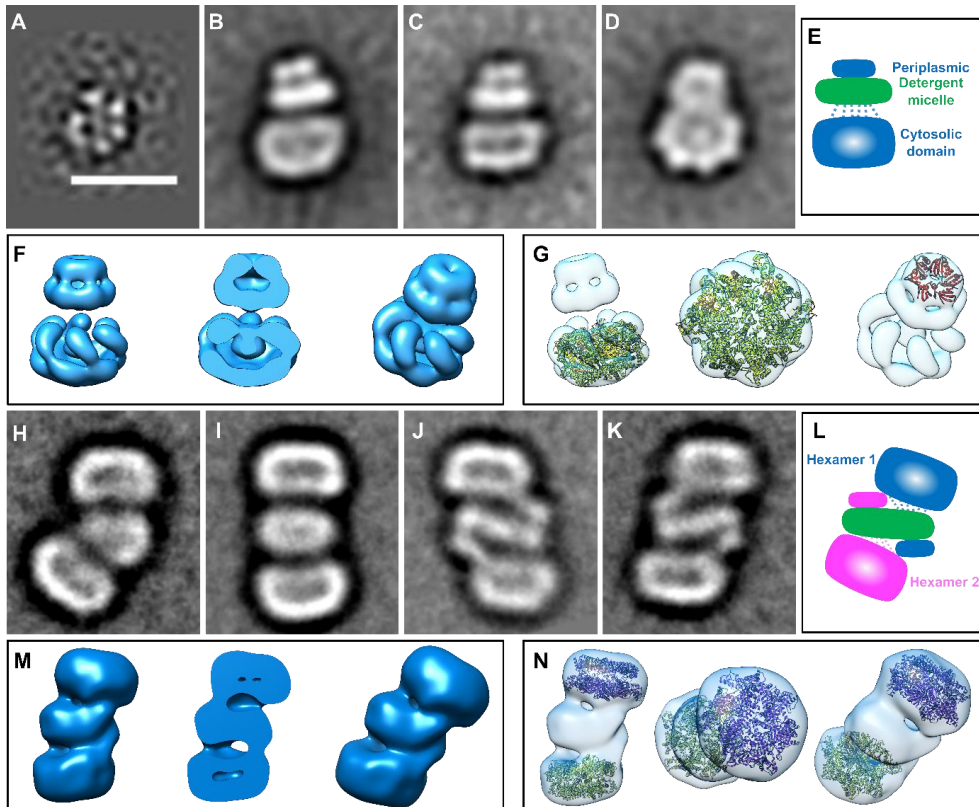


**Figure 4.4 - Class averages of negatively stained FtsH complexes and 3D maps.** Class averages (A-D, H-K) represent top views (A), side views (B and C) and a view of a tilted hexamer (D), and different conformations of dodecamers (H-K). E and L – Schematic representation of the class averages highlighting with dashed lines six linking peptides present in the protein sequence. F, M – 3D maps of AaFtsH full length hexamer and dodecamer, respectively. G – Fitting of the crystal structure of the cytoplasmic domain of AaFtsH (PDB 4WW0) and the crystal structure of the periplasmic domain of *E. coli* FtsH (PDB 4V0B) to the hexamer map. N – Fitting of two cytoplasmic domains (PDB 4WW0) to the dodecamer map. Scale bar equals 110 Å.

#### 4.3.4 2D Class averages of the large AaFtsH complex highlights large conformational changes

15000 projections of the larger elongated complex yielded class averages that document the conformational flexibility of AaFtsH dodecamers (Figure 4.4 H, I). To obtain a 3D map of the dodecamers, class averages that correspond to a cylindrical (Figure 4.4 I- K) rather than a bent conformation (Figure 4.4 H) were selected to

calculate an initial model that was subsequently refined against all projections of these classes without imposing any symmetry. Figure 4.4 M and N illustrate the resulting 3D map and indicate how the structure of the AaFtsH cytosolic domain (PDB 4WW0) fit. As displayed in Figure 4.4 L, class averages and 3D maps suggest that the AaFtsH dodecamer is kept in solution by a single LMNG micelle that embraces 2x12 transmembrane helices (green), while the periplasmic domains of each hexamer contact the cytosolic domains of the other hexamer (pink and blue).

#### **4.3.5 Dimensions of FtsH subunits and their conformational changes**

Using ten class averages from both AaFtsH hexamers and dodecamers we measured that the detergent micelle, highlighted in green (Figure 4.4 E,L), has a thickness of  $40 \pm 4 \text{ \AA}$  for the hexamer and  $43 \pm 2 \text{ \AA}$  for the dodecamer, which is close to the lipid bilayer thickness. The measured micelle/helical bundle width is  $100 \pm 18 \text{ \AA}$  for the hexamer and  $126 \pm 7 \text{ \AA}$  for the dodecamer. The estimated length of the 3D map for the full hexamer is  $167 \pm 5 \text{ \AA}$  (SD, N = 10) and its width is  $131 \pm 7 \text{ \AA}$  (SD, N = 10). When compared with the dimensions of *A. aeolicus* FtsH crystal structure, a similar width is reported ( $120 \text{ \AA}$ ) (16). In hexamers, the cytoplasmic domain has a height of  $83 \pm 7 \text{ \AA}$ , and the periplasmic domain has a height of  $31 \pm 3 \text{ \AA}$  and a width of  $63 \pm 6 \text{ \AA}$ . The estimated length of the dodecamer 3D map is  $243 \pm 8 \text{ \AA}$ , nevertheless it accommodates two tilted and distorted hexamers. The height of the volume encompassing the micelle plus the two periplasmic domains is  $90 \pm 6 \text{ \AA}$ , which is comparable to twice the periplasmic domain ( $31 \text{ \AA}$ ) plus the micelle height ( $40 \text{ \AA}$ ). Albeit the medium resolutions achieved ( $25 \text{ \AA}$  for the dodecamer and  $20 \text{ \AA}$  for the hexamers of AaFtsH), the orientation of the cytosolic domain with respect to the detergent micelle is clearly apparent. All the dodecamer classes and some of the hexamer classes show that the plane of the protease domain is at an angle relative to the detergent micelle creating a gap at the substrate entry site. This is more evident in the dodecamer conformations (Figure 4.4 J-L), where a gap as large as  $20 \text{ \AA}$  is observed between the central pore of AaFtsH cytosolic domain and the detergent micelle, and a gap of  $\sim 30 \text{ \AA}$  between the edge of that domain and the

micelle (Supplementary Figure 4.2). This gap is large enough to accommodate the whole periplasmic domain of the second hexamer to which it is complexed.

### 4.3.6 Full-length AaFtsH hexamers and dodecamers show similar ATPase and protease activity

ATP hydrolysis rates were assessed by measuring the inorganic phosphate (Pi) released (Material & Methods). The first assessment to phosphate release was measured after 60 min in presence of 2 or 5 mM ATP and 2  $\mu$ g of AaFtsH dodecamers or hexamers (Figure 4.5 A). The results show that the release of phosphate is higher in presence of a bigger amount of ATP, indicating that the amount of ATP is a limiting factor to measure the ATPase activity.

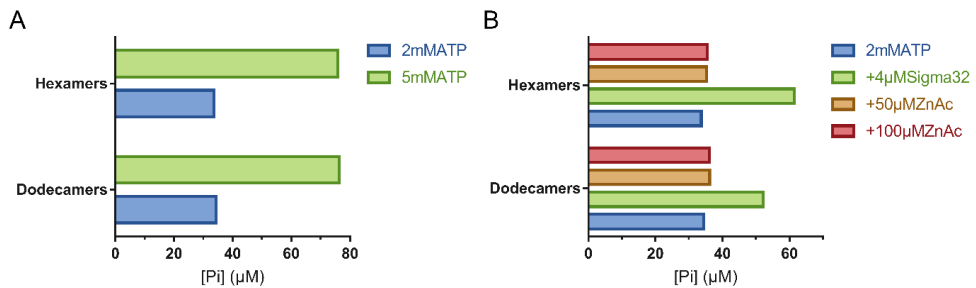


**Figure 4.5 – Inorganic phosphate release of AaFtsH hexamers and dodecamers.** In presence of 2 or 5 mM ATP (A). The same assay was performed in presence of 2 mM ATP adding 4  $\mu$ M Sigma 32 or 50 or 100  $\mu$ M ZnAc (B).

The ATPase activity of AaFtsH hexamers is not affected by the change in concentration of ZnAc (Figure 4.5 B orange and red bars), but doubles in presence of 4  $\mu$ M of Sigma 32 (Figure 4.5 B green bar). While the AaFtsH dodecamers behaviour is the same, the ATPase activity in presence of Sigma 32 is higher but not exactly double.

The initial velocity of the ATP hydrolysis reactions is extracted from the concentration of Pi released in the first 10-minutes interval (Supplementary Figure 4.3). From this, specific ATPase activities of 338 nmol/min/mg and 340 nmol/min/mg were calculated for AaFtsH hexamers and dodecamers, respectively. To further compare the activity of FtsH in the hexameric and dodecameric forms, Michaelis Menten constants ( $K_M$

and  $K_{cat}$ ) were fitted using initial velocities calculated at various ATP concentrations (Figure 4.6 A, B), with the use of FtsH monomer concentrations in the calculations [10,11]. The results of the fits show that the dodecamer fraction has a  $K_M = 518 \mu\text{M}$  (95% Confidence Interval (CI): 432 – 625  $\mu\text{M}$ ) and a  $K_{cat} = 61 \text{ min}^{-1}$  (95% CI: 57 – 66  $\text{min}^{-1}$ ). The hexamer fraction has a  $K_M = 600 \mu\text{M}$  (95% CI: 480 - 754  $\mu\text{M}$ ) and a  $K_{cat} = 63 \text{ min}^{-1}$  (95% CI: 58 – 69  $\text{min}^{-1}$ ), identical to the values for the dodecameric AaFtsH within error limits. ATPase activity was measured at 60°C. The optimal growth temperature of *Aquifex aeolicus* is 85°C (26); however, LMNG-solubilized AaFtsH aggregates at 80°C. To ensure that it is valid to perform the Malachite Green assay at 60°C, a control experiment was performed to calculate the measured release of Pi in absence of AaFtsH (Supplementary Figure 4.3).

Next, we assessed the proteolytic activity of the hexamer and the dodecamer forms of AaFtsH. As previously reported [2,29], we used resorufin-labelled casein substrate (Roche) to test the proteolytic activity over a range of AaFtsH concentrations (Material & Methods). The initial rates of proteolytic activity were calculated from the concentration of resorufin released in the first 30-minutes interval (Supplementary Figure 4.4). We assessed initial velocities for different AaFtsH monomer concentrations using the dodecamer (Figure 4.6 C) and the hexamer (Figure 4.6 D) fractions. The hexamers and the dodecamers reaction rates both increased linearly with AaFtsH concentrations at a slope of  $\sim 1.8 \text{ nM}$  of resorufin per minute per  $\mu\text{M}$  of AaFtsH. This validates the idea that both fractions have the same proteolytical activity, suggesting that their active centres are not only well folded, but also equally accessible for protein entrance.

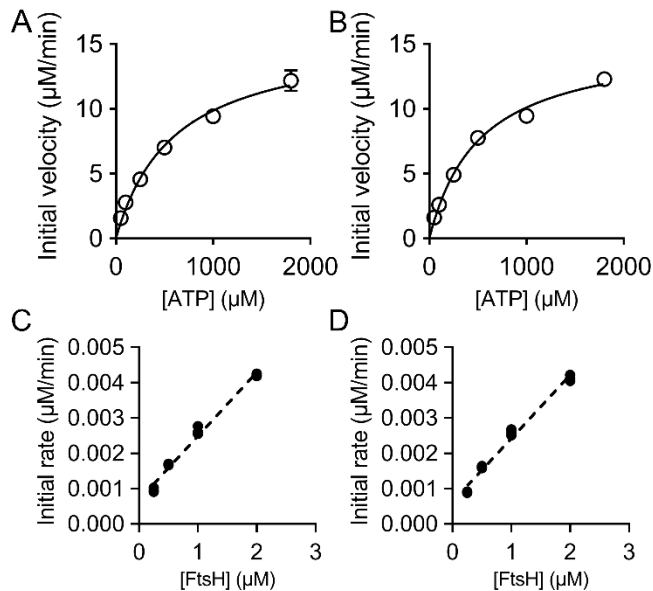


**Figure 4.6 - ATPase and protease activity assays.** A, B – Steady-state velocities for the ATP hydrolysis by 0.25 μM AaFtsH dodecamers (A) and hexamers (B). The average and SD of three replicas for each reaction are plotted (SD bars are not visible for some points due to their small sizes). C, D – Initial velocities of proteolysis of 50 μM resorufin-labelled casein by AaFtsH dodecamers (C) and hexamers (D) as a function of AaFtsH concentration. All the reactions were measured three times and all points are plotted.

#### 4.3.7 AaFtsH hexamers and dodecamers show similar degradation behaviour in presence of the physiological substrate Sigma 32

AaFtsH dodecamers and hexamers capability to degrade the known FtsH physiological substrate sigma32 (with MW around 32 kDa) [10,11,30–32] was analysed by SDS-Page gel. In Figure 4.7 A, the degradation of 1 μM of Sigma 32 in presence of 2 μM of AaFtsH eluted from the HisTrap column was tested. Results demonstrate that after 120 min the total amount of Sigma 32 is not completely degraded in presence of ATP, as described in literature [10,11]. Although degradation is observed from the 0 min to the 120 min time point in the presence of ATP, there is no degradation in presence of ADP.

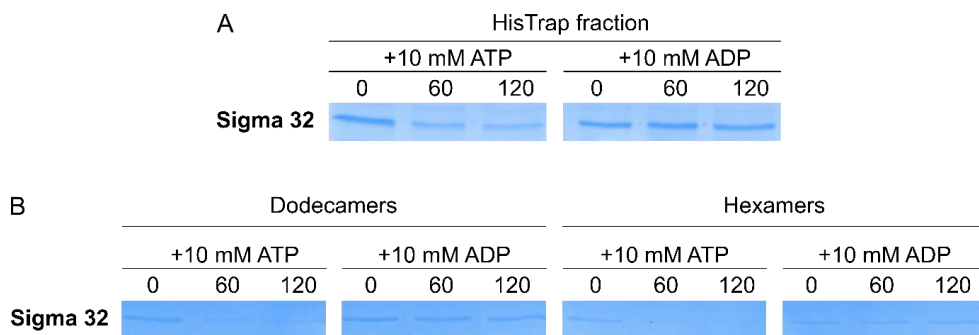


**Figure 4.7 - SDS-Page gels analysis of Sigma 32 degradation by AaFtsH.** A show the degradation by the AaFtsH fraction which eluted directly from the HisTrap step. Moreover, B shows the degradation of Sigma 32 by Dodecamers and Hexamers in presence ATP or ADP.

The Sigma 32 degradation by AaFtsH dodecamers and hexamers was also tested in presence of ATP or ADP (Figure 4.7 B). Both fractions are capable to degrade Sigma 32 in presence of ATP, but no degradation is seen with ADP.

### 4.3.8 Bioinformatics tools identify a linker region of ~20aa

To gain a better understanding of the unexpected conformational flexibility of AaFtsH complexes, we compared the *E. coli* and *Aquifex aeolicus* FtsH protein sequences and mapped the available crystal structures onto the sequence alignment (Supplementary Figure 4.5). Different transmembrane helix predictors identified both the N-terminal helix and the one linking the periplasmic to the ATPase domain. A region of ~20 aa remained between the second transmembrane helix and the cytoplasmic domain (Figure 4.8 A). Basic Local Alignment Search Tool (BLAST) [23] finds that this 20aa sequence is unique to membrane bound AAA+ proteases. When tested with different structure predictors, this region exhibits extended loop conformation with a weak signal for a short helix at its end (Supplementary Figure 4.6). Analysis of residue conservation by ConSurf [24] shows 13 highly conserved or conserved residues in this 20 aa region (Supplementary Figure 4.6).

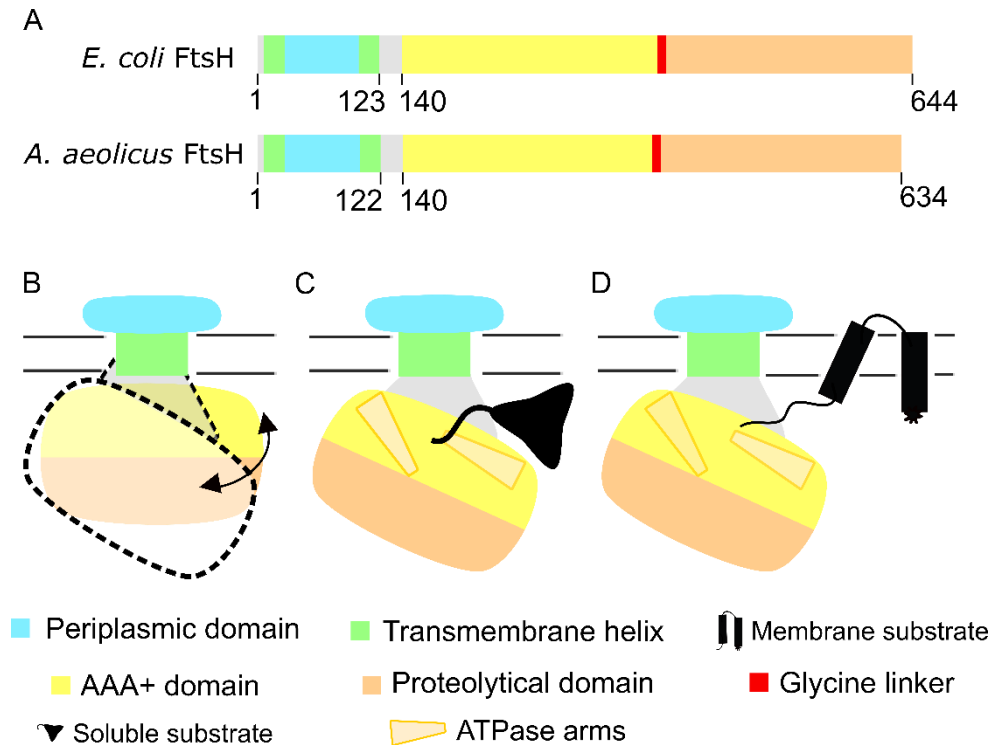


**Figure 4.8 - Schematic representation of AaFtsH sequence and proposed model for substrate entry.** A – Bioinformatics tools and available structures of FtsH domains, from *E. coli* and *A. Aeolicus*, show the presence of a loop-like peptide structure with ~20 aa between the membrane and the AAA domains. The N-terminal periplasmic domain (green) is between two transmembrane helices (yellow). The second transmembrane helix is followed by a loop region (grey; see text), which is the link to the AAA+ domain (blue). Connected by the glycine linker (red), the C-terminal protease domain is shown in purple. B - A new model for substrate entry is proposed. The ~20 aa flexible linker could allow the cytoplasmic domain of FtsH to tilt in relation to the membrane, creating a 30 Å wide gap that provides access of cytoplasmic (pink, C) and membrane protein substrates (black, D) to the central pore in a partially folded state.

#### 4.4 Discussion and conclusions

In this work, we have purified full-length *Aquifex aeolicus* FtsH and characterized both its structure with negative stain EM and its ATPase and proteolytic activities. The purification of full-length FtsH hexamers proved to be challenging with size exclusion chromatograms reproducibly showing two species of AaFtsH in closely overlapping fractions. Negative stain EM and image analysis confirmed that the low molecular weight fraction corresponds to AaFtsH hexamers, and the high molecular weight fraction to AaFtsH dodecamers (Figure 4.3 and Figure 4.4). Importantly, both fractions show highly similar specific ATPase activities: 340 nmol/min/mg for AaFtsH dodecamers and 338 nmol/min/mg for AaFtsH hexamers. This compares well to values reported for the *E. coli* FtsH, 230 nmol/min/mg [11] and 193 nmol/min/mg [10]. Also, the Michaelis Menten constants are similar for the dodecameric and hexameric forms, with  $K_M$  (518 and 600  $\mu\text{M}$ , respectively) and  $K_{cat}$  (61 and 63  $\text{min}^{-1}$ , respectively). The  $K_M$  values obtained for ATPase activity of hexamers and dodecamers are between 7x [11] and 20x [10] higher than reported for *E. coli* FtsH solubilised in a different detergent and under different conditions. Both fractions of LMNG-solubilized AaFtsH can degrade a casein substrate at comparable proteolytic rates (Figure 4.6 C, D). Our results also document that AaFtsH hexamer and dodecamer both show high proteolytic activity, since the same amount of casein can be degraded by 10x less LMNG-AaFtsH when compared with AaFtsH solubilized in n-Dodecyl- $\beta$ -D-Maltoside (DDM) [2]. In summary, we demonstrate that the AaFtsH kept in solution by LMNG exists as equally active dodecamers and hexamers. Both AaFtsH are also capable of degrading the known physiological substrate Sigma 32 [10,11,32] only in presence of ATP as opposed to ADP. However, the total degradation of Sigma 32 in the medium was not observed after 120 min. The ATP concentration present during the assay is also limiting the amount of phosphate released by FtsH, shown in Figure 4.5 A. Both AaFtsH fractions show an increase of ATPase activity in presence of Sigma 32 presence as reported in literature, showing that both hexamers and dodecamers ATPase domains are equally available to bind Sigma 32 in presence of ATP and that when this nucleotide is replaced by ADP no

degradation is observed. The stimulation of the ATPase activity in presence of higher amounts of  $Zn^{2+}$  in the medium is not observed (Figure 4.5 B).

Molecular weight estimates from SEC suggest that for the hexamer, the LMNG micelle and the bound lipid molecules account together for  $\sim 300$  kDa (Figure 4.1). Combined SEC and MALDI-TOF MS measurements showed that the dimeric ABC transporter BmrA, comprised of 12 transmembrane helices modelled as a cylinder of 40 Å diameter, binds an LMNG micelle of 157 kDa [19]. In AaFtsH hexamers, the LMNG micelle containing the 12-helix ring has a width of 100 Å (Figure 4.3). According to previous reports the LMNG belt is  $\sim 20$  Å thick [33–35]. Therefore, the cylindrical transmembrane domain of the hexamer has a diameter of  $\sim 60$  Å, accommodating  $1.5 \times 157$  or 240 kDa of LMNG. The ring of twelve tilted helices emanating from the periplasmic domain (PDB 4V0B) also exhibits a diameter of  $\sim 60$  Å, consistent with the above estimate. Transmembrane helix 1 (TM1) corresponds in length to TM4 of aquaporin 1 (AQP1; PDB 1FQY) [36] and is likely tilted by  $29^\circ$ . TM2 corresponds to TM6 of AQP1 and is thus probably tilted by  $36^\circ$ . Modelling helices as 10 Å wide tilted cylinders, the cross section of the helical bundle is  $6 \times \pi \times 52 (1/\cos(29^\circ) + 1/\cos(36^\circ)) \text{ \AA}^2$ , and the bilayer cross section inside the ring then amounts to  $1700 \text{ \AA}^2$ . Taking  $50 \text{ \AA}^2$  per lipid molecule into account, the ring houses about 34 lipid pairs, which make  $\sim 50$  kDa. From the dimension of the membrane domain with its LMNG belt measured by EM, the LMNG micelle and the lipid molecules are estimated to represent  $\sim 290$  kDa, close to the molecular weight estimate from SEC. Such a molecular weight estimate is less accurate for the AaFtsH dodecamer, because it elutes outside the range of calibration proteins used. In addition, the hexamer has possibly different migration properties compared to the compact elongated dodecamer composed of two intertwined hexamers (Figure 4.3).

Further we report here the first full length bacterial FtsH 3D map at a resolution of 20 Å, which is related to the negative staining used for visualizing the protein complexes, as well as their intrinsic flexibility. As documented in Figure 4.3 G this map accommodates X-ray structures of cytosolic and periplasmic fragments. The density of the X-ray structure of *Aquifex aeolicus* cytosolic domain (PDB 4WW0)

rendered at 20 Å resolution fits well with the cytosolic domain of the 3D map presented here. There is also a similar match of the periplasmic domain with the periplasmic crystal structure of *E. coli* FtsH (PDB 4V0B). The reported intermembrane domain of m-AAA is larger [9], as it comprises ~25% more amino acids than the AaFtsH periplasmic domain. Nevertheless, except for the periplasmic domain, the yeast full-length m-AAA cryoEM map rendered at 20 Å also fits well with the 3D map of the AaFtsH hexamer.

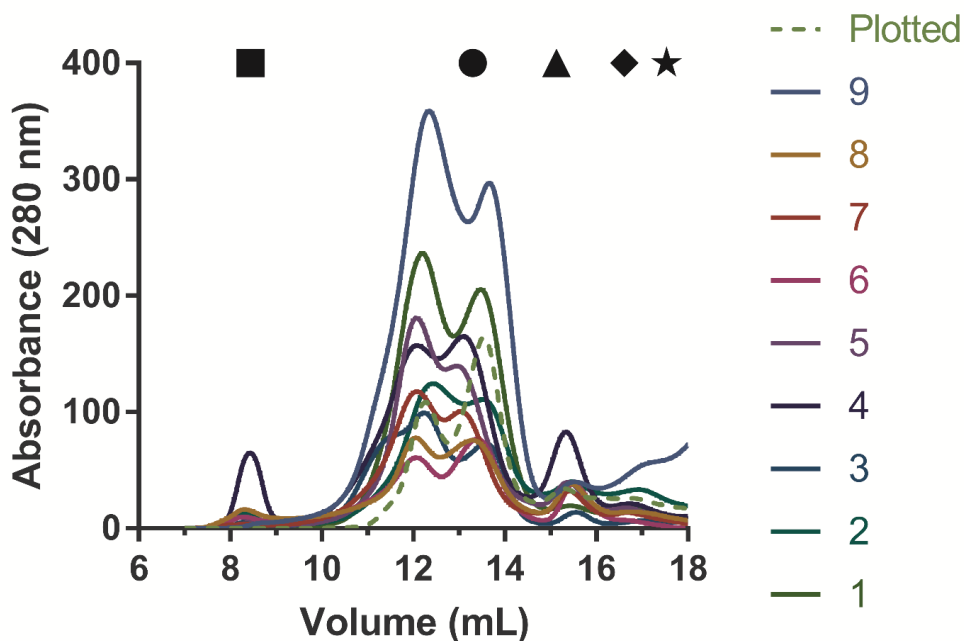
The unexpected AaFtsH dodecamers consistently observed (Figure 4.1 and Figure 4.2) exhibit highly variable conformations (Figure 4.3 H and I), with periplasmic domains strongly tilted with respect to cytosolic domains. These dodecamers composed of intertwined hexamers that share a single LMNG micelle reveal a large flexibility of the region that links the membrane and ATPase domains. While the 12 Å cryo-EM structure of m-AAA shows these thin links clearly [9], the subsequent model of the full-length *E. coli* FtsH predicts transmembrane helices projecting into the ATPase domain [8], which would not allow the conformational flexibility we observe. However, this model is neither compatible with the thin links shown by Lee et al., 2011, nor with the significant stain-penetrated gap between the cytosolic AaFtsH domain and membrane domain visualized in Figure 4.3.

Based on these results we propose a new model for substrate entry. Conformational variations demonstrated by the AaFtsH dodecamers (Figure 4.3) indicate that FtsH is flexible enough for the large cytosolic domain to tilt significantly with respect to the membrane plane, thus accommodating larger substrates (Figure 4.5 B-D). In the fully active dodecamer, the space between the cytosolic domain and the membrane compares to the height of the AaFtsH periplasmic domain. Thus, our results suggest that the gap at the edge of the cytosolic domain of the native, hexameric AaFtsH may open up to ~30 Å. Such a gap is enabled by the ~20aa linker present between the second transmembrane helix and the cytosolic domain sequence (Figure 4.5 A, grey). This linker appears to have remarkable properties: it exhibits a length of ~13 Å in its quiescent state, but can extend like a spring at least up to ~30 Å. Structure predictors produce similar models that include a possible elongation of TM2,

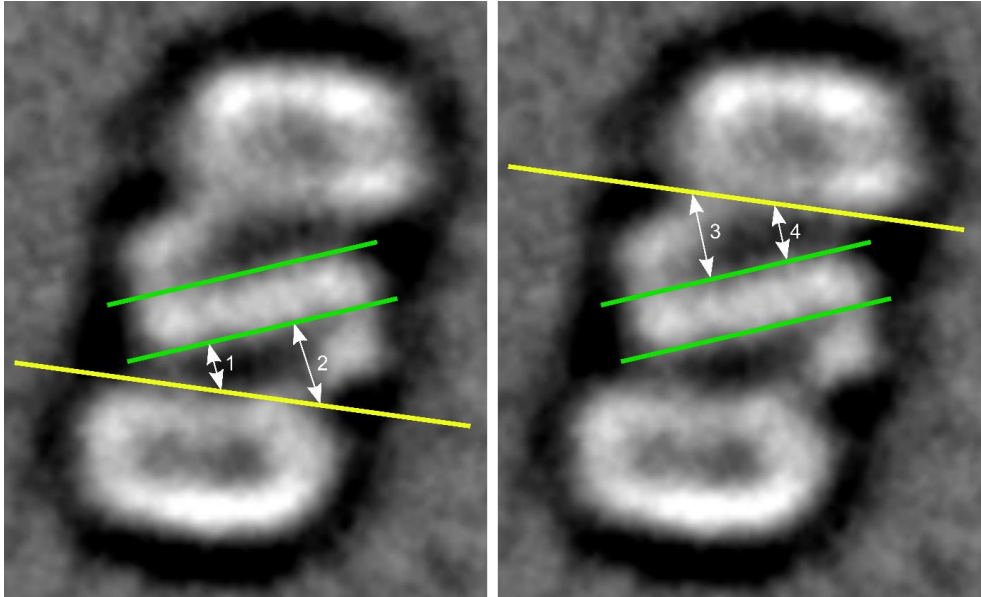
comprising at most the highly conserved RQM(S) motif, followed by a loop (GGGNVN), and a conserved region that may adopt loop, extended strand or helical configurations (RAFNFGKSRA) (Supplementary Figure 4.5). This linker's possible extended loop conformation explains the structural variation of the dodecameric form (Figure 4.3 H-K), and would also accommodate the large movements of the ATPase domain predicted by X-ray crystallography [1]. Endpoints of 20 aa loops are separated by a minimum distance of  $\sim 10$  Å in known proteins structures, but can extend or be stretched up to a maximum of 60-80 Å [37,38]. These large tilting movements of the cytosolic domain of FtsH would allow misfolded proteins to access the pore (Figure 4.5 B-D), without the need for an unfolded polypeptide to snake through a 13 Å channel before reaching to translocating loops [9].

Although we do not anticipate FtsH to form dodecamers in bacteria, we propose that the large tilting movements observed here are likely achieved during proteolytic activity in vivo. A higher resolution model of full-length FtsH would give us more details on how FtsH interacts with its substrates. This has however proven to be difficult, precisely due to the high flexibility of the 20 aa linker at the membrane junction.

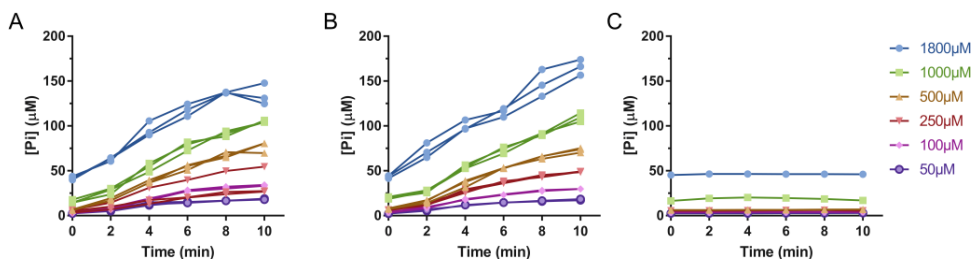
## 4.5 Supplementary information



**Supplementary Figure 4.1 – SEC profiles of 10 runs, showing the reproducibility of the results obtained.** Numbers indicate different runs and the dashed green line represents the chromatogram profile shown in Figure 4.1 A. Blue Dextran (■) used to calculate the void volume of the column (8.47mL). The elution volumes of standard proteins used to estimate the molecular weight of the eluted fractions are shown on the top of the graph: (●) Tyroglobulin (MW: 669 kDa; Ve: 13.27 ml), (▲) Ferritin (MW: 440 kDa; Ve: 15.13 ml), (◆) Aldolase (MW: 158 kDa; Ve: 16.62 ml) and (★) Ovalbumin (MW: 44kDa; Ve: 17.76 ml).

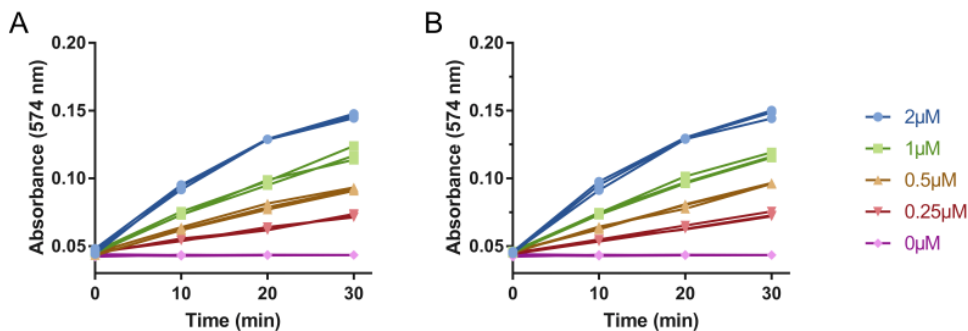


**Supplementary Figure 4.2 - Measurements between the cytosolic domain and the detergent micelle.** The distance between the central pore of AaFtsH cytosolic domain (delimited by the yellow line) and the detergent micelle (green lines) is approximately 20 Å (distances 1 and 4 are 18 Å and 20 Å, respectively), while ~30 Å (distances 2 and 3 are 32 Å and 33 Å, respectively) is measured between the edge of that domain and the micelle. This gap is large enough to accommodate partially folded proteins comparable in size to the periplasmic domain.



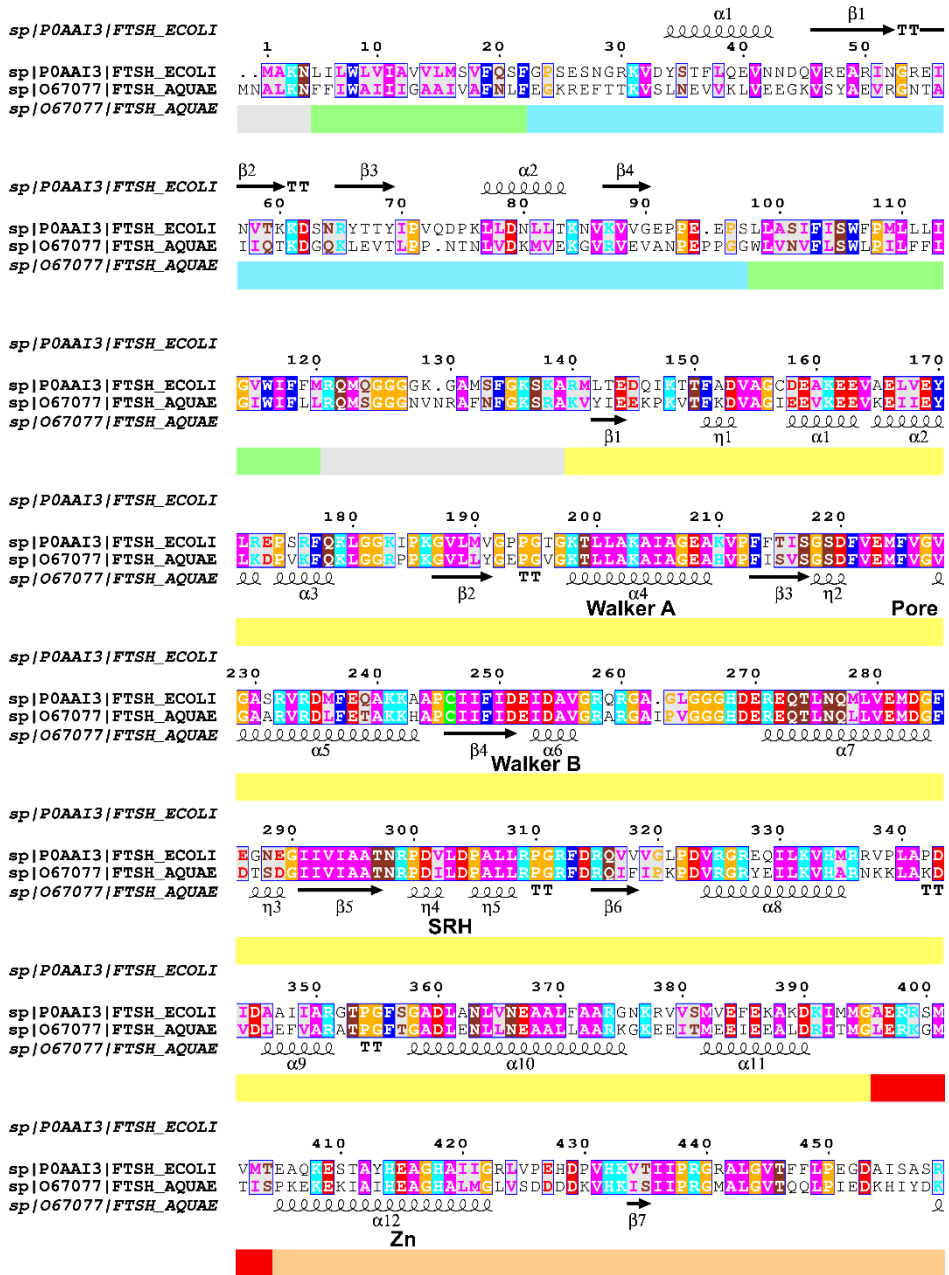
### Supplementary Figure 4.3 - Raw data for the inorganic phosphate release.

Free phosphate was measured using the Malachite Green assay kit for 0.25  $\mu\text{M}$  of AaFtsH dodecamer (A) and hexamer (B) fractions incubated with different ATP concentrations for 10 min. C – The free phosphate measurements in absence of AaFtsH.

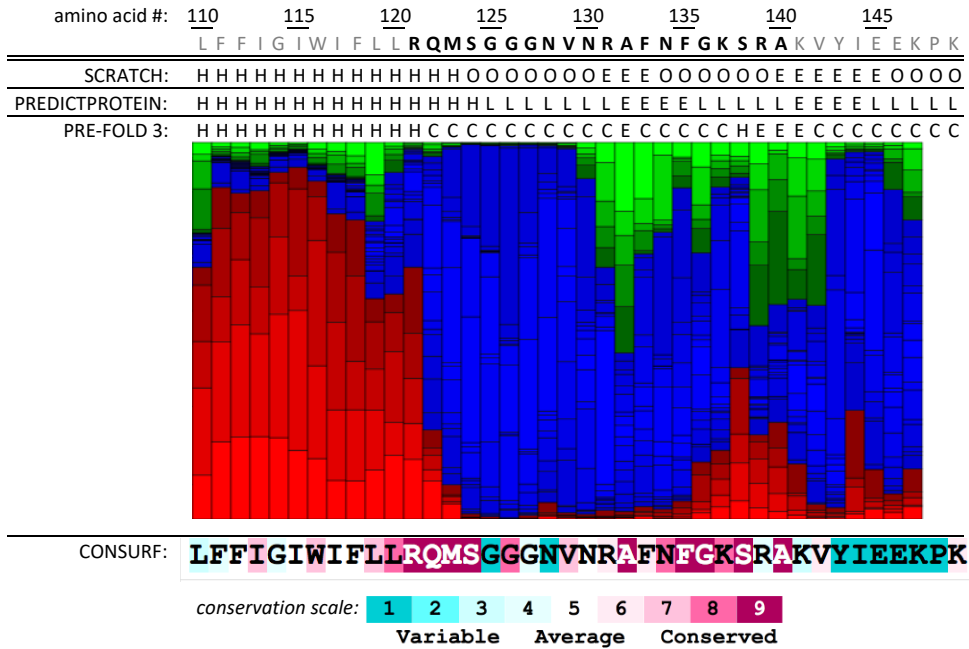


### Supplementary Figure 4.4 - Protease activity assays raw data.

Resorufin release was measured over 30 minutes for 50  $\mu\text{M}$  of Resorufin labelled casein incubated with dodecamer (A) and hexamer fractions (B) at different concentrations.







**Supplementary Figure 4.6 - Structure of the ~20 aa region (amino acids in black) between the TM2 and the AAA-domain of *Aquifex aeolicus* FtsH,** as predicted by the structure predictors SCRATCH, PREDICTPROTEIN and PRE-FOLD 3 (H: helical; E: extended; L: loop; C: coil; O: other). Residue conservation scores are obtained from the ConSurf server (scale at the bottom).

## 4.6 References

- [1] C. Bieniossek, B. Niederhauser, U.M. Baumann, The crystal structure of apo-FtsH reveals domain movements necessary for substrate unfolding and translocation., *Proceedings of the National Academy of Sciences of the United States of America*. 106 (2009) 21579–21584.
- [2] M. Vostrukhina, A. A. Popov, B. E. Brunstein, C. M.A. Lanz, D. A. R. Baumgartner, A. C. Bieniossek, E. A. M. Schacherl, C. A. Ulrich, Baumann, C, \*, The structure of *Aquifex aeolicus* FtsH in the ADP-bound state reveals a C2-symmetric hexamer, *Acta Crystallogr D Biol Crystallogr*. D71 (2015) 1307–1318.
- [3] R. Suno, M. Shimoyama, A. Abe, T. Shimamura, N. Shimodate, Y.-H. Watanabe, Y. Akiyama, M. Yoshida, Conformational transition of the lid helix covering the protease active site is essential for the ATP-dependent protease activity of FtsH, *FEBS Letters*. 586 (2012) 3117–3121.
- [4] R. Suno, H. Niwa, D. Tsuchiya, X. Zhang, M. Yoshida, K. Morikawa, Structure of the Whole Cytosolic Region of ATP-Dependent Protease FtsH, *Molecular Cell*. 22 (2006) 575–585.
- [5] C. Bieniossek, T. Schalch, M. Bumann, M. Meister, R. Meier, U. Baumann, The molecular architecture of the metalloprotease FtsH., *Proceedings of the National Academy of Sciences of the United States of America*. 103 (2006) 3066–3071.
- [6] S.H. Kim, G.B. Kang, H.E. Song, S.J. Park, M.H. Bea, S.H. Eom, Structural studies on *Helicobacter pylori* ATP-dependent protease, FtsH., *Journal of Synchrotron Radiation*. 15 (2008) 208–10.
- [7] H. Niwa, D. Tsuchiya, H. Makyio, M. Yoshida, K. Morikawa, Hexameric ring structure of the ATPase domain of the membrane-integrated metalloprotease FtsH from *Thermus thermophilus* HB8, *Structure*. 10 (2002) 1415–1423.
- [8] F. Scharfenberg, J. Serek-Heuberger, M. Coles, M.D. Hartmann, M. Habeck, J. Martin, A.N. Lupas, V. Alva, Structure and Evolution of N-domains in AAA Metalloproteases., *Journal of Molecular Biology*. 427 (2015) 910–923.
- [9] S. Lee, S. Augustin, T. Tatsuta, F. Gerdes, T. Langer, F.T.F. Tsai, Electron cryomicroscopy structure of a membrane-anchored mitochondrial AAA protease, *Journal of Biological Chemistry*. 286 (2011) 4404–4411.
- [10] R.L. Bruckner, Robert C.; Gunyuzlu, Paul L. and Stein, Coupled Kinetics of ATP and Peptide Hydrolysis by *Escherichia coli* FtsH Protease, *Biochemistry*. 42 (2003) 10843–10852.

- [11] T. Tomoyasu, J. Gamer, B. Bukau, M. Kanemori, H. Mori, A.J. Rutman, A.B. Oppenheim, T. Yura, K. Yamanaka, H. Niki, *Escherichia coli* FtsH is a membrane-bound, ATP-dependent protease which degrades the heat-shock transcription factor sigma 32., *The EMBO Journal*. 14 (1995) 2551–2560.
- [12] T. Okuno, T. Yamada-Inagawa, K. Karata, K. Yamanaka, T. Ogura, Spectrometric analysis of degradation of a physiological substrate sigma32 by *Escherichia coli* AAA protease FtsH., *Journal of Structural Biology*. 146 (2004) 148–54.
- [13] H. Grosjean, V. de Crécy-Lagard, C. Marck, Deciphering synonymous codons in the three domains of life: co-evolution with specific tRNA modification enzymes., *FEBS Letters*. 584 (2010) 252–64.
- [14] A. Rose, S. Lorenzen, A. Goede, B. Gruening, P.W. Hildebrand, RHYTHM--a server to predict the orientation of transmembrane helices in channels and membrane-coils., *Nucleic Acids Research*. 37 (2009) W575-80.
- [15] L. Dobson, I. Reményi, G.E. Tusnády, CCTOP: a Consensus Constrained TOPology prediction web server., *Nucleic Acids Research*. 43 (2015) W408-12.
- [16] A. Krogh, B. Larsson, G. von Heijne, E.L. Sonnhammer, Predicting transmembrane protein topology with a hidden markov model: application to complete genomes, *Journal of Molecular Biology*. 305 (2001) 567–580.
- [17] G.E. Tusnády, I. Simon, The HMMTOP transmembrane topology prediction server., *Bioinformatics (Oxford, England)*. 17 (2001) 849–50.
- [18] K.D. Tsirigos, C. Peters, N. Shu, L. Käll, A. Elofsson, The TOPCONS web server for consensus prediction of membrane protein topology and signal peptides., *Nucleic Acids Research*. 43 (2015) W401-7.
- [19] K. Hofmann, W. Stoffel, TMbase-A database of membrane spanning proteins segments, *Biol Chem*. 374 (1993) 166.
- [20] J. Cheng, A.Z. Randall, M.J. Sweredoski, P. Baldi, SCRATCH: a protein structure and structural feature prediction server., *Nucleic Acids Research*. 33 (2005) W72-6.
- [21] A. Lamiable, P. Thévenet, J. Rey, M. Vavrusa, P. Derreumaux, P. Tufféry, PEP-FOLD3: faster de novo structure prediction for linear peptides in solution and in complex., *Nucleic Acids Research*. 44 (2016) W449-54.
- [22] B. Rost, G. Yachdav, J. Liu, The PredictProtein server., *Nucleic Acids Research*. 32 (2004) W321-6.
- [23] S.F. Altschul, T.L. Madden, A.A. Schäffer, J. Zhang, Z. Zhang, W. Miller, D.J. Lipman, Gapped BLAST and PSI-BLAST: a new generation of protein database search programs., *Nucleic Acids Research*. 25 (1997) 3389–402.

- [24] H. Ashkenazy, S. Abadi, E. Martz, O. Chay, I. Mayrose, T. Pupko, N. Ben-Tal, ConSurf 2016: an improved methodology to estimate and visualize evolutionary conservation in macromolecules., *Nucleic Acids Research*. 44 (2016) W344-50.
- [25] J.M. Rosa-Trevín de la, A. Quintana, L. del Cano, A. Zaldívar, I. Foche, J. Gutiérrez, J. Gómez-Blanco, J. Burguet-Castell, J. Cuenca-Alba, V. Abrishami, J. Vargas, J. Otón, G. Sharov, J.L. Vilas, J. Navas, P. Conesa, M. Kazemi, R. Marabini, C.O.S. Sorzano, J.M. Carazo, Scipion: A software framework toward integration, reproducibility and validation in 3D electron microscopy, *Journal of Structural Biology*. 195 (2016) 93–99.
- [26] S.J. Ludtke, Single-Particle Refinement and Variability Analysis in EMAN2.1, *Methods in Enzymology*. 579 (2016) 159–189.
- [27] E.F. Pettersen, T.D. Goddard, C.C. Huang, G.S. Couch, D.M. Greenblatt, E.C. Meng, T.E. Ferrin, UCSF Chimera - A visualization system for exploratory research and analysis, *Journal of Computational Chemistry*. 25 (2004) 1605–1612.
- [28] P.S. Chae, S.G.F. Rasmussen, R.R. Rana, K. Gotfryd, R. Chandra, M.A. Goren, A.C. Kruse, S. Nurva, C.J. Loland, Y. Pierre, D. Drew, J.-L. Popot, D. Picot, B.G. Fox, L. Guan, U. Gether, B. Byrne, B. Kobilka, S.H. Gellman, Maltose-neopentyl glycol (MNG) amphiphiles for solubilization, stabilization and crystallization of membrane proteins., *Nature Methods*. 7 (2010) 1003–1008.
- [29] Y. Akiyama, Proton-motive force stimulates the proteolytic activity of FtsH, a membrane-bound ATP-dependent protease in *Escherichia coli*., *Proceedings of the National Academy of Sciences of the United States of America*. 99 (2002) 8066–8071.
- [30] L.-M. Bittner, J. Arends, F. Narberhaus, When, how and why? Regulated proteolysis by the essential FtsH protease in *Escherichia coli*, *Biological Chemistry*. 398 (2017) 625–635.
- [31] A. Kihara, Y. Akiyama, K. Ito, Different pathways for protein degradation by the FtsH/HflKC membrane-embedded protease complex: an implication from the interference by a mutant form of a new substrate protein, YccA, *Journal of Molecular Biology*. 279 (1998) 175–188.
- [32] Y. Shotland, S. Koby, D. Teff, N. Mansur, D.A. Oren, K. Tatematsu, T. Tomoyasu, M. Kessel, B. Bukau, T. Ogura, A.B. Oppenheim, Proteolysis of the phage lambda CII regulatory protein by FtsH (HflB) of *Escherichia coli*, *Molecular Microbiology*. 24 (1997) 1303–1310.
- [33] V. Chaptal, F. Delolme, A. Kilburg, S. Magnard, C. Montigny, M. Picard, C. Prier, L. Monticelli, O. Bornert, M. Agez, S. Ravaud, C. Orelle, R. Wagner, A. Jawhari, I. Broutin, E. Pebay-Peyroula, J.-M. Jault, H.R. Kaback, M. le Maire, P. Falson, Quantification of Detergents Complexed with Membrane Proteins., *Scientific Reports*. 7 (2017) 41751.

- [34] K.W. Huynh, M.R. Cohen, S. Chakrapani, H.A. Holdaway, P.L. Stewart, V.Y. Moiseenkova-Bell, Structural insight into the assembly of TRPV channels., *Structure* (London, England : 1993). 22 (2014) 260–8.
- [35] A. Vahedi-Faridi, B. Jastrzebska, K. Palczewski, A. Engel, 3D imaging and quantitative analysis of small solubilized membrane proteins and their complexes by transmission electron microscopy., *Microscopy* (Oxford, England). 62 (2013) 95–107.
- [36] Y. Fujiyoshi, K. Murata, K. Mitsuoka, T. Hirai, T. Walz, P. Agre, J.B. Heymann, A. Engel, Structural determinants of water permeation through aquaporin-1, *Nature*. 407 (2000) 599–605.
- [37] Y. Choi, S. Agarwal, C.M. Deane, How long is a piece of loop?, *PeerJ*. 1 (2013) e1.
- [38] S.R.K. Ainavarapu, J. Brujic, H.H. Huang, A.P. Wiita, H. Lu, L. Li, K.A. Walther, M. Carrion-Vazquez, H. Li, J.M. Fernandez, Contour length and refolding rate of a small protein controlled by engineered disulfide bonds., *Biophysical Journal*. 92 (2007) 225–33.



# Chapter 5

## Cryo-electron microscopy: A look into FtsH structure

High resolution protein structural characterization has witnessed an important advance in recent years. The breakthrough to achieve high resolution atomic models was the appearance of new and more sophisticated detectors, which lead to the development of the imaging processing tools. In this chapter, the work done using cryo-electron microscopy and tomography are shown.

\*Parts of this chapter is included in: Current Protocols in Protein Science, e72, 2018.

## 5.1 Introduction

The increment of the atomic structures determined by 3D cryo-electron microscopy (cryo-EM) deposited in the EMDataBank shows a huge development of the cryo-EM technique [1]. The diverse advances of cryo-EM [2,3] conjugated with the development of membrane protein purification and stabilization protocols [4] lead to the opportunity to solve the atomic structure of membrane proteins.

The ice vitrification technique, established in 1981 [5–7] by Dubochet et al., allows the vitrification of particles in solution. The well establish modern method of cryo-EM enables the imaging at low dose and atomic resolution since decades, but the recent breakthrough is a direct consequence of the direct electron detecting cameras [8–10]. These devices not only transmit every electron carrying information from the sample to the detector, but also to acquire images at a rate of 40-400 frames/sec. This allows particles projections to be recorded at a signal to noise ratio limited by sample contrast and electron counting statistics only, and permits the motions of the sample induced by the electron beam to be corrected [11]. Therefore, motion corrected images exhibit noisy particle projections at atomic resolutions. Image processing allows such high-resolution information to be extracted and 3D maps of proteins at 2 Å resolution to be calculated [3]. Within a few years, powerful schemes were developed to acquire movies with sufficiently sparse electron hits per frame that each single electron detected is localized with subpixel accuracy [11]. A small stack ( $\sim 10$ ) of such frames is summed up producing a signal that allows the sample movement to be detected by correlating the sum of the current stack with that of the next one. Experience based weighting of frames according to the accumulated dose, elimination of the first few frames, and summation of properly shifted frames leads to a drift corrected image of unprecedented optical quality as judged by the number of visible Thon rings in the power spectrum of corrected images. Availability of the Thon ring signal then allows to accomplish contrast transfer function (CTF) correction to a resolution of  $\sim 3$  Å [12,13].

Several single particle processing software packages [14–18] have been developed to classify and average such projections, and to reconstruct the 3D structure of the

protein complexes under study. It thus becomes now possible to determine the structure of membrane proteins without the need of crystallization. Moreover, cryo-electron tomography (cryo-ET) [19,20] of membrane proteins reconstituted into proteoliposomes combined with subtomogram averaging [21–23] has made progress and demonstrated that sub-nanometre resolution can be reached [24], increasing the knowledge about how proteins integrate in the lipid bilayer. Cryo-ET of proteoliposomes provides an excellent opportunity to assess a membrane protein in its “native environment”.

The major advantage of cryo-EM is to enable membrane protein structure determination when the protein is solubilized in detergent complexes and when reconstituted into proteoliposomes, which allows a close to native environment of the membrane protein to be restored. No 3D crystals are required to reach atomic resolution. Moreover, only small protein amounts are needed, although overexpression is still required for preparing pure samples. Because the result depends on sample quality, the protocol for expression, solubilization and purification needs to be optimized for each membrane protein addressed. All conditions of sample preparation and optimization must be studied till a high structure resolution is obtained. Without a pure sample, imaging processing of automatically collected data sets will be difficult.

In this chapter, we present the data obtained for the negatively stained tilt pairs, the cryo-EM and cryo-ET data of AaFtsH. We take in account the knowledge obtained in the last chapter, where we present the best conditions to purify AaFtsH, but also acquired knowledge for structural features recognition. The main goal of this chapter is to display the initial structural information obtained from cryo-EM and cryo-ET data acquisition and processing and to explain the difficulties, to provide a basis for future work with such a flexible protein as AaFtsH.

## **5.2 Materials and methods**

### **5.2.1 Tilting pairs in negative stain**

Negatively stained grids of the second peak eluted from the SEC (more detailed information in 4.3.1) were prepared. Imaging acquisition was performed in the same area tilting the specimen at 0° or 45°. Forty tilt pairs were acquired in a FEI Tecnai T12 (120 kV) equipped with a TVIPS F416 CMOS camera (4k x 4k) with a pixel size of 2.5 Å/pixel. Imaging processing was performed using the Scipion 1.0.1 interface choosing the option of Random Conical Tilt processing. For particle picking and 2D averaging Xmipp software and for the construction of a first initial model EMAN2.1 software, were used. The classification was performed using 8000 particles, manually picked, and 27 2D class averages were produced. Several rounds of particle grouping, and re-classification was performed resulting in 7500 particles assigned to 27 2D class averages.

### **5.2.2 Single particle data acquisition and imaging processing in cryo-EM**

A drop of 3-5 µl of the sample containing AaFtsH hexamers was applied to a Quantifoil holey carbon film Q3.5/1 grid, previously glow discharged for 1 min. After blotting the grid (one or double sided), the sample was plunged into liquid ethane using a FEI Vitrobot Mark IV. Grids were then imaged using different electron microscopes equipped with different cameras/detector: Philips CM200FEG TEM (200kV) equipped with a TVIPS F416 CMOS camera; FEI Polara TEM (300kV) equipped Gatan K2 Summit DED plus a custom-built Medipix detector and FEI Titan Krios TEM (300kV) equipped with Gatan K2 Summit direct electron detector. Image processing was performed on a set of 1400 images acquired with Titan Krios TEM (300kV) using Relion 2.1 [25]. Gautomatch was used for automatically picking of the particles a set of 207 742 particles. Several particle selections and 2D classification cycles were run. The best set of particles (10 994) were then used for 2D class averaging to form 10/15 classes. In attempt to get a finer 2D classification the criteria of Relion 2.1 software was changed using the command: `-maxsig 5` which slowed down convergence of the 2D averages (Supplementary Figure 5.1). These

classes were used to build a first initial 3D model. Attempts of 3D classification and refinement the model failed.

### **5.2.3 AaFtsH reconstitution into proteoliposomes and imaging reconstruction**

AaFtsH hexamers fractions, at a concentration of 0.5 mg/mL, were incubated at a lipid protein ratio (LPR) of 0.5 (w/w) for 30 min at room temperature. *E. coli* Polar lipids (Anatrace) were previously prepared to a final concentration of 5 mg/mL in 1% LMNG. After incubation, 10 mg of pre-treated biobeads (BioRad) were added and the mix was incubated for 10 days at 4°C. The biobeads were previously washed two times in methanol for 15 min, followed by three washes in MiliQ water. The results were initially checked by negative stain (as described in 4.2.2) and thereafter analysed by Cryo-electron tomography (cryo-ET).

Gold nanoparticles of 10 nm diameter were added to the proteoliposomes prior to grid vitrification as reference for imaging of by cryo-ET. Gold nanoparticles help in aligning the different images at recorded at different tilting angles. Tomograms were acquired in the Titan Krios TEM (300kV) equipped with Gatan K2 Summit direct electron detector camera at a resolution of 1.054 Å/pixel. The unaligned tomograms were then aligned using Imod 1.3.1 software [26], using the fiducial marks to align the tilt series from -60° to 60° acquired every 3°. Aligned sub tomograms were processed using Dynamo software [21,22]. The integrity of the monomeric AaFtsH after reconstitution was tested by SDS-Page gel. The proteolytical activity was measured using 2 µM of monomeric AaFtsH incubated with 50 µM of resorufin-labelled casein for 60 min at 60°C, as described in 4.2.4.

## **5.3 Results**

### **5.3.1 Random conical tilt of negatively stained pairs**

The acquisition of negatively stained tilt pairs was performed as illustrated in Figure 5.1 A. Image pairs were recorded at 0° and 45° by manually shifting from the search/focus to exposure mode. The goal of using random conical tilt pairs is to

obtain an initial 3D model from the negatively stained FtsH preparation. Tilting a 3D object during a projection in 2D will give more insight of sides of the object than only imaging it at  $0^\circ$ . The precise location of the recorded area was assured using a dust present in most grid squares guiding the user in the different Search/Focus and Exposure modes (Figure 5.1). This allowed the random conical tilt program of Xmipp 1.12 to be used under control of Scipion 1.1 [14]. 40 tilt pairs were acquired, and 7 500 particles were picked manually.

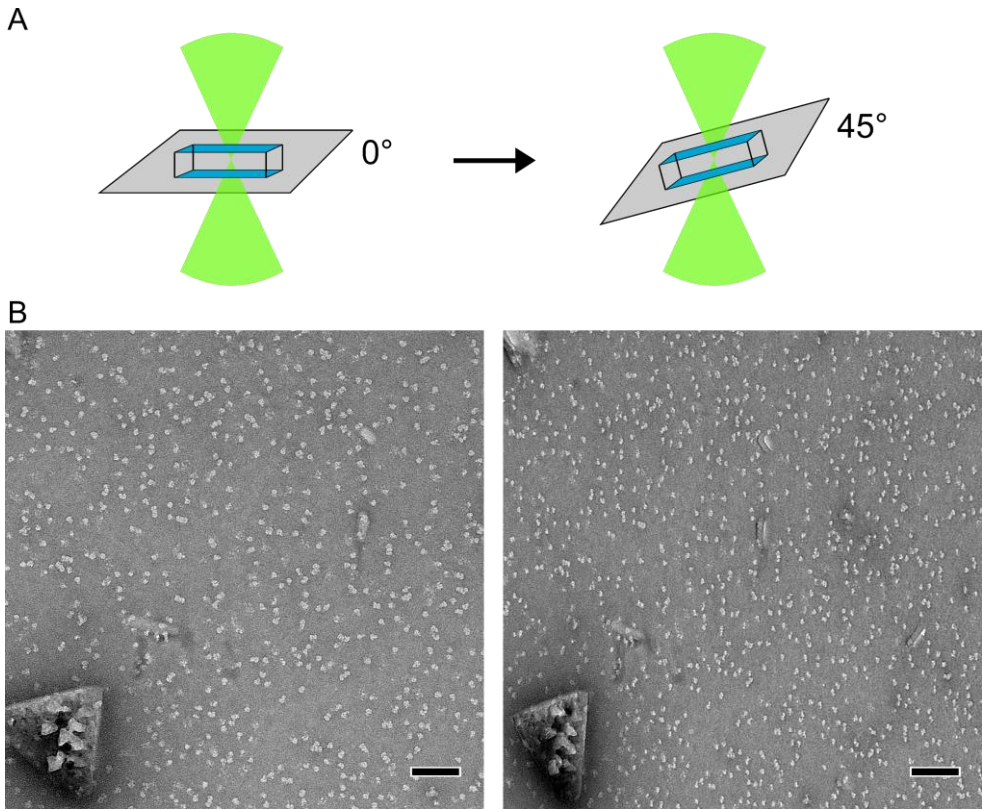
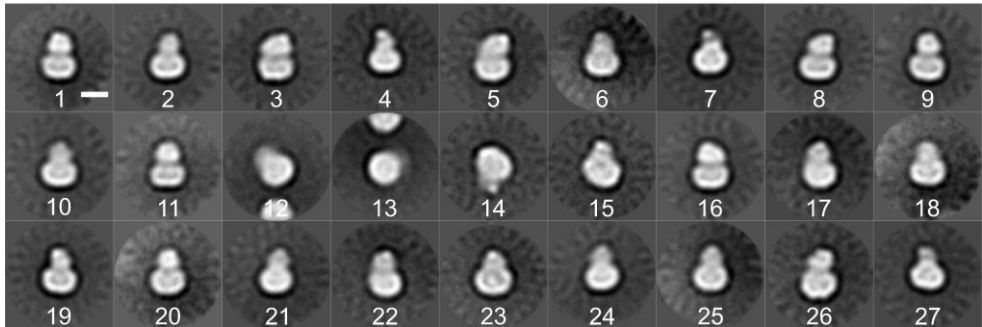


**Figure 5.1 – Tilting pairs acquisition of negatively stained sample.** Schematic representation of the tilt pairs acquisition inside the electron microscope at  $0$  and  $45^\circ$  (A). The tilt pairs were acquired using as guide the dust present on the grid by the uranyl acetate stain (left corner of both figures in B). Scale bar represents 100 nm.

After several classification cycles using Xmipp, a final group of 27 classes was formed (Figure 5.2 A). Preferentially side views were observed, as described previously in

Chapter 4 for negatively stained AaFtsH hexamers. Nevertheless, some tilted views can be recognized as in class averages number 6, 7, 12, 14, 15 and 27 in Figure 5.2 A. A clear bottom view is observed in class number 13. The tilting pairs 2D class average show, complementary structural information to that presented in Chapter 4. In the 2D classification, it is also possible to recognise side views with the same tilted features of the intermembrane domain in relation to the cytoplasmic domain. Examples of this are classes number 4, 8, 9, 19 and 26 of Figure 5.2 A.

A



B

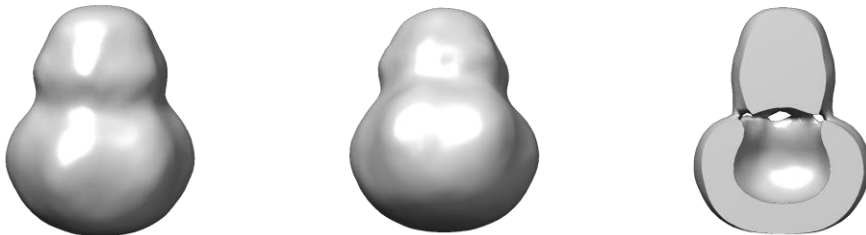


**Figure 5.2 - The imaging processing of tilted pairs at 0 and 45° results.** The 2D classification of particles resulted into 27 classes (A). With these classes a first initial model was obtained by random conical tilt (B, side, tilted and internal view). This map does not have enough resolution to reveal further structural details. Scale bar is 100 Å.

An initial model was constructed using Relion 2.1, inside Scipion 1.1, although no valuable information could be extracted since the refinement of this model failed. Other attempts to characterize the AaFtsH structure were performed although none of the classification and refinement of the tilted structure could increase the information provided by the first model obtained in Chapter 4.

### **5.3.2 Single particle image processing of cryo-EM AaFtsH**

Imaging proteins in vitreous ice is a challenging technique as explained before (in 5.1). Figure 5.3 A, displays two micrographs which are representative of the vitrified FtsH imaged by cryo-EM. These images show a low contrast signal. Although particles can be discerned, it is a challenging task to identify each particle by naked eye. For that reason, particles were picked using the automatic picking tool in Relion 2.1 software [25]. After automatically picking 207 742 particles, imaging processing was performed to form 7 final classes and using only 72 000 particles. The first set of 2D classification shows clear bottom (class 1 and 2) and side views (class 3) (Figure 5.3 B).

2D class averaging optimization lead to the exclusion of part of the initial particle set and a new set of 10 994 particles was used to form 9 averages (Supplementary Figure 5.1). This method allowed to increase the type of averages seen, clear top views (class 2, 7 and 9 of Figure 5.3 C) show the six-fold symmetry of AaFtsH since more classes were formed. While tilted top views are seen in class 3, side views were in class 5 and bottom view in class 1 of Supplementary Figure 5.1. However, the appearance of the classes did not improve, looking fuzzier than the previous classification showed in Figure 5.3 B.

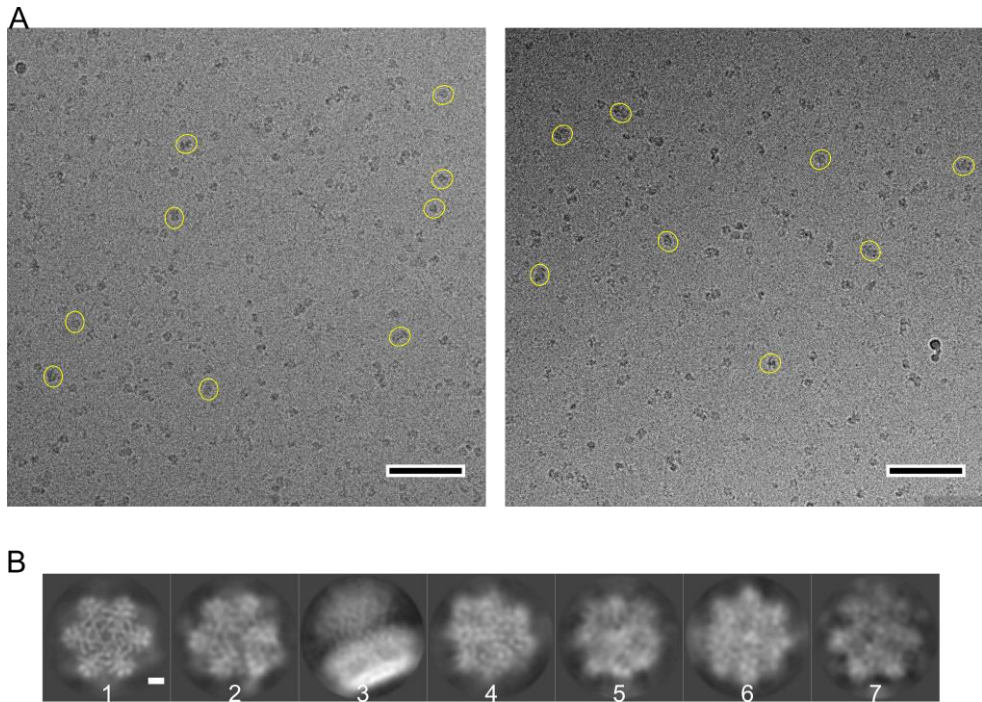


**Figure 5.3 – Cryo electron microscopy results.** The images reveal a low contrast of the particles with respect to the background (A). In B the seven classes after the first round of particle selection show a clear bottom view (class 1 and 2) and a side view (class 3). The scale bar of A is 100 nm and B is 10 Å.

An attempt to refine the first initial model shown in Figure 5.4 failed to converge to a high-resolution map. Because particle picking was considered as the probable reason for this fact, particles after automatic picking were excluded from the 2D classification. Changing the picking factors neither resulted in a higher resolution nor in the refinement of the model presented in Figure 5.3 B. The symmetry of the atomic model C6 was imposed and determined by the top and bottom view classes presented in Figure 5.3 B, classes 1 and 2.

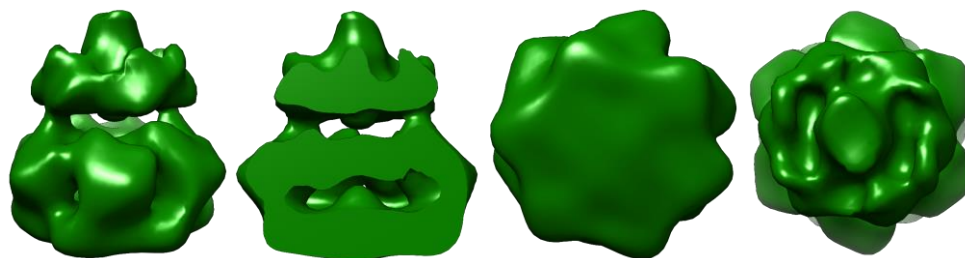
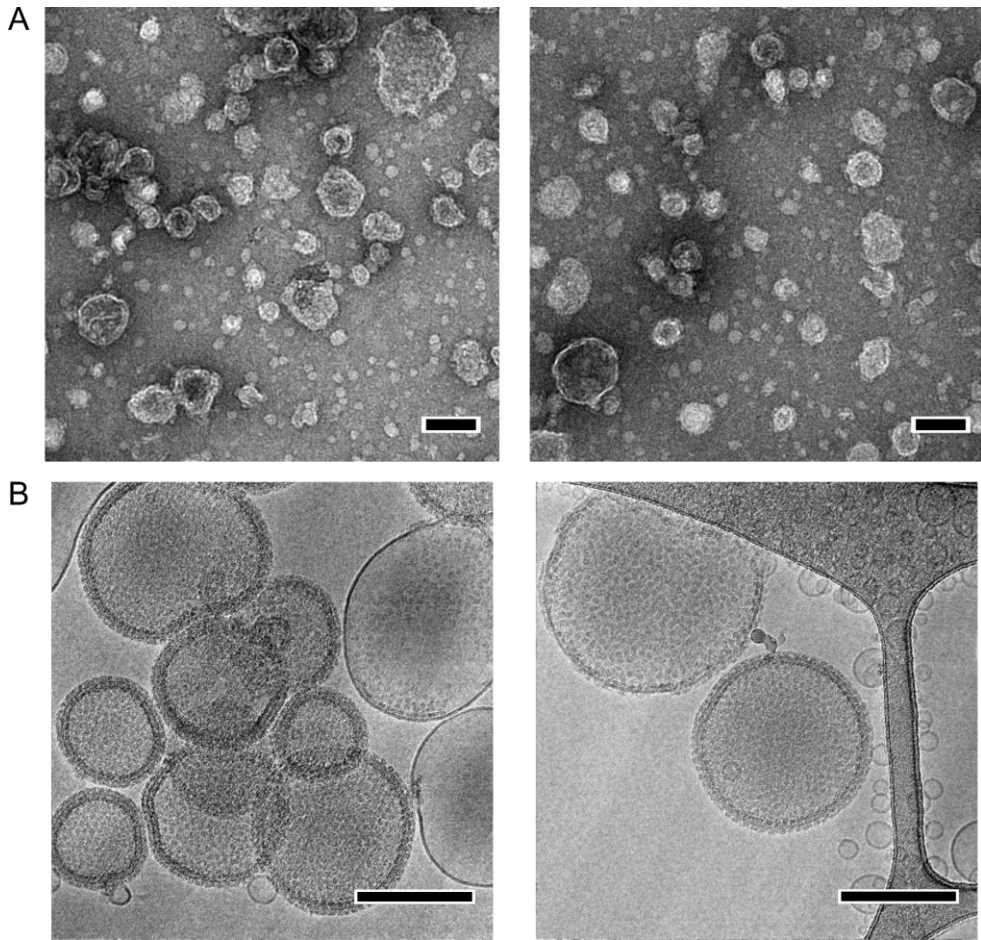


Figure 5.4 – Initial model from Relion 2.1 image processing. Different views are represented in a side, side half cut, bottom and top view.

### 5.3.3 Proteoliposomes, a magical recipe for native AaFtsH

Proteoliposomes are lipid vesicles with membrane proteins integrated in the lipid bilayer. These structures allow the study of membrane proteins in a more native like environment. We reconstituted AaFtsH into *E. coli* polar lipid membranes forming structures of about 50-100 nm. In Figure 5.5 A the negative stain micrographs show the success of the reconstitution of the second peak from the SEC, comprised of AaFtsH hexamers. The reconstitution of the first peak from the SEC was also attempted, although no clear vesicles were formed as the ones observed in the negatively stained sample. Cryo-EM shows the lipid vesicles to be densely packed with FtsH hexamers that form crystalline and mosaic patterns (Figure 5.3 B). The double lipid membrane is distinct and confirms that AaFtsH indeed was included in the membrane, where it adopts a more native like conformation. A comparison can be made with the vesicles that did not include proteins, as shown on the right side of Figure 5.5 B.



**Figure 5.5 – Proteoliposomes experiment results.** Negatively stained samples of the proteoliposomes in A show the vesicle shape and also the background of smaller vesicles formed during the reconstitution. Protein can be identified in some of the vesicles. With cryo-EM (B) it is possible to observe the mosaic like structure of the proteoliposomes as well as the double lipid membrane. Some small empty vesicles are also observed on the right panel in B. The scale bars represent 100 nm.

Reconstitute AaFtsH into proteoliposomes presents the advantage of resolving a potentially more native like structure of the protein with sub-tomography averaging and image processing. However, it is necessary to assure that the protein maintains its function throughout the reconstitution process. AaFtsH was loaded into an SDS-Page gel before or after reconstitution and the results can be compared in Figure 5.6 A. The SDS-Page proves that no degradation of the monomeric AaFtsH occurred. A Native-PAGE gel would prove that the hexameric form of AaFtsH was not

disturbed, but this turned to be difficult since AaFtsH had again to be solubilized from the proteoliposomes for analysis. Tests were performed incubating the proteoliposomes with different concentrations and different time points with 2% LMNG, but no solubilization was done.

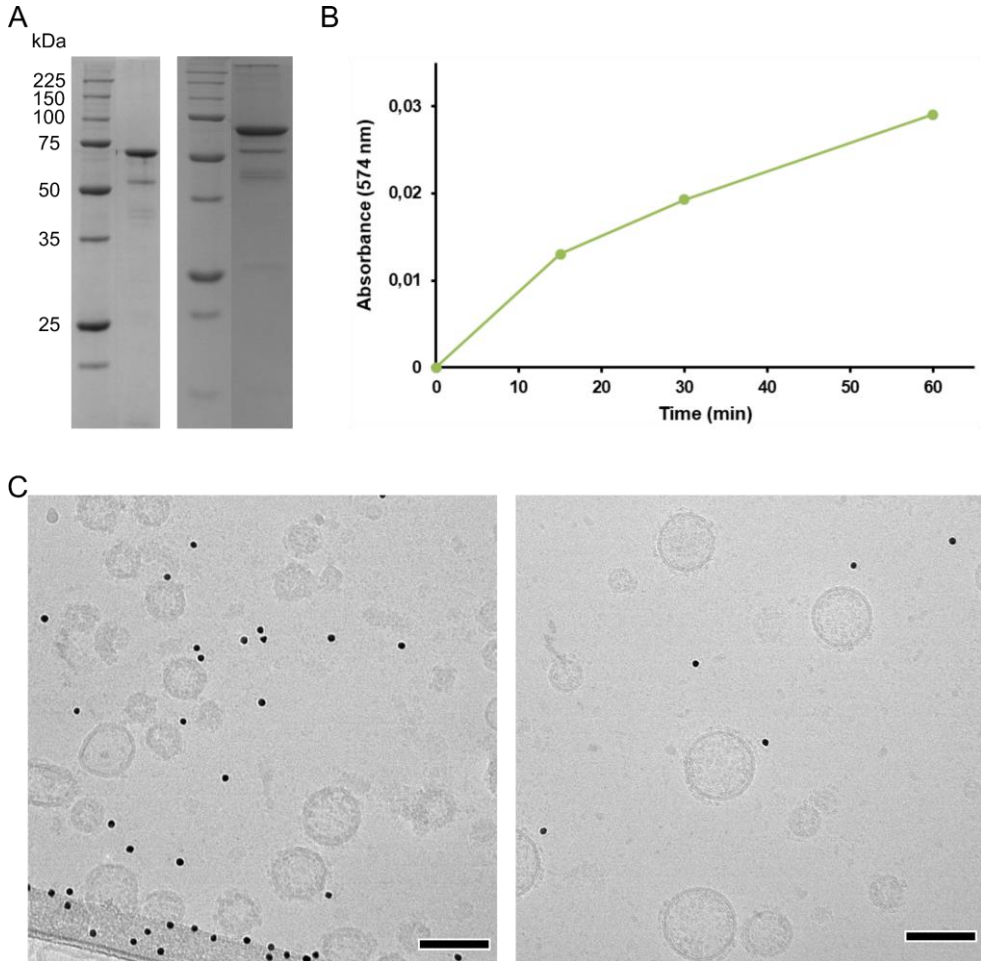


**Figure 5.6 – Cryo-ET was performed in proteoliposomes.** The integrity of AaFtsH monomers after reconstituted was tested by SDS-PAGE gel in A. The first gel (left) is the result of the sample that directly eluted from the SEC, and the second gel (right), the sample after reconstitution into proteoliposomes. The proteolytical activity of the proteoliposomes was tested using resorufin-labelled casein substrate incubated for 60 min at 60°C (B). The micrographs in C represent the projections of a slice of two subtomogram from tilt series aligned by the movie mode, while the gold nanoparticles are used to align the tilt series before the 3D reconstruction. The scale bar represents 100 nm.

Moreover, activity measurements using the same protocol as in 4.2.4 were performed in duplicates (Figure 5.6 B), showing that the proteolytic activity of the same concentration of AaFtsH monomers and AaFtsH reconstituted into proteoliposomes is different. The reconstituted AaFtsH appears to have less than double activity as the AaFtsH hexamers fraction solubilised with LMNG. This can be further explained by the uncertainty that not all monomers are incorporated in the lipid bilayer during reconstitution as entire hexamers, which would result in part of the protein not integrating the membrane and aggregating, thus having less activity than the one solubilised. Also, the resorufin-labelled casein substrate cannot penetrate the lipid bilayer, which can explain the lower activity measured compared with the one obtained for the protein in solution with detergent. Proteolytic assays using the physiological substrate described in 4.2.5 were also tested although the analysis of such assays proved to be difficult since the SDS-PAGE gels tended to be clogged by the proteoliposomes.

Despite the difficulties to prove that the protein was kept functional in the lipid bilayer, cryo-electron tomography (cryo-ET) was performed using a FEI Titan Krios TEM (300kV) and a tilting series of  $-60^{\circ}$  to  $60^{\circ}$ . As Castaño-Diez et al describe, the low signal to noise ratio of the images used in cryo-EM to avoid radiation damage are a limitation when averaging a sample [21]. The use of cryo-ET allows to collect data of the same sample at different angles and compile more information for the reconstitution of the average [21]. To calculate a meaningful 3D average of an FtsH complex many hundreds of single particle subtomograms are required. Close to a hundred full tomograms were collected and aligned with Imod 2.1. Alignment is necessary since during the acquisition of the tilt series there are shifts during tilting and focusing, which are not fully corrected. To facilitate alignment, nanogold beads of 20 nm are included during the grid preparation and freezing steps (see Figure 5.6). In Figure 5.6 C, two different areas of the grid are shown. The image processing was then performed using *Dynamo* software [21]. The first steps of identifying the double membrane for class averaging processing was performed although some difficulties related to the few number of particles identified by naked eye emerged.

The image processing of the tomograms is still in progress and more tomograms need to be acquired to produce stronger data.

## 5.4 Discussion and conclusion

AaFtsH has proven to be a protein difficult to structurally characterize which is explainable by the protein flexibility observed during this thesis. The negatively stained tilting pairs of Figure 5.1, processed by random conical tilting image processing (Figure 5.2), proved not to provide further information to the 3D model shown in the last Chapter 4 [27]. The acquisition of tilting pairs at the microscope is a challenging technique since there is a need to acquire an image in the same area of the correspondent tilting pair. When tilting the specimen inside the microscope there is always a shift, which has to be compensated when performing the imaging of a pair (Figure 5.1 A). In this case, we used stain artefacts, characteristic of that location, to detect the area where the image of the untitled sample was acquired, as shown in Figure 5.1 B. Although a few tilted views gave some insight of the top and bottom views, their resolution did not suffice to improve the negatively stained 3D model presented in Chapter 4. The other goal of the random conical tilt approach was to confirm the symmetry of the protein as it has been suggested by other crystal structures [28–33]. However, the views of tilted negatively stained particles had an insufficient resolution to also confirm the C6 symmetry (Figure 5.2). For this reason, we decided to acquire cryo-EM images of vitrified samples conserved in liquid nitrogen. The creation of vitreous ice allows the imaging of protein samples in the most native state without artefacts of crystallization and negative stain [34]. Because the signal to noise ratio of cryo-EM images is low and low recording doses must be used to prevent radiation damage, micrographs need to be acquired at very high under focus to discern particles. However, this results in difficulties during image processing [35] as can be seen in Figure 5.3. Taking images closer to focus would guarantee a higher resolution because the CTF envelope declines slower than at a strong under focus. In the set of 1 371 micrographs, acquired with the FEI Titan Krios TEM (300kV), the resulting 2D class average formed by Relion 2.1 did not provide enough resolution for a 3D model of AaFtsH, despite of the effort to run

several picking cycles it seems that instead of improving the results, the classification becomes more blurry (Figure 5.3 B and Supplementary Figure 5.1). Nevertheless, results from multiple particle picking and classification cycles confirmed that the protein has a six-fold symmetry, clearly demonstrated by class number 1 and 2 of Figure 5.3 B. Class number 2 confirms that the protease domain is a well conserved robust structure since this class average indicates atomic resolution. Although progress in AaFtsH structures was achieved with cryo-EM, these preliminary data did not generate a high-resolution 3D model. The reason for this is related to the flexibility of the protein in its ATPase and linker domains, which introduces a conformational variability in the intermembrane and intramembrane domains (as can be observed in class 5 of Supplementary Figure 5.1). This corroborates our observations described in Chapter 4 that the flexibility of the linker domain is higher than previously described. The resolution of structures resolved by cryo-EM have been increasing since the availability of direct detector cameras [8–10], and advances in image processing [1,16,21,36,37]. However, to automatically pick projections of proteins as flexible as AaFtsH, novel approaches are required, such as autolearning algorithms based on convolutional neural networks. The time was not available to explore EMAN 2.2, which offers a neural network particle auto picker, which with minimal information is capable of search for image characteristics in a more efficient and faster ways than what the human brains needs [38]. With the development of the microscope technology and the software used in single particle processing, AaFtsH 3D model will be successfully resolved to a high-resolution, provided that more data can be recorded.

Cryo-ET is the second approach used nowadays for resolving the structure of membrane proteins in their native environment. However, this technique is challenging since for the acquisition of tilt series the stability and quality of the microscope used must be at its maximum. AaFtsH has been reconstituted in the past into proteoliposomes by Akiyama et al. [39]. Here also, we successfully reconstituted the protein into proteoliposomes as Figure 5.5 and Figure 5.6 show. Both negatively stain samples and cryo-EM show that the protein is included in the lipid membrane, some smaller vesicles without protein and debris are also identifiable by both

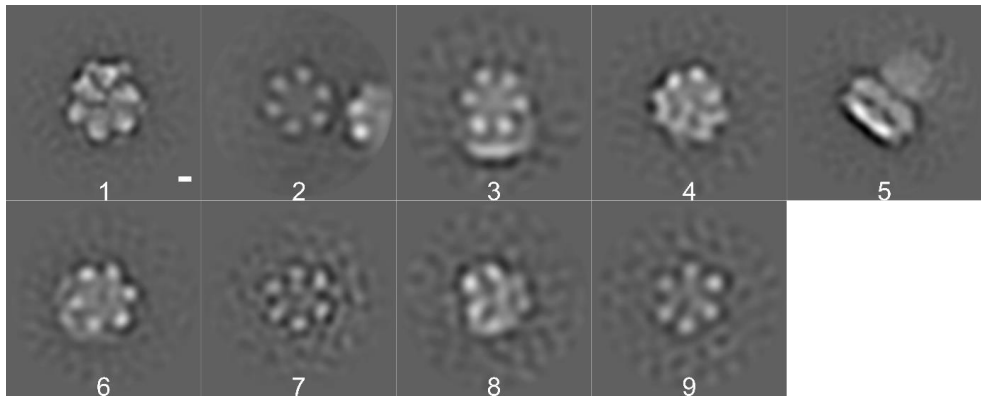
techniques (Figure 5.5). The integrity of the FtsH monomer was confirmed by SDS-PAGE by comparing the bands obtained before and after forming proteoliposomes (Figure 5.6 A). Moreover, the proteolytic activity of these vesicles was tested using resorufin-labelled casein showing that some activity is present after reconstitution, although at a smaller level when compared to the wild type AaFtsH solubilised with LMNG (as described in Chapter 4). This is a rather unexpected result since it has been proven that membrane proteins are more stable and active when incorporated into proteoliposomes. However, because casein carries a fluorophore that is unable to pass through the membrane, and in general proteoliposomes harbour reconstituted membrane proteins in both orientations, only half of the AaFtsH hexamers would be accessible for recognition. Moreover, the crowdedness of the membrane, in a proteoliposome form, may interfere with casein access to FtsH loops. Therefore, a different assay must be established to test the proteolytical activity of the generated proteoliposomes. One of the main challenges of this assay is that the protein is inserted into the lipid bilayer and disrupting this membrane by a second solubilization will not allow to study the protein in its native state. The use of the physiological substrate sigma32 (as described in Chapter 4) would not give enough insight since its degradation is not fully complete as shown in Chapter 4. It might be helpful to use a smaller substrate that would be immediately recognized by AaFtsH without having to increase the temperature to 60°C. One alternative is the use of the small peptide Phe- Gly-His-<sup>NO<sub>2</sub></sup>Phe-Phe-Ala-Phe-OMe used by Bruckner et al [40], whose degradation would be identifiable by mass-spectrometry.

Nevertheless, seventy sub tomograms were processed in this work. Acquisition of the tomograms was performed using a FEI Titan Krios TEM (300kV) equipped with a Gatan K2 Summit direct electron detector to maximize the resolution obtained from the data sets. To acquire and align tilt series from -60° to 60°, recording an image every 3°, gold nanoparticles allow sample shifts to be identified and compensated. We used the fiducial model approach implemented in Imod 1.2.3 [26], and the image processing package *Dynamo* [21]. Although the image processing of the proteoliposomes revealed to be difficult because proteins were inserted in the lipid bilayer in both orientations, and only few particles were found per proteoliposomes

used for the sub tomogram session. Manual picking of the particles was performed to start, but no satisfactory 2D classification average was achieved. This problem can be overcome with the acquisition of a bigger set of data including more particles per proteoliposome, which will increase the signal obtained for the 2D classification.

AaFtsH revealed to be a challenging membrane protein to structurally characterize, but our work demonstrates that it is possible to obtain good cryo-EM preparations with no particle aggregation on the grid. Further optimizing the protein conditions may be helpful for a future structural characterization. The advances in science will lead to the structure characterization of AaFtsH, which will reveal further details of the ATP hydrolysis and substrate degradation by AaFtsH.

## 5.5 Supplementary information



**Supplementary Figure 5.1 – Attempt to create a better classification than in Figure 5.3.** The automatic picking of particles seems not to converge to a better resolution. Although the resolution is small, it is possible to observe more orientations of the particles in this classification round. Example of this is class numbers 3, 6 and 8 which are AaFtsH tilted views that can be observed by naked eye. Although this information does not seem to fit in the algorithm run into Relion 2.1. The scale bar corresponds to 10 Å.

## 5.6 References

- [1] A. Patwardhan, IUCr, Trends in the Electron Microscopy Data Bank (EMDB), *Acta Crystallographica Section D Structural Biology*. 73 (2017) 503–508.
- [2] W. Kühlbrandt, Cryo-EM enters a new era, *ELife*. 3 (2014) e03678.
- [3] A. Merk, A. Bartesaghi, S. Banerjee, V. Falconieri, P. Rao, M.I. Davis, R. Pragani, M.B. Boxer, L.A. Earl, J.L.S. Milne, S. Subramaniam, Breaking Cryo-EM Resolution Barriers to Facilitate Drug Discovery, *Cell*. 165 (2016) 1698–1707.
- [4] A. Pandey, K. Shin, R.E. Patterson, X.-Q. Liu, J.K. Rainey, Current strategies for protein production and purification enabling membrane protein structural biology, *Biochemistry and Cell Biology*. 94 (2016) 507–527.
- [5] J. Dubochet, M. Adrian, J. Lepault, A.W. McDowell, Emerging techniques: Cryo-electron microscopy of vitrified biological specimens, *Trends in Biochemical Sciences*. 10 (1985) 143–146.
- [6] J. Dubochet, M. Adrian, J.-J. Chang, J.-C. Homo, J. Lepault, A.W. McDowell, P. Schultz, Cryo-electron microscopy of vitrified specimens, *Quarterly Reviews of Biophysics*. 21 (1988) 129.
- [7] J. Dubochet, A.W. McDowell, VITRIFICATION OF PURE WATER FOR ELECTRON MICROSCOPY, *Journal of Microscopy*. 124 (1981) 3–4.
- [8] A.R. Faruqi, R. Henderson, L. Tlustos, Noiseless direct detection of electrons in Medipix2 for electron microscopy, *Nuclear Instruments and Methods in Physics Research Section A: Accelerators, Spectrometers, Detectors and Associated Equipment*. 546 (2005) 160–163.
- [9] N. Grigorieff, Direct detection pays off for electron cryo-microscopy, *ELife*. 2 (2013) e00573.
- [10] G. McMullan, A.R. Faruqi, D. Clare, R. Henderson, Comparison of optimal performance at 300 keV of three direct electron detectors for use in low dose electron microscopy, *Ultramicroscopy*. 147 (2014) 156–163.
- [11] X. Li, P. Mooney, S. Zheng, C.R. Booth, M.B. Braunfeld, S. Gubbens, D.A. Agard, Y. Cheng, Electron counting and beam-induced motion correction enable near-atomic-resolution single-particle cryo-EM, *Nature Methods*. 10 (2013) 584–590.
- [12] T. Grant, N. Grigorieff, Automatic estimation and correction of anisotropic magnification distortion in electron microscopes, *Journal of Structural Biology*. 192 (2015) 204–208.
- [13] K. Zhang, Gctf: Real-time CTF determination and correction, *Journal of Structural Biology*. 193 (2016) 1–12.

- [14] J.M. Rosa-Trevín de la, A. Quintana, L. del Cano, A. Zaldívar, I. Foche, J. Gutiérrez, J. Gómez-Blanco, J. Burguet-Castell, J. Cuenca-Alba, V. Abrishami, J. Vargas, J. Otón, G. Sharov, J.L. Vilas, J. Navas, P. Conesa, M. Kazemi, R. Marabini, C.O.S. Sorzano, J.M. Carazo, Scipion: A software framework toward integration, reproducibility and validation in 3D electron microscopy, *Journal of Structural Biology*. 195 (2016) 93–99.
- [15] G. Tang, L. Peng, P.R. Baldwin, D.S. Mann, W. Jiang, I. Rees, S.J. Ludtke, EMAN2: An extensible image processing suite for electron microscopy, *Journal of Structural Biology*. 157 (2007) 38–46.
- [16] S.H.W. Scheres, Processing of Structurally Heterogeneous Cryo-EM Data in RELION, *Methods in Enzymology*. 579 (2016) 125–157.
- [17] T.R. Shaikh, H. Gao, W.T. Baxter, F.J. Asturias, N. Boisset, A. Leith, J. Frank, SPIDER image processing for single-particle reconstruction of biological macromolecules from electron micrographs, *Nature Protocols*. 3 (2008) 1941–1974.
- [18] M. van Heel, G. Harauz, E. V. Orlova, R. Schmidt, M. Schatz, A New Generation of the IMAGIC Image Processing System, *Journal of Structural Biology*. 116 (1996) 17–24.
- [19] W. Baumeister, J. Ortiz, S. Nickell, J. Plitzko, Mapping Molecular Landscapes inside Cells, (n.d.).
- [20] V. Lučić, A. Rigort, W. Baumeister, Cryo-electron tomography: The challenge of doing structural biology in situ, *J Cell Biol*. 202 (2013) 407–419.
- [21] D. Castaño-Díez, M. Kudryashev, M. Arbeit, H. Stahlberg, Dynamo: A flexible, user-friendly development tool for subtomogram averaging of cryo-EM data in high-performance computing environments, *Journal of Structural Biology*. 178 (2012) 139–151.
- [22] D. Castaño-Díez, M. Kudryashev, H. Stahlberg, Dynamo Catalogue: Geometrical tools and data management for particle picking in subtomogram averaging of cryo-electron tomograms, *Journal of Structural Biology*. 197 (2017) 135–144.
- [23] J.R. Meyerson, T.A. White, D. Bliss, A. Moran, A. Bartesaghi, M.J. Borgnia, M.J. V de la Cruz, D. Schauder, L.M. Hartnell, R. Nandwani, M. Dawood, B. Kim, J.H. Kim, J. Sununu, L. Yang, S. Bhatia, C. Subramaniam, D.E. Hurt, L. Gaudreault, S. Subramaniam, Determination of molecular structures of HIV envelope glycoproteins using cryo-electron tomography and automated subtomogram averaging., *Journal of Visualized Experiments : JoVE*. (2011).
- [24] T.A.M. Bharat, D. Kureisaite-Ciziene, G.G. Hardy, E.W. Yu, J.M. Devant, W.J.H. Hagen, Y. V. Brun, J.A.G. Briggs, J. Löwe, Structure of the hexagonal surface layer on *Caulobacter crescentus* cells, *Nature Microbiology*. 2 (2017) 17059.

- [25] S.H.W. Scheres, RELION: implementation of a Bayesian approach to cryo-EM structure determination., *Journal of Structural Biology*. 180 (2012) 519–30.
- [26] D.N. Mastronarde, S.R. Held, Automated tilt series alignment and tomographic reconstruction in IMOD, *Journal of Structural Biology*. 197 (2017) 102–113.
- [27] S.H.W. Scheres, R. Núñez-Ramírez, C.O.S. Sorzano, J.M. Carazo, R. Marabini, Image processing for electron microscopy single-particle analysis using XMIPP., *Nature Protocols*. 3 (2008) 977–90.
- [28] M. Vostrukhina, A. A. Popov, B. E. Brunstein, C. M.A. Lanz, D. A. R. Baumgartner, A. C. Bieniossek, E. A. M. Schacherl, C. A. Ulrich, Baumann, C. \*, The structure of Aquifex aeolicus FtsH in the ADP-bound state reveals a C2-symmetric hexamer, *Acta Crystallogr D Biol Crystallogr*. D71 (2015) 1307–1318.
- [29] R. Suno, H. Niwa, D. Tsuchiya, X. Zhang, M. Yoshida, K. Morikawa, Structure of the Whole Cytosolic Region of ATP-Dependent Protease FtsH, *Molecular Cell*. 22 (2006) 575–585.
- [30] R. Suno, M. Shimoyama, A. Abe, T. Shimamura, N. Shimodate, Y.-H. Watanabe, Y. Akiyama, M. Yoshida, Conformational transition of the lid helix covering the protease active site is essential for the ATP-dependent protease activity of FtsH, *FEBS Letters*. 586 (2012) 3117–3121.
- [31] C. Bieniossek, B. Niederhauser, U.M. Baumann, The crystal structure of apo-FtsH reveals domain movements necessary for substrate unfolding and translocation., *Proceedings of the National Academy of Sciences of the United States of America*. 106 (2009) 21579–21584.
- [32] S.H. Kim, G.B. Kang, H.E. Song, S.J. Park, M.H. Bea, S.H. Eom, Structural studies on *Helicobacter pylori* ATP-dependent protease, FtsH., *Journal of Synchrotron Radiation*. 15 (2008) 208–10.
- [33] Y. Shotland, D. Teff, S. Koby, O. Kobiler, A.B. Oppenheim, Characterization of a conserved  $\alpha$ -helical, coiled-coil motif at the C-terminal domain of the ATP-dependent FtsH (HflB) protease of *Escherichia coli*, *Journal of Molecular Biology*. 299 (2000) 953–964.
- [34] R. Fernandez-Leiro, S.H.W. Scheres, Unravelling biological macromolecules with cryo-electron microscopy, *Nature*. 537 (2016) 339–346.
- [35] S. Jonic, C. Vénien-Bryan, Protein structure determination by electron cryo-microscopy., *Current Opinion in Pharmacology*. 9 (2009) 636–42.
- [36] J.M. Bell, M. Chen, P.R. Baldwin, S.J. Ludtke, High resolution single particle refinement in EMAN2.1, *Methods*. 100 (2016) 25–34.
- [37] S.J. Ludtke, Single-Particle Refinement and Variability Analysis in EMAN2.1, *Methods in Enzymology*. 579 (2016) 159–189.

- [38] M. Chen, W. Dai, S.Y. Sun, D. Jonasch, C.Y. He, M.F. Schmid, W. Chiu, S.J. Ludtke, Convolutional neural networks for automated annotation of cellular cryo-electron tomograms, *Nature Methods*. 14 (2017) 983–985.
- [39] Y. Akiyama, K. Ito, Reconstitution of membrane proteolysis by FtsH, *Journal of Biological Chemistry*. 278 (2003) 18146–18153.
- [40] R.L. Bruckner, Robert C.; Gunyuzlu, Paul L. and Stein, Coupled Kinetics of ATP and Peptide Hydrolysis by *Escherichia coli* FtsH Protease, *Biochemistry*. 42 (2003) 10843–10852.



# Chapter 6

## Conclusion and Outlook

Membrane protein structural characterization has been explored, for decades now, by the scientific community. Despite the growth of solved structures in the last decades it is clear that much progress is expected to happen in the next years. In this thesis we explored the application of diverse techniques to study the FtsH structure as well as its activity to increase the knowledge in the field of membrane AAA proteases. This chapter summarizes the contributions of this thesis to the scientific knowledge about FtsH and presents a future perspective of what can be done.

## **6.1 Summary and contributions to the field**

Proteolysis is one of the most interesting mechanism operated by proteins, since proteins are the ones controlling the degradation of other proteins. This is a mechanism that includes a high demand of cell organization but also of energy consumption. When proteolysis is performed in the lipid bilayer through the involvement of a membrane protein, which is an intriguing process for the scientific community. FtsH has been studied for decades, and despite the advances in resolving the cytoplasmic conformational changes comparing several crystal structures, not much information is provided about the way this protein can degrade soluble and insoluble substrates. Also, how it coordinates this degradation mechanism with the burning of ATP energy remains an open question. All these reasons lead me to explore the conditions to express and purify FtsH, to study its activity and structure.

In this thesis Chapter 2 explores the expression conditions, some of them already published before, but the majority with novel approaches based on more recent cell strains and testing how different buffers and columns impact the purification results. The EcFtsH solubilization revealed to be difficult since the protein is not stable enough to be maintained in an aqueous solution with the detergent tested, as shown by the low activity levels. For that reason, in Chapter 3 we use a homologous thermophile sequence to explore FtsH expression and purification. The use of thermophiles to improve expression and stability of proteins is common in the scientific community [1–5]. With this construct, not only the solubilization and purification of the wild-type mutant was investigated but also mutants that inhibit the ATPase or/and the protease of the protein. Furthermore, in Chapter 4 a detailed study is performed to reveal a novel conformational state that FtsH is capable of maintaining while solubilized: the dodecamer conformation. Negatively stained single particle imaging processing lead to a 3D model for both the hexamer and the dodecamer particles. Despite the low resolution of these models, we show that the protein is capable of maintaining its ATPase and proteolytical activity even in presence of a physiological substrate. Our findings show that this protein is capable

of undergo large movements in relation to the membrane: tilting the cytoplasm domain to form an angle higher than  $13 \text{ \AA}$ , bigger than what was previously described in literature [6]. Finally, in Chapter 5, we present the cryo-EM studies several 2D class averages that do not converge to a high-resolution model due to the high flexibility of the ATPase domain shown in the previous chapter. Moreover, we show that there is another approach that could be followed to further explore FtsH structural characterization: using proteoliposomes. The inclusion of FtsH into proteoliposomes was successful. The use of cryo-ET to characterize the structure of FtsH within the proteoliposomes is still under development. Although it was not possible to reach a high-resolution model from the natively embedded protein, I believe that these results bring new knowledge about FtsH.

## 6.2 Future work

The knowledge gathered in this thesis concerns different approaches to purify FtsH and explore its structure and can be used for future studies in a useful manner. The application of optical tweezers to study the kinetics of the protein degradation as used by Aubin-Tam et al. is one of the goals of the bigger research project where this PhD thesis was included [7]. This type of study will deepen the understanding at the single molecule level, improving our knowledge not only for this specific protein but for the whole proteolytical mechanism.

The different activity assays run during this work revealed. The degradation kinetics with a commercial substrate, facilitating the activity tests of future experiments. The proteolytical activity can be further characterized by using physiological substrates that can be fluorochrome labelled in order to trace in a more specific manner FtsH proteolytical activity, as suggested in 5.4.

The last chapter of this thesis demonstrates the potential of cryo-EM, since a new set of micrographs increasing the number of particles picked during the imaging processing may lead to high-resolution models of the different conformations of full-length FtsH. Such model will answer the questions of how substrates are recognized and transferred to the site of degradation during the process of ATP hydrolysis.

Despite in the newest work published about FtsH [8], it is possible to have a better look into the structural rearrangements that this protein adapts during ATP hydrolysis, it is not clear how the full structure in its native environment supports these structural changes. This is the potential of the data acquired by cryo-tomography. The characterization of FtsH structure inserted in the lipid bilayer will show the rearrangements that occur in the membrane domain. Furthermore, if the FtsH proteoliposomes can be mixed with membrane resident substrate labelled, for example with gold-nanobead. This will lead to the knowledge how insoluble proteins access the central pore of the proteolytical chamber.

In addition, to the use of detergents was I was also involved in studies using styrene maleic acid (SMA), which is a polymer capable of forming nanodiscs disrupting the membrane and leaving the protein trap inside this disc. These results were present in [9,10]. Their work confirmed that FtsH extraction from the membrane is not an easy task. Nevertheless, this approach is worth exploring for FtsH stabilization in solution since more and novel polymers are being developed with different ionic characteristics.

It would not make sense to pursue FtsH high-resolution resolution model if we forget the biological importance of this protein. This is a crucial protein for *E. coli* survival and malformations of its homologous leads to severe forms of paraplegia in humans. Not only, can FtsH protein structural solve biological questions, but it may also be a route to new drugs, which is important for the human health. We should find strategies to annihilate bacteria in a specific way, rather than using broad spectrum antibiotics. Also, increased knowledge about this protein structure will deepen our knowledge about the disease mechanisms in humans and create a transversal knowledge not only about FtsH itself but also about proteolytical mechanisms, an important vital control mechanism inside the cell.

### 6.3 References

- [1] M. de Champdoré, M. Staiano, M. Rossi, S. D'Auria, Proteins from extremophiles as stable tools for advanced biotechnological applications of high social interest., *Journal of the Royal Society, Interface.* 4 (2007) 183–91.
- [2] A. Razvi, J.M. Scholtz, Lessons in stability from thermophilic proteins., *Protein Science : A Publication of the Protein Society.* 15 (2006) 1569–78.
- [3] B. Boussau, S. Blanquart, A. Necsulea, N. Lartillot, M. Gouy, Parallel adaptations to high temperatures in the Archaean eon, *Nature.* 456 (2008) 942–945.
- [4] L. Schweizer, L. Mueller, Protein Conformational Dynamics and Signaling in Evolution and Pathophysiology, in: *Biased Signaling in Physiology, Pharmacology and Therapeutics*, Elsevier, 2014: pp. 209–249.
- [5] J. Ruprecht, J; Nield, Determining the structure of biological macromolecules by transmission electron microscopy, single particle analysis and 3D reconstruction, *Progress in Biophysics and Molecular Biology.* 75 (2001) 121–164.
- [6] S. Lee, S. Augustin, T. Tatsuta, F. Gerdes, T. Langer, F.T.F. Tsai, Electron cryomicroscopy structure of a membrane-anchored mitochondrial AAA protease, *Journal of Biological Chemistry.* 286 (2011) 4404–4411.
- [7] M.-E. Aubin-Tam, A.O. Olivares, R.T. Sauer, T.A. Baker, M.J. Lang, Single-molecule protein unfolding and translocation by an ATP-fueled proteolytic machine., *Cell.* 145 (2011) 257–67.
- [8] Z.A. Ripstein, R. Huang, R. Augustyniak, L.E. Kay, J.L. Rubinstein, Structure of a AAA+ unfoldase in the process of unfolding substrate, *ELife.* 6 (2017) e25754.
- [9] N. de Lange, Proteolytic activity of membrane protein FtsH, TUDelft, 2017.
- [10] F. Honig, Preparation and purification of SMA-FtsH nanodiscs, TUDelft, 2016.



# Summary

Proteins are one of the most important constituents of cells, since they are responsible for various processes such as replication, translation, etc. Interestingly, proteins are also responsible for the degradation of proteins that do not assemble well, and/or which are not necessary anymore inside the cell. This process of proteins destruction and recycling of amino acids is called proteolysis. Without this process, the cell would accumulate toxic waste and would not survive for long. This highlights the importance of this process. This process occurs not only in the cell cytoplasm but in the cell lipid bilayer leading to the degradation of soluble and membrane integral proteins. In bacteria, the protein responsible for this mechanism is vital and it is called FtsH. FtsH is part of the AAA+ proteases family, which are deeply investigated since they are responsible for many important biological mechanisms inside the cell.

In this thesis, we aimed to answer the question of how can FtsH not only degrade soluble proteins, but also degrade insoluble proteins. In a complex mechanism in which soluble/insoluble proteins are unfolded passing through an ATPase domain, and into a protease domain for degradation. The curiosity about this mechanism is also high, regarding how can this protein coordinate this ATP hydrolysis and coordinate it with the proteolytical process.

To answer these questions, this thesis presents a series of purification protocols for *E. coli* FtsH (Chapter 2) and for an orthologous of FtsH, a thermophile called *Aquifex aeolicus* (presented in Chapter 3). During this thesis, we show that the movements that the ATPase domain can undergo in relation to the membrane are larger than

what was previously described in literature (Chapter 4). The assembling of this protein into dodecamers, in the solubilized form, showed that the intermembrane loops are more flexible than what was thought before. A kinetic characterization of the ATPase and protease activity is also assessed showing that both forms are equally functional. Finally, in Chapter 5, we explore the use of cryo-electron microscopy and tomography to perform an exhaustive single particle study. Although the cryo-TEM results showed in this chapter are preliminary 2D class averages, it is possible to observe the six-fold symmetry structure of this protein, which is an incentive to pursue the studies with this technique. The same is true for the cryo-tomography performed on FtsH in the proteoliposomes which will provide further insights about the protein insertion into the membrane and allow to the study how substrates can access the ATPase domain loops.

This thesis describes the efforts made in the FtsH purification protocol optimization to get a sample as pure and stable as possible. This thesis showed that FtsH undergoes much larger conformational changes than previously thought and challenges the currently accepted model for the substrate to access FtsH active site.

In the future cryo-electron microscopy of single particles and cryo-tomography of proteoliposomes must be explored too deepen our knowledge of the full-length FtsH structure, and more generally our knowledge about proteolytical mechanisms in cells.

# Samenvatting

Eiwitten zijn een van de belangrijkste bestanddelen van cellen, omdat ze verantwoordelijk zijn voor verschillende processen zoals replicatie, translatie, etc. Interessant is dat eiwitten ook verantwoordelijk zijn voor de afbraak van eiwitten die niet goed assembleren en/of niet noodzakelijk zijn meer in de cel. Dit proces van eiwitvernietiging en recycling van aminozuren wordt proteolyse genoemd. Zonder dit proces zou de cel giftig afval verzamelen en zou het niet lang overleven. Dit benadrukt het belang van dit proces. Dit proces vindt niet alleen plaats in het celcytoplasma, maar ook in de cellipide dubbellaag die leidt tot de afbraak van oplosbare en membraan-integrale eiwitten. In bacteriën is het eiwit dat verantwoordelijk is voor dit mechanisme van vitaal belang en wordt het FtsH genoemd. FtsH maakt deel uit van de AAA<sup>+</sup> proteasenfamilie, die diep onderzocht omdat ze verantwoordelijk zijn voor vele belangrijke biologische mechanismen in de cel.

In dit proefschrift hebben we ons gericht op het beantwoorden van de vraag hoe FtsH niet alleen oplosbare eiwitten kan afbreken, maar ook onoplosbare eiwitten kan afbreken. In een complex mechanisme waarin oplosbare/onoplosbare eiwitten worden ontvouwen door een ATPase-domein en in een proteasedomein voor afbraak. De nieuwsgierigheid naar dit mechanisme is ook groot, met betrekking tot hoe dit eiwit deze ATP-hydrolyse kan coördineren en coördineren met het proteolytische proces.

Om deze vragen te beantwoorden presenteert dit proefschrift een reeks zuiveringsprotocollen voor *E. coli* FtsH (hoofdstuk 2) en voor een ortholoog van FtsH,

een thermofiel genaamd *Aquifex aeolicus* (gepresenteerd in hoofdstuk 3). Tijdens dit proefschrift laten we zien dat de bewegingen die het ATPase-domein kan ondergaan in relatie tot het membraan groter zijn dan wat eerder in de literatuur werd beschreven (Hoofdstuk 4). De assemblage van dit eiwit in dodecamers, in de oplosbare vorm, liet zien dat de intermembrane lussen flexibeler zijn dan eerder gedacht. Een kinetische karakterisering van de ATPase en protease activiteit wordt ook beoordeeld, hetgeen aantoont dat beide vormen even functioneel zijn. Ten slotte verkennen we in hoofdstuk 5 het gebruik van cryo-elektronenmicroscopie en tomografie om een uitputtende studie van een enkel deeltje uit te voeren. Hoewel de cryo-TEM-resultaten in dit hoofdstuk voorlopige 2D-klassengemiddelden zijn, is het mogelijk de zesvoudige symmetriestructuur van dit eiwit waar te nemen, wat een stimulans is om de studies met deze techniek voort te zetten. Hetzelfde geldt voor de cryo-tomografie die wordt uitgevoerd op FtsH in de proteoliposomen, wat verdere inzichten zal verschaffen over de eiwitinvloeging in het membraan en het mogelijk zal maken om te bestuderen hoe substraten toegang hebben tot de ATPase-domeinlussen.

Dit proefschrift beschrijft de inspanningen die zijn geleverd in de optimalisatie van het FtsH-zuiveringsprotocol om een monster zo zuiver en stabiel mogelijk te krijgen. Dit proefschrift liet zien dat FtsH veel grotere conformatieveranderingen ondergaat dan eerder werd gedacht en daagt het momenteel geaccepteerde model voor het substraat uit om toegang te krijgen tot de actieve site van FtsH.

In de toekomst moet cryo-elektronenmicroscopie van afzonderlijke deeltjes en cryo-tomografie van proteoliposomen worden onderzocht om onze kennis van de FtsH-structuur van volledige lengte en meer in het algemeen onze kennis over proteolytische mechanismen in cellen te verdiepen.

# Acknowledgements

Four years ago, when this adventure started I was far from imagine that I would be seated writing these words in Sweden, although this journey has taught me a lot. I have growth as an individual and as a professional (which I believe it is the main objective of a PhD degree) and for that "Thank you" to all that made part of my life during this time. Science revealed to be a difficult journey for me the high competition and the eager for higher impact than for precious knowledge was a major disappointment for me. Although, I met great people during this journey who do science for the right reasons, for the eager of knowledge and to help the society to evolve. I believe this is what a scientist should remember in the lab every day. And as one of the most admirable men I met, Jacques Dubochet, in his Nobel prize presentation said: "scientists should worry in becoming as good humans as they are scientists".

First, I would like to thank you Marie-Eve for giving me the opportunity to explore this project and for the daily guidance. You always encouraged me to continue even in the tough times. I admire your spirit and your determination to pursue science, having a beautiful family and your faith. Thank you, also to you Andreas for the opportunity to learn with such an experience and young spirit as yours. I always had the feeling that you had more energy than me which fascinated me. Thank you for all your advices and for receiving me at your place and giving me the chance to meet your lovely wife. Moreover, I would like to thank Barbara for receiving me inside your house even without knowing me. I wish you all of you, all the happiness and success for you and your families.

I would like to thank the members of the committee Professor Claire, Professor Ulrich, Professor Marileen and Dr. Arjen. Thank you for the honour of discussing my work with you.

Thanks to Andreas I also had the opportunity to visit C-CINA in Basel and meet great professionals. I thank to Doctor Henning Stahlberg for the opportunity to collaborate during the project with your group. Mohamed, thank you so much for all your patience, teaching and guidance during the times that I visit Basel but also when I needed help from Delft. You were one of the most fascinating scientists that I met in these four years due to your generosity and truly dedication to science. Moreover, I also would like to thank for the honour you gave me belonging to my thesis committee. I wish you the best and your family. In this journey I cannot forget Daniel also for your help and for hearing me during the times I was in Basel: Muchas gracias por todo! To the rest of Henning's group, which helped me during my stay: Ricardo, Paul, Paula, Karen and many others thank you for your help and specially for your welcoming in the lab. Wish you guys enormous success!

The life in Delft was not easy for me, the adaptation to a new country so different from my native country, the PhD project that did not work as planned, and I struggle with, and the realization that after the PhD I needed to find a solution for my life wouldn't be possible without: good friends. So the next lines are for you my friends. Victor, no sé por dónde empezar la verdad es que todavía me imagino en la oficina cuando me hiciste la entrevista, te acuerdas? Me da la risa imaginarlo, tu cara de que no te creías que hablaba español. Fuiste siempre un bon compañero y sin ti ahí en la oficina talvez no hubiera terminado. Espero que podamos mantener esta amistad por mucho en nuestras vidas mismo que estemos lejos en diferentes países. iiMuchísimas gracias y lo logramos!! A ti y a Fabiola os deseo el mejor que sean muy felices y que yo y Nuno estemos aquí para verlos construir una bonita vida. Alicia, has sido la primera persona que me acogió en Holanda y siempre estuviste ahí en los peores y sobre todo en los mejores momentos en Delft. Aunque no hablemos todos los días y que estemos lejos estarás siempre en mi corazón, es como una hermanita más pequeña que no he tenido. A ti y a Roland, os deseo la mayor

felicidad. ¡Aquí estaré siempre para una buena charla! ¡Ah, y gracias a ti y a Victor por haber aceptado defenderme en este día! Roland, first thank you so much for all your patience with me to teach me commands and all those stuffs, I know I was not an easy student. Thank you for taking such good care of us always with a smile. I imagine that staying is also not easy, and for that I admire your courage and I hope you find what you expect from life.

Mihaela, thank you very much for all your teaching and friendship during this tuff period. I wish you all the happiness girl and that you find what you are looking for in life. Dominik, a contrast with my "Latin" spirit, but always a smile for me, your kindness and calm helped me a lot. I wish you and Mathili a happy life. Ewa, despite we connected only at the end (I feel sorry for that) I envy your optimism facing life, it is admirable. Keep strong there is so many places in the world to discover and so many books to read. I am always here if you need a talk. Da, my "desk neighbour", thank you for being you it was a pleasure working with you. Aurora, I feel sorry that we met so late, but I hope we can keep in touch and thank you for listening and the cafe time! Mariana and Abram, it was a joy to see the beginning of your family. I wish you all the happiness for your beautiful family. Fabrizio, Andrea, Richard, Orkide, Theo, Mathia, Benjamin, Luuk, Humberto, Esengül, Helena, Laura, Louis, Fayezeah and Greta thank to you all, that in one way or the other helped to make my life more cheerful in Delft. I would like to thank you Joljin for all your help during these years. Thank you to my students: Kamil, Florian, Ester, Stella and Nick for all your help in the lab. I also would like to thank Irfan, despite we don't know each other well, thank you for your open spirit and for your help finishing the "unfinished" work. Enormous success to all of you!

I would also like to thank Josefina, that gave me the opportunity to start at Vironova, even knowing that I was still finishing my PhD. To all the rest of the team at Vironova: Mathieu, Rickard, Lin, Johan, Mehedi and Manu; thank you for the support. Carin thank you so much for the help with word and making the formatting of this document.

Gostava de te agradecer a ti Joana, pela tua amizade e que apesar de longe sempre me ajudaste a superar dias menos bons. Há pessoas assim com quem não precisamos de muito tempo ou até de falar muito para sabermos que estão lá para o resto da vida. Obrigada! Pónei Eliana, já sabes que nos somos assim, mas tu és uma daquelas amigas distantes que sempre que é preciso estão lá, obrigada por isso Pónei. Pessoal, apesar da mudança para outro país ter sido dura e nos termos afastado não posso de deixar de vos agradecer pela amizade que é o que deve comandar as nossas vidas: Paulo, Sara, Marcos, Maria (e agora o Dioginho), Diogo, Sopas, Verónica, Sarinha, Jorge, Filipa, Alice, Cristina, Sonia, Neto, Iris. Estais sempre lá quando é preciso, mesmo que às vezes longe, e espero que continuemos a poder fazer parte das vossas vidas por muitos e longos anos.

Família, não sei o que vos diga! Obrigada por essa alma nossa que tanto nos caracteriza e que me ensinou que nada é impossível, desde que o queiramos com força. Infelizmente, a emigração afasta-nos de algumas pessoas, mas elas estarão sempre no meu coração. Nando, Xande, Carla, Bruno e Pedro gosto muito de vocês e espero que um dia possamos partilhar boas recordações. As coisas não foram fáceis com esta mudança e com outros problemas e tristezas que surgiram nestes quatro anos, mas com isso acredito que temos que aprender e tornar-nos mais fortes para enfrentar a vida com um sorriso. Sofia e Nuno apesar de longe sempre senti que na vossa casa estou em casa, não tenho palavras para vos agradecer por isso e pela forma como cuidaram da minha mãe. Obrigada! O mesmo vos digo a vocês, Catarina e Fábio. Será sempre memorável o vosso casamento para mim, não por esses motivos que vocês estão a pensar, mas porque foi uma verdadeira festa de alegrias e de família. Sejam felizes, estarei aqui para assistir e comemorar com vocês a essa felicidade. Tio Henrique e tia Goreti, obrigada por me receberem sempre na vossa casa e haver sempre qualquer coisa especial porque vimos de fora.

Matilde, a minha pequenina que foi crescendo ao longo destes quatro anos. Que sejas sempre muito, muito feliz pequenita e a prima estará aqui sempre para te ajudar no que precisares. Não te esqueças que há um mundo de oportunidades onde quer que queiras ir, o mundo é enorme! Não te esqueças de cuidar do teu irmão, é

tua responsabilidade agora, e que eu sei que vais desempenhar essa tarefa muito bem. Gosto muito, muito de ti miúda!

Micas, muito, muito obrigada por tudo o que fazes e fizeste por mim e pela minha mãe, sinto que és como uma segunda mãe. Muito obrigada pela tua generosidade! D. Fátima e Sr. Adelino muito obrigada por todo o apoio e por me aceitarem na vossa família como uma segunda filha, e claro por criarem um filho maravilhoso. Sr. António nunca será esquecido e não se preocupe cuidarei bem do seu netinho, obrigada!

Infelizmente a vida é feita de perdas e a maior que sofri até hoje foi a tua avó, fico triste por não ter chegado a tempo para te dizer adeus e por não partilhares este momento de alegria connosco, mas sei que estejas onde estiveres estás feliz por nós. És a grande inspiração das nossas vidas e acredito que a nossa família te deve muito, a generosidade, a amabilidade, a alegria, a simpatia, o amor e sempre, sempre a coragem de enfrentar a vida. Essa coragem que transmitiste à mulher mais forte que conheço, a minha mãe! Mamã sei que não é, nem foi fácil, ver-me partir para longe e sei que a vida não nos tem recompensado da melhor forma pelos nossos esforços por sermos melhores. Mas como tu sempre dizes: "Cá se fazem cá se pagam!". O que significa que ainda muita coisa boa está para vir e estarei aqui para disfrutar contigo. Obrigada por todo o teu apoio e pela boa mãe que és e por sempre me teres posto à frente de tudo na tua vida. A ti e à avó vos dedico esta tese, por ela simbolizar para mim o empenho, a dedicação e a coragem para enfrentar as adversidades da vida que vocês me ensinaram. Obrigada às duas pelos vossos sorrisos!

Cuquinhas ou talvez devesse dizer meu marido... Eheheh! Obrigada não é suficiente por me acompanhares nesta maratona que é a vida. Sei que não é fácil aturar-me todos os dias e que principalmente estes quatro anos não foram fáceis para ti, mas mantiveste-te lá ao meu lado. Sempre com esse teu otimismo inabalável e determinação. Não só o teu amor é admirável, mas a tua amizade. Não sei onde iremos parar, mas sei que aconteça o que acontecer estarei para sempre aqui para ti. Amo-te muito meu amor e obrigada por tudo!

E como a canção diz:

*“Eles não sabem, nem sonham, que o sonho comanda a vida. Que sempre que o homem sonha o mundo pula e avança como bola colorida entre as mãos de uma criança.”*

*Fin*

# Curriculum Vitae

## **Vanessa Isabel Dias Ribeiro de Carvalho**

16-03-1985      Born in Viana do Castelo, Portugal

2000 – 2003      Secondary Education

Escola Secundária de Santa Maria Maior, Viana do Castelo - Portugal

2004 – 2009      B.Sc. in Anatomical Pathology

School of Allied Health Sciences - Polytechnic Institute of Porto,  
Portugal

2011 – 2012      M.Sc. of Science in Applied Biology – Molecular Biology

Aveiro University, Portugal

2013 – 2018      Ph.D. research

Department of Bionanoscience, Technical University of Delft

*Promotor:* Prof. dr. Andreas Engel

*Copromotors:* Dr. Marie-Eve Aubin-Tam



# Publications

**Carvalho V**, Kieffer R, de Lange N, Engel A, Aubin-Tam ME. Large conformational changes in FtsH create an opening for substrate entry. (BioRxiv, 209445, 2017).

**Carvalho V**, Pronk JW, Engel AH. Characterization of Membrane Proteins Using Cryo-Electron Microscopy. *Current Protocols in Protein Science*, e72, 2018.

Lindhoud S, **Carvalho V**, Pronk JW, Aubin-Tam ME. SMA-SH: Modified Styrene-Maleic Acid Copolymer for Functionalization of Lipid Nanodiscs. *Biomacromolecules*, 17(4):1516-22, 2016.